UNIVERSITY OF OKLAHOMA

GRADUATE COLLEGE

NON-FICKIAN THREE-DIMENSIONAL MOISTURE ABSORPTION IN

POLYMERIC COMPOSITES: DEVELOPMENT AND VALIDATION OF

HINDERED DIFFUSION MODEL

A DISSERTATION

SUBMITTED TO THE GRADUATE FACULTY

in partial fulfillment of the requirements for the

Degree of

DOCTOR OF PHILOSOPHY

By

LANDON GRACE
Norman, Oklahoma
2012

NON-FICKIAN THREE-DIMENSIONAL MOISTURE ABSORPTION IN
POLYMERIC COMPOSITES: DEVELOPMENT AND VALIDATION OF
HINDERED DIFFUSION MODEL


A DISSERTATION APPROVED FOR THE
SCHOOL OF AEROSPACE AND MECHANICAL ENGINEERING




BY


_____
Dr. M. Cengiz Altan


_____
Dr. David P. Miller


_____
Dr. Mrinal C. Saha


_____
Dr. Zahed Siddique


_____
Dr. Mark Yeary

# Acknowledgements

First and foremost, I would like to thank my advisory committee for their support and guidance throughout my graduate studies, both in the classroom and as members of my committee. The encouragement and insight of Dr. David Miller, Dr. Mrinal Saha, Dr. Zahed Siddique, and Dr. Mark Yeary has been invaluable. Particular thanks are owed to my advisor, Dr. Cengiz Altan, without whom a long and arduous road would have been immeasurably longer and more arduous. Dr. Altan's expectations were matched only by the quality of his advice and guidance. Most graduate students are not afforded an opportunity to work under conditions so conducive to success, and for that I am thankful.

The dedication and persistence required to complete my degree were by no means solely my own. The unwavering support of my friends and family throughout this endeavor was my motivation when my own was lacking, as was sometimes the case. I owe a particular debt of gratitude to my wife for her encouragement, support, and understanding, without which this and many other milestones could not have been reached.

## Table of Contents

# List of Tables

# List of Figures

# Abstract

The importance of environmental damage consideration in the design of polymeric composite structures is discussed, with emphasis on the relationship between absorbed moisture content and material property degradation. A brief overview of existing predictive models of moisture diffusion and their limitations is presented. The three-dimensional anisotropic Fickian diffusion model is expanded to include the effects of the interaction of diffusing molecules with the chemical and physical structure of polymeric composites. The numerical solution of this novel hindered diffusion model is obtained for a three-dimensional, anisotropic domain by using a forward-time centered-space finite difference technique. The numerical solution method is verified by comparing the results to known analytical solutions of a one-dimensional, "Langmuir-type" diffusion model and for the limiting case of the three-dimensional Fickian model. The proposed three-dimensional anisotropic hindered diffusion model (3D HDM) and its one-dimensional isotropic version are successfully applied to three experimental moisture absorption data sets reconstructed from existing literature.

An analytical solution based on a judicious approximation to the 3D HDM is developed in an effort to increase the utility of the model in the recovery of polymeric composite diffusion properties from experimental data. The effectiveness of the recovery of absorption properties is assessed using artificially generated "synthetic" experimental data.  The anisotropic

diffusivities, equilibrium moisture content ($M_\infty$), and molecular binding ($\gamma$)

and unbinding ($\beta$) probabilities that govern three-dimensional hindered

diffusion are recovered using least-squares regression. Using both Fickian and

non-Fickian synthetic moisture absorption data, diffusivities and equilibrium

moisture content are recovered with less than 1% error. Values of $\gamma$ and $\beta$ are

recovered with less than 3% error in the non-Fickian diffusion case. It is

shown that equilibrium moisture content can be successfully determined much

earlier using only partial gravimetric data obtained from the initial phases of

moisture absorption, even in the presence of considerable measurement error.

The three-dimensional anisotropic moisture absorption behavior of a quartz-fiber-

reinforced bismaleimide (BMI) laminate is investigated by collecting 21 months

of experimental gravimetric data. Laminates of six, twelve, and forty plies and

various planar aspect ratios are used to determine the three-dimensional

anisotropic diffusion behavior when exposed to full immersion in distilled water

at 25°C. The long-term moisture absorption behavior deviates from the widely-

used Fickian model, but excellent agreement is achieved between experimental

gravimetric data and the 3D HDM. Diffusion through the laminate edges occurs

15 times faster on average than diffusion through the thickness, further

highlighting the importance of anisotropic diffusion consideration.

# Chapter 1: Environmentally Induced Damage in Polymeric Composites

Polymers and their fiber-reinforced composites have a wide variety of desirable mechanical, electrical, and thermal properties which have led to their widespread use in the aerospace, automotive, and electronics industries. Particularly in applications which require low weight and high strength, fiber-reinforced composites have seen a rapid increase in application. This high strength-to-weight ratio is especially beneficial in the automotive and aerospace industries, where better fuel efficiency as a result of lower weight is increasingly important. In addition, the ability to orient the fiber reinforcement in the direction of the applied load in structural applications offers a unique advantage in certain applications. Further, a high-strength material which is also an excellent electrical insulator due to low dielectric constant is essential in applications such as printed circuit boards or radar-protecting structures on aircraft. As a result of these unique capabilities and benefits of polymeric composites, usage of these materials has seen a sharp increase over the last three decades. As polymer composite technology becomes more established, an increasing number of composite structures are being used in long-service-life applications in potentially damaging environmental conditions. Research has shown that environmentally induced physical damage has a significant effect on the mechanical, thermal, and electrical properties of polymer composites. The extent to which these physical damages affect the mechanical

and electrical properties of polymeric composites plays an important role in structural design decisions and service life estimations for composite structures. Therefore, substantial effort has been made to characterize the degradation of polymer composites under adverse environmental conditions such as ultraviolet radiation exposure, galvanic corrosion when coupled with metals, exposure to atmospheric oxygen at high temperatures, and exposure to moisture in the form of liquid water or humid air.

## (1.1)  Common Types of Polymeric Composite Environmental Degradation

Exposure to ultraviolet (UV) radiation is a common composite operating condition and has been shown to have a deleterious effect on composite mechanical properties. Polymer matrix material contains many types of bonds that are capable of absorbing ultraviolet light, which can lead to photochemical reactions and dissolution of the chemical bonds of the exposed polymer.  As a result, composite polymer resins are particularly susceptible to degradation due to ultraviolet radiation.  The ultraviolet components of solar radiation on the surface of the earth are in the 290-400 nm band. The energy associated with these UV photons is typically comparable to the dissociation energies of the covalent bonds in polymers. As a result, these photons result in photo-oxidative reactions that alter the chemical structure of the polymer in the form of chain scission and/or

crosslinking [1]. Photochemical reactions can potentially lead to loss of

mechanical properties and discoloration of the polymer, even for very short

exposure times. In one study, degradation was observed in the top 0.5-1μm of an

epoxy resin after 30 minutes of exposure to ultraviolet radiation in the 220-300

nm wavelength range [2].  In a study on the effects of UV radiation on carbon

fiber-reinforced epoxy, Kumar et al. [1] observed a significant decrease in the

matrix-dominated mechanical properties after only 1000 hours of cyclic exposure

to ultraviolet radiation. The transverse tensile strength of the laminate, for

example, decreased by 29% during this time.  High magnification optical

micrographs of machined specimens of carbon fiber / epoxy exposed to 500 hours

of UV radiation are shown in Ref. [1]. These images reveal the formation of

microcracks in the resin. This microcracking is attributed to excessive resin

brittleness caused by the UV radiation-induced photo-oxidation reactions [1].


Environmental degradation of polymer composites may also proceed through the

galvanic corrosion process. In a study performed to assess the effect of galvanic

corrosion on the strength of graphite/bismaleimide composites, Cochran et al.

report resin degradation in composites galvanically coupled to aluminum alloys.

The authors report significant cracking and deterioration of the resin, which is

attributed to hydroxyl ion generation in the cathodic reaction [3].  Fischer and

DeLuccia report that electrochemical measurements indicate a relatively large

potential difference of approximately 1V between graphite/epoxy composites and

aluminum alloys. This is particularly problematic in the naval air/sea environment, in which sea water increases the effect by acting as an electrolyte [4]. In a study on the formation of blisters on graphite-reinforced vinyl ester coupled with steel in seawater, Tucker and Brown [5] found visible blister formation occurred after approximately three weeks of full immersion in seawater. Control samples which were not galvanically coupled to steel under the same conditions exhibited no blister formation. Evidence of this blister formation on the graphite/vinyl ester composite is provided in an image in Ref. [5].

A relatively common operating environment for polymer composites is elevated temperature coupled with exposure to environmental oxygen. This condition can cause a significant reduction in mechanical properties and mass loss, commonly referred to as "thermo-oxidative" aging. Damage of this type is nonreversible and typically manifests in the form of mass loss, matrix-fiber debonding, and resin microcracks. The degradation is caused by the diffusion of oxygen into the composite, which is accelerated at increased temperatures [6]. The process of thermo-oxidative degradation in polymer composites is autocatalytic, i.e., it will self-propagate once the process has been initiated. Free radicals, an unstable atom or group of atoms with at least one unpaired electron, have a high affinity for reacting with oxygen to form unstable peroxy radicals. Once formed, these peroxy radicals abstract neighboring labile hydrogen atoms from the polymer chain, which weakens and degrades the polymer and produces more free radicals to begin the process anew [7]. It has been observed in surface weight-loss rate

experiments performed on unidirectional carbon-fiber reinforced polyimide, that oxygen diffusion and consequent weight loss exhibit anisotropic behavior. Weight loss transverse to the fiber direction is lower than weight loss for neat resin, due to a retarding effect of the carbon fiber on oxygen diffusion. Weight loss in the fiber direction, however, proceeds much faster due to the interactions between fiber, matrix, and the fiber/matrix interface. The authors speculate that thermal oxidation causes shrinkage of the polymer, which is responsible for the initiation of debonds. Therefore, oxygen penetration into the laminate is accelerated, which leads to additional thermal oxidation. Evidence of this fiber/matrix debond due to thermo-oxidative resin shrinkage can be seen in a micrograph in Ref [8].

One of the primary disadvantages of polymeric composites is the tendency of these materials to absorb moisture when exposed to humid and / or wet environments for long periods of time. Moisture absorption into polymer composites is a critical consideration, both due to the damage induced by absorbed water and the ubiquitous nature of moisture. Moisture absorption into composite structures depends largely on the climatic conditions, such as the range and temporal variations of ambient temperature and humidity levels, to which they are exposed. Even in geographic locations with typically hot, dry conditions, a measurable amount of moisture absorption has been reported [9].

## (1.2)    Moisture Induced Damage in Polymeric Composites

Significant research effort has been focused on understanding the mechanisms of moisture ingress and the detrimental effects of moisture in polymeric composites. Abdel-Magid et al. [10] investigated the effect of moisture conditioning combined with mechanical loading on E-glass/epoxy composites and observed a noticeable reduction in strength, strain-to-failure, and modulus. The influence of moisture on the mechanical and thermal properties of Kevlar/epoxy laminates was studied by Akay et al. [11], who reported deterioration of the compressive, interlaminar shear, and flexural strength of the laminate in the presence of absorbed moisture. Specifically, the compressive, interlaminar shear, and flexural strength decreased by 5, 4, and 2%, respectively, per 1% absorbed moisture by weight [11].  A lowering of the glass transition temperature of the laminate due to resin plasticization was also observed. Typically, the maximum service temperature of polymeric composites is related to the value of the glass transition temperature, $T_g$ [12].  As a result, the determination of service temperature, an important design consideration, must take into account the moisture content of the composite. Similarly deleterious effects due to moisture have been observed in thermoplastic resins, in addition to thermosets. For example, a decrease in the tensile and interlaminar shear strengths of carbon or glass-fiber-reinforced polyetherimide in the presence of absorbed moisture was reported by Viña et al. [13].  A general reduction in the static material properties of fiber-reinforced polymers has been

reported by a number of sources and for a number of fiber/matrix combinations, such as glass/polyester [14], glass/epoxy [15], glass/vinylester [16], and carbon fiber/epoxy [17]. In addition, adverse effects on the mechanical properties of unreinforced epoxy resins have been reported in the case of a diglycidyl ether of bisphenol A (DGEBA) epoxy cured with dethylenetriamine (DETA) [18], as well as DGEBA cured with dicyandiamide (DDA) [19]. The degradation of the mechanical properties in the DGEBA/DETA system is attributed to hydrogen bonding that is formed between the water molecules and the polar groups of the polymer. Resin degradation due to moisture limits the load-transferring ability of the matrix by loosening the bond between fiber and resin, as observed during tensile and short-beam shear tests performed on glass/epoxy resin transfer molded composites by Aktas et al. [20-21]. This decrease in mechanical properties was attributed to loosening of the fiber as evidenced by fiber pullouts on the surface of tested samples. Similar results were found by Barraza et al. [22] in water sorption studies to assess the hydrolytic stability and wet-adhesion properties of resin transfer molded glass fiber/epoxy composites with different elastomer fiber coatings. Regardless of the fiber coating, wet composites were found to suffer from interfacial debonding, matrix craze, and fiber pullout with a subsequent decrease in mechanical properties. Significant degradation of a carbon fiber / nylon 6 composite was reported by Pillay et al. [23] in the form of surface cracks and fiber/matrix interface damage after exposure to water at 100°C for 100 hours as evidenced by scanning electron microscopy images provided in Ref. [23].

Decreased flexural strength, flexural modulus, and shear strength were also reported by Wan et al. [24] in three-dimensional braided carbon-epoxy prepared by vacuum assisted resin transfer molding. In addition to these specific cases, the bulk of existing literature indicates a near universal consensus on the undesirable decrease in material properties due to absorbed moisture in polymeric composites.

In addition to the deterioration of mechanical properties, the presence of moisture in polymeric composites has been shown to degrade electrical performance. Desirable electrical properties in the form of low dielectric constant and loss tangent are essential for polymeric composites used as electrical insulators and as part of the radar protecting structure (radome) on aircraft. As part of the radome structure, polymer composites must be transparent to radar of varying frequencies. This electromagnetic transparency can potentially be compromised by the presence of moisture within the polymer matrix due to the high dielectric constant (~ 80) of water relative to the low dielectric constant (~3) of most quartz or glass-reinforced polymers [25]. In addition, glass-reinforced polymer composites are used as an alternative to porcelain as high voltage insulators. In this role, moisture ingress has been shown to lead to electrical failure of glass reinforced polymer composites exposed to a moist environment of 80% relative humidity at 50°C [26]. Further, Cotinaud et al. [25] report changes in the electrical properties of a glass-fiber reinforced epoxy composite in the form of a 40% increase in relative permittivity for a 1% increase in moisture content by weight.

# Chapter 2:  Modeling Moisture

# Absorption in Polymeric Composites

In order to predict the extent of material property degradation in polymeric

composites, the moisture absorption dynamics and equilibrium moisture content

(i.e. maximum moisture content, $M_\infty$) must be well known. Thus, accurate

prediction of the amount of moisture within a composite structure at a given time

is necessary to prevent potential in-service failure of these materials. In an effort

to meet this requirement, numerous predictive models of moisture absorption

have been developed. During the past few decades, Fick's law of diffusion [27]

has been among the most widely-used models.  Numerous experimental results of

moisture absorption in polymeric composites seem to follow a Fickian diffusion

process [28-33], particularly in the initial linear uptake region. Many other

experimental results, however, indicate varying degrees of non-Fickian behavior

exist in polymeric composites [34-51]. For example, non-Fickian absorption

followed by Fickian desorption [50] or Fickian behavior at low temperatures and

non-Fickian behavior at higher temperatures [51] have been reported.  The wide

variety of moisture absorption behavior reported in the literature for various

polymer systems often necessitates the use of multiple models. Among these are

traditional Fickian diffusion model [27], a dual-mode sorption model generally

referred to as the "Langmuir-type" model of diffusion [52], a time-varying

diffusion coefficient model [53], a dual-diffusivity model taking into account the

two-phase nature of composite materials proposed by Jacobs and Jones [41] which was later modified by Maganna and Pissis [54], and a coupled diffusion-relaxation model [55-56].

## (2.1) Fickian Diffusion Model

Moisture absorption in composite panels is typically modeled as a one-dimensional process through a semi-infinite plate in which diffusion through the edges of composite panels is neglected. The most basic absorption model is based on Fick's second law [27], and in the one-dimensional case is governed by the equation

$$\frac{\partial n}{dt} = D_z \frac{\partial^2 n}{dz^2} \tag{1}$$

where $n$ is the moisture concentration, $D_z$ is the diffusion coefficient, $t$ is time, and $z$ is the spatial coordinate.

Assuming an initially dry slab of thickness $h$ exposed to a constant moisture environment on both sides, the boundary and initial conditions are

$$n(z, 0) = 0 \quad \text{for} \quad |z| < \frac{h}{2} \qquad \text{and}$$

$$\tag{2}$$

$$n\left(\frac{h}{2}, t\right) = n\left(-\frac{h}{2}, t\right) = n_\infty \qquad \text{for all } t$$

where $n_\infty$ is the moisture concentration at equilibrium.

The coordinate system, geometry, and diffusion directions used throughout this work are shown in Figure 1. The solution to the problem defined by Equations (1) and (2) is given as

$$n(z,t) = n_\infty - 4\frac{n_\infty}{\pi} \sum_{p=0}^{\infty} \frac{(-1)^p}{(2p+1)} \cos\left(\frac{\pi(2p+1)}{h}z\right)$$

(3)

$$\times \ \exp\left[-\left(\frac{\pi(2p+1)}{h}\right)^2 D_z t\right]$$

Integration of the moisture concentration profile defined by Equation (3) over the surface and time yields the total mass entering the specimen. Considering absorption from both sides, the mass gain function for one-dimensional Fickian diffusion becomes

$$M(t) = M_\infty - \frac{8M_\infty}{\pi^2} \sum_{p=0}^{\infty} \frac{1}{(2p+1)^2} \ e^{-\pi^2 t\left(\frac{D_z\,(2p+1)^2}{h^2}\right)}$$

(4)

where $M(t)$ is the percent mass gain of the composite sample as a function of time, $M_\infty$ is the percent mass gain at equilibrium, and $h$ is the thickness of the sample in the $z$ direction.

In the initial stages of Fickian diffusion, the moisture content $M(t)$ varies linearly

with the quantity $\sqrt{t}$. The diffusion coefficient $D_z$ can be calculated based on the

initial slope $s$ of the diffusion curve [57]

$$D_z = \pi \left(\frac{sh}{4M_\infty}\right)^2 \tag{5}$$

where

$$s = \frac{M_2 - M_1}{\sqrt{t_2} - \sqrt{t_1}} \tag{6}$$

The typical shape of the moisture absorption curve when the moisture content is

plotted against the square root of time is shown in Figure 2. An illustration of the

measured values used in the determination of the one-dimensional diffusion

coefficient (Equation 6) is shown as well.
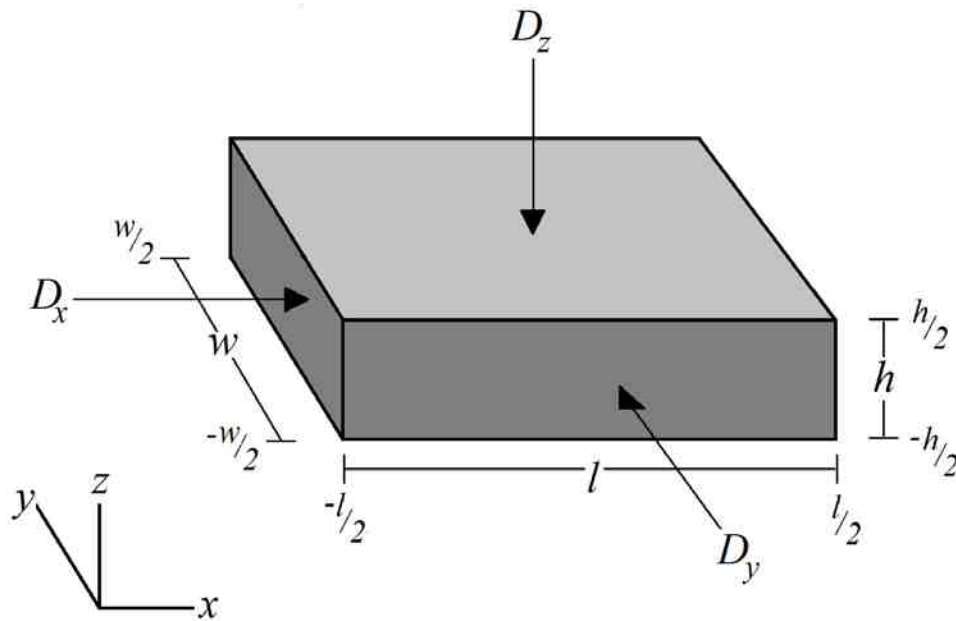


**Figure 1 - Dimensions and moisture ingress directions used in this work.**

In the one-dimensional Fickian diffusion model, the diffusion coefficient of specimens without moisture-impermeable coating at their edges should be corrected. This edge correction, intended to account for moisture ingress through the edges of a composite slab, was proposed by Shen and Springer [57] and is given by

$$D_c = D_z \left(1 + \frac{h}{l} + \frac{h}{w}\right)^{-2} \qquad (7)$$

where $D_c$ is the corrected value of the diffusion coefficient $D_z$, and $l$ and $w$ are the length and width of the specimen, respectively.
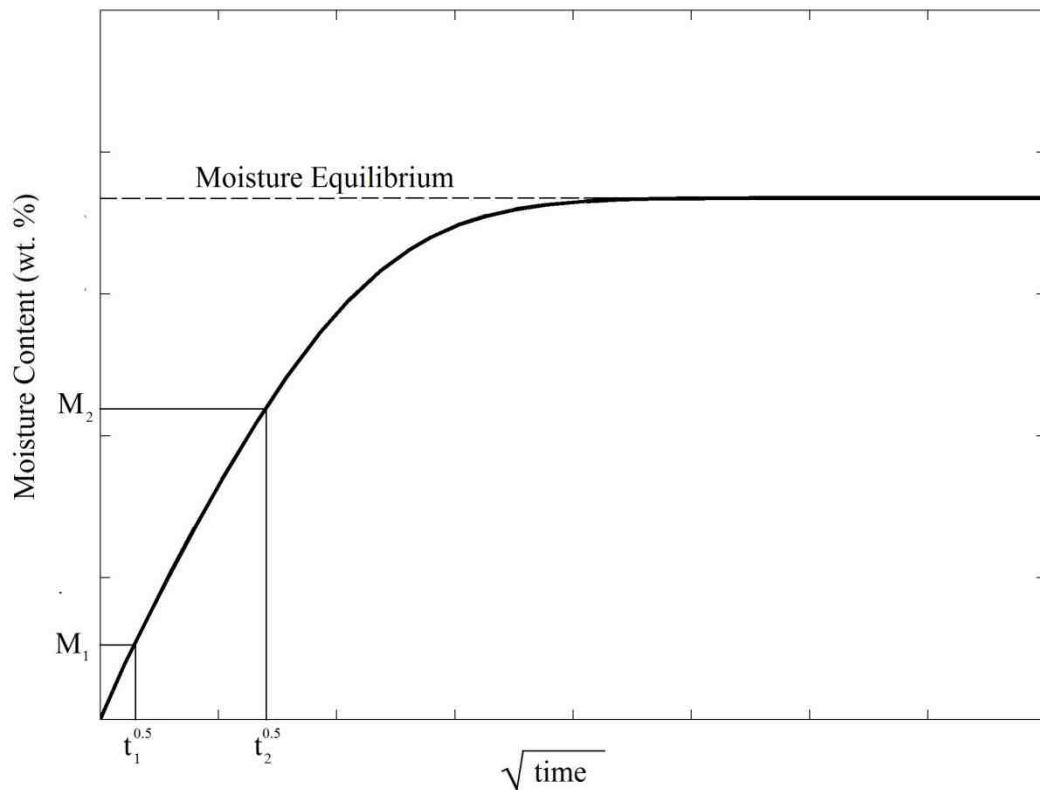


**Figure 2 - Depiction of a typical Fickian moisture absorption curve and measured values used to determine one-dimensional diffusivity.**

## (2.2) Time-Varying Diffusivity Model

Cai and Weitsman [58] developed a one-dimensional diffusion model with time-varying diffusivity within the framework of Fickian diffusion. The model assumed variation in the diffusion coefficient with temperature, which could be represented by a time-dependent function. The model requires an iterative numerical procedure for evaluation of the time-varying boundary conditions. Weitsman proposes that the diffusion coefficient is highly sensitive to temperature, and can be summarized by

$$D = D_0 e^{-\frac{B}{\theta}} \tag{8}$$

where $D_0$ and $B$ are material constants and $\theta$ is absolute temperature.

As a result, Weitsman concludes that a composite structure exposed to time-varying temperature would also be subjected to time-varying diffusivity. Therefore, a function was defined such that

$$e^{-\frac{B}{\theta}(t)} = h(t) \tag{9}$$

so that the diffusion coefficient can then be defined as

$$D = D_0 h(t) \tag{10}$$

The governing equation for moisture diffusion with time varying diffusivity can then be expressed as

$$\frac{\partial n}{dt} = D_0 h(t) \frac{\partial^2 n}{dz^2} \tag{11}$$

If $h(t) = 1$, the model given in Equation (11) reduces to the one-dimensional

Fickian diffusion model with constant diffusivity.

The time-varying diffusion model is expanded and improved by Roy et al. [53].

The governing equation is expressed as

$$\frac{\partial n}{dt} = D_z(t) \frac{\partial^2 n}{dz^2} \tag{12}$$

where $D_z(t)$ is the diffusion coeffiecient, which varies with time but is uniform

through the thickness of the polymer.

Assuming an initially dry slab of thickness $h$, the boundary conditions for

moisture concentration are given by

$$n\left(-\frac{h}{2}, t\right) = n\left(\frac{h}{2}, t\right) = n_\infty \tag{13}$$

subject to the initial condition

$$n(z, 0) = 0 \tag{14}$$

Assuming that the diffusivity can be expressed in the form of a Prony Series,

$$D(t) = D_0 + \sum_{r=1}^{R} D_r \left(1 - e^{-\frac{t}{\tau_r}}\right) \tag{15}$$

where $D_0$ and $D_r$ are the unknown Prony coefficients and $\tau_r$ is the corresponding retardation time.

The corresponding expression for moisture concentration as a function of distance and time is

$$\frac{n}{n_\infty} = 1 - \frac{4}{\pi} \sum_{p=0}^{\infty} \frac{(-1)^p}{2p+1} \times exp\left\{\frac{-(2p+1)^2\pi^2}{h^2}\right.$$
$$\times \left\{D_0 t + \sum_{r=1}^{R} D_r\left[t + \tau_r\left(e^{-\frac{t}{\tau_r}} - 1\right)\right]\right\}\right\} \cos\frac{(2p+1)\pi z}{h} \tag{16}$$

Integration of moisture concentration over slab thickness yields the moisture weight-gain fraction as a function of time, given as

$$\frac{M(t)}{M_\infty} = 1 - \frac{8}{\pi^2} \sum_{p=0}^{\infty} \frac{1}{(2p+1)^2} \times exp\left\{\frac{-(2p+1)^2\pi^2}{h^2}\right.$$
$$\times \left\{D_0 t + \sum_{r=1}^{R} D_r\left[t + \tau_r\left(e^{-\frac{t}{\tau_r}} - 1\right)\right]\right\}\right\} \tag{17}$$

## (2.3) Dual-Diffusivity Model

A dual-diffusivity model was developed by Jacobs and Jones [41] to describe the moisture absorption behavior of a two-phase polymer. The diffusion characteristics of the dense and less dense polymer phases are determined and incorporated into a comprehensive one-dimensional model for the system. The two phases of the polymer are assumed to absorb moisture at different rates and reach different equilibrium saturation values. A representation of the typical dual-diffusion moisture uptake is shown in Figure 3 based on Ref. [41]. The initial absorption (Region I) is assumed to take place in both dense and less dense phases. Once the less dense phase has reached equilibrium, absorption continues in the dense phase alone (Region II).
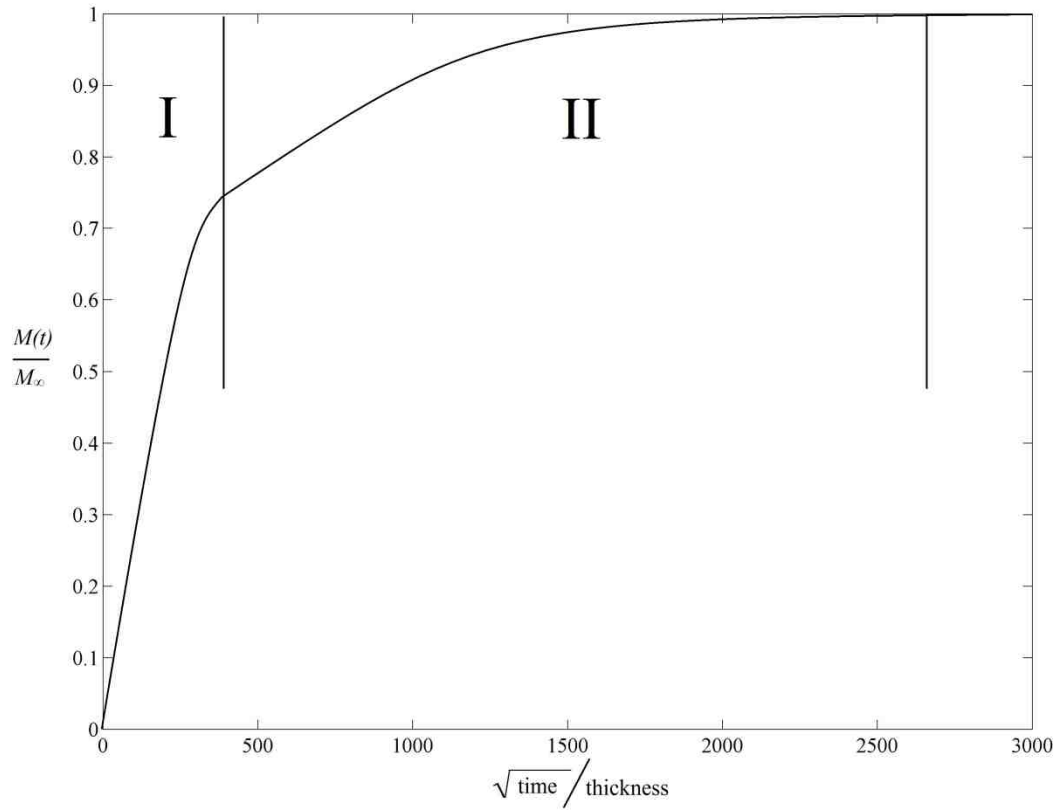
**Figure 3 - Typical moisture absorption profile for the dual-diffusivity model proposed by Jacobs and Jones highlighting the two absorption regions, denoted by I and II [41].**

An average diffusion coefficient $D_z$ can be calculated in the same manner as the Fickian case using the slope of the curve in Region I.

$$D_z = \pi \left( \frac{sh}{4M_\infty} \right)^2 \qquad (18)$$

where $M_\infty$ is the overall equilibrium moisture content, $s$ is the slope of the initial section of the moisture absorption curve, and $h$ is the thickness of the sample.

In order to determine the diffusion coefficients of the dense and less dense phases, denoted by $D_d$ and $D_l$, respectively, the equilibrium moisture content ($M_d$ and $M_l$) of each phase must be known. The equilibrium moisture content of the less dense phase is found by extrapolating the slope of the curve in Region II, denoted $m_d$, back to the moisture content axis. The equilibrium moisture content of the dense phase is found by subtracting $M_l$ from $M_d$. The diffusion coefficients of the individual phases, therefore, can be expressed as:

$$D_d = \pi \left( \frac{m_d h}{4M_d} \right)^2 \tag{19}$$

and

$$D_l = \pi \left( \frac{m_l h}{4M_l} \right)^2 \tag{20}$$

The volume fraction of the dense phase relative to the total system, $V_d$ can be expressed as

$$V_d = \frac{(B_d + 2)\left[ \left( \frac{D_z}{D_l} \right) - 1 \right]}{(B_d - 1)\left[ 2 + \left( \frac{D_z}{D_l} \right) \right]} \tag{21}$$

where

$$B_d = \frac{D_d}{D_l} \tag{22}$$

The normalized moisture absorption curve (assuming Fickian diffusion behavior in each phase) for the two phase system can therefore be expressed as

$$M(t) = V_d \left\{ 1 - exp\left[ -7.3 \left( \frac{D_d t}{h^2} \right)^{0.75} \right] \right\}$$

(23)

$$+ (1 - V_d) \left\{ 1 - exp\left[ -7.3 \left( \frac{D_l t}{h^2} \right)^{0.75} \right] \right\}$$

The model proposed by Jacobs and Jones was later modified by Maggana and Pissis [54] and applied to an epoxy resin. Diffusion was assumed to take place in two phases due to the existence of a plasticizer that led to formation of products with different cross-linking densities and/or hydrophilic characteristics. Unlike the model proposed by Jacobs and Jones, this model does not assume that the diffusion process is dependent only on the density of each phase. Instead, phase density and/or different amounts of interaction between water molecules and hydroxyl groups of the resin are assumed to contribute to the dual sorption behavior.

The Jacobs-Jones model is transformed by Maggana and Pissis to [54]

$$M(t) = M_1 \left\{ 1 - exp\left[ -7.3 \left( \frac{D_1 t}{h^2} \right)^{0.75} \right] \right\}$$

$$+ M_2 \left\{ 1 - exp\left[ -7.3 \left( \frac{D_2 t}{h^2} \right)^{0.75} \right] \right\}$$

(24)

where $D_1$ and $D_2$ and $M_1$ and $M_2$ are the diffusion coefficient and equilibrium

moisture content of the two phases, respectively.

As in the Jacobs-Jones model, the diffusion coefficient $D_2$ refers to the dense

phase and must be at least one order of magnitude less than $D_1$, as the diffusion of

water in this region is hindered by increased crosslinking density.  According to

the authors, this assumption is valid for systems where water molecules are not

strongly attached to polar groups of the polymer. Further, the authors demonstrate

that this assumption is not always valid, as strong interactions between water

molecules and polymer sometimes exist.

## (2.4)  Dual-Mode Sorption Model

A dual-mode sorption model assumes that two modes of penetrant sorption occur

concurrently within a microheterogeneous medium. The first sorption mode is

controlled by dissolution of mobile molecules due to random molecular motion, as in the Fickian diffusion model. The second sorption mode is due to interaction between the penetrant and sites within the medium [59]. Assumptions about the nature of this interaction vary, though one of the more widely-used models assumes interaction between polar water molecules and molecular groups of the resin. This model, generally referred to as "Langmuir-type," was first proposed by Carter and Kibler [52] and has since been successfully applied to the absorption behavior of several polymers and their composites [33, 34, 40, 43, 52], albeit only in one dimension. The diffusive characteristics of the model are related to neutron transport theory, and the classification of diffusing water molecules into strongly bound and mobile types is related to the Langmuir theory of adsorption isotherms [52]. The model proposed by Carter and Kibler is essentially the one-dimensional isotropic Fickian diffusion model modified by an additional term to account for sources and sinks of diffusing molecules. According to Ref. [52], these sources and sinks are likely due to interactions between polar water molecules and the molecular groups of the resin, which is the same phenomenon reported to be the cause of mechanical degradation in a DGEBA/DETA epoxy resin [18].

In the one-dimensional domain, the concentration at position $z$ and time $t$ in the "Langmuir-type" model of diffusion satisfy the coupled pair of partial differential equations,

$$D\frac{\partial^2 n}{\partial z^2} = \frac{\partial n}{\partial t} + \frac{\partial N}{\partial t}$$

(25)

$$\frac{\partial N}{\partial t} = \gamma n - \beta N$$

where $n$ represents the mobile molecules per unit volume, $N$ represents the bound molecules per unit volume, $\gamma$ is the probability per unit time that a mobile molecule will become bound, and $\beta$ is the probability per unit time that a bound molecule will become mobile. The absorption process continues until the temporal variation of bound molecules per unit volume vanishes. Thus, when the equilibrium conditions are reached, the following equation is satisfied.

$$\gamma n = \beta N \qquad\qquad (26)$$

Assuming an initially dry slab of thickness $h$ exposed to a constant moisture environment on both sides, the boundary and initial conditions are

$$n(z,0) = 0, \quad N(z,0) = 0 \quad \text{for} \quad |z| < \frac{h}{2} \quad \text{and}$$

(27)

$$n\left(\frac{h}{2}, t\right) = n\left(-\frac{h}{2}, t\right) = n_\infty \qquad \text{for all } t$$

An exact solution for the spatial distribution of mobile molecules in this one-dimensional isotropic model of diffusion has been obtained by means of Laplace transforms.

$$n(z,t) = n_\infty \left\{ 1 - \frac{4}{\pi} \sum_{p=1}^{\infty(odd)} \frac{(-1)^{\frac{p-1}{2}}}{p(r_P^+ - r_P^-)} \right.$$

$$\times \left[ r_P^+ \exp(-r_P^- t) - r_P^- \exp(-r_P^+ t) \right] \cos\frac{p\pi z}{h} \Bigg\}$$

(28)

$$+ n_\infty \frac{4}{\pi\beta} \sum_{p=1}^{\infty(odd)} \frac{(-1)^{\frac{p-1}{2}}}{p(r_P^+ - r_P^-)} (r_P^+ r_P^-)[\exp(-r_P^- t)$$

$$- \exp(-r_P^+ t)] \cos\frac{p\pi z}{h}$$

where

$$r_P^\pm = \frac{1}{2}\left[ (kp^2 + \gamma + \beta) \pm \sqrt{(kp^2 + \gamma + \beta)^2 - 4k\beta p^2} \right]$$

(29)

and

$$k = \frac{\pi^2 D}{(h)^2}$$

(30)

The corresponding solution for the spatial distribution of bound molecules is given by

$$N(z,t) = \frac{\gamma}{\beta} n_\infty \left\{ 1 - \frac{4}{\pi} \sum_{p=1}^{\infty(odd)} \frac{(-1)^{\frac{p-1}{2}}}{p(r_P^+ - r_P^-)} \right.$$

$$\left. \times [r_P^+ \exp(-r_P^- t) - r_P^- \exp(-r_P^+ t)] \cos \frac{p\pi z}{h} \right\}$$

(31)

The solution process was detailed in Ref. [52], where integration of the exact expression for concentration over slab thickness yields the following:

$$M(t) = M_\infty \left\{ 1 - \frac{8}{\pi^2} \sum_{p=1}^{\infty(odd)} \frac{[r_P^+ \exp(-r_P^- t) - r_P^- \exp(-r_P^+ t)]}{p^2(r_P^+ - r_P^-)} + \frac{8}{\pi^2}\left(\frac{k\beta}{\gamma+\beta}\right) \sum_{P=1}^{\infty(odd)} \frac{[\exp(-r_P^- t) - \exp(-r_P^+ t)]}{r_P^+ - r_P^-} \right\}$$

(32)

In Equation (32), $M$ is the weight of absorbed moisture after time $t$ given an equilibrium moisture weight percent, $M_\infty$.

When the parameter, $k$, that determines the rate of saturation is much larger than $\gamma$ and $\beta$, which is almost always the case in polymeric composites, the following approximation is valid:

25

$$\frac{M(t)}{M_\infty} = \frac{\beta}{\gamma + \beta} \left[ 1 - \frac{8}{\pi^2} \sum_{P=0}^{\infty} \frac{1}{(2P+1)^2} \, e^{-\pi^2 t \left( \frac{D_z \, (2P+1)^2}{h^2} \right)} \right]$$

$$+ \left( 1 - \frac{\gamma}{\gamma + \beta} e^{-\beta t} - \frac{\beta}{\gamma + \beta} \right) \tag{33}$$

This expression can be further simplified and written as

$$M^* = \mu \left( 1 - \frac{8}{\pi^2} \sum_{P=0}^{\infty} \frac{1}{(2P+1)^2} \, e^{-\pi^2 t \left( \frac{D_x \, (2P+1)^2}{h^2} \right)} \right) + (1 - \mu)(1 - e^{-\beta t})$$

where, $\tag{34}$

$$M^* = \frac{M(t)}{M_\infty} \qquad \mu = \frac{\beta}{\gamma + \beta}$$

### (2.5)  Diffusion-Relaxation Model

In an effort to model concurrent diffusive and polymer relaxation controlled

moisture absorption mechanisms, Berens and Hopfenberg [55, 56] considered the

moisture uptake by each mechanism to be superimposable with the total moisture

uptake. Therefore, net moisture uptake is separated into diffusion controlled

uptake and polymer relaxation controlled uptake as defined by

$$m(t) = m_D(t) + m_R(t) \tag{35}$$

where $m_R$ and $m_D$ represent moisture uptake due to relaxation and diffusion,

respectively.

The moisture uptake due to diffusion was assumed to follow the typical one-

dimensional Fickian process. The relaxation process is defined as

$$\frac{dm_R}{dt} = \Omega\big(m_{R,e} - m_R\big) \tag{36}$$

where $\Omega$ is a relaxation rate constant and $m_{R,e}$ is the equilibrium moisture content

due to the relaxation process. In order to account for multiple viscoelastic

processes within the polymer with different relaxation rates, Berens and

Hopfenberg proposed the more general expression

$$m_R = \sum_{i=1}^{N} \big(m_{R,e}\big)_i (1 - e^{-\Omega_i t}) \tag{37}$$

The solution to the diffusion-relaxation model was rewritten by Bond [59] as

$$M^* = \Phi\left(1 - \frac{8}{\pi^2}\sum_{P=0}^{\infty}\frac{1}{(2P+1)^2}\, e^{-\pi^2 t\left(\frac{D_x\,(2P+1)^2}{h^2}\right)}\right) + (1-\Phi)(1-e^{\Omega t}) \quad (38)$$

by setting

$$m_{D,e} = \Phi m_e$$

$$m_{R,e} = (1-\Phi)m_e \quad (39)$$

$$M^* = \frac{m}{m_e}$$

where $m_{D,e}$ is the equilibrium moisture content due to the diffusive process, $m_e$ is the net equilibrium moisture content due to both processes, and $\Phi$ is the "diffusive absorption fraction" which varies from 0 to 1.

Notice that the diffusion-relaxation solution proposed by Bond in Equation (38) is mathematically equivalent to the "Langmuir-type" dual-mode sorption model presented in Equation (34) under certain conditions. Namely, the two models are mathematically equivalent when we set $m_{D,e}$ and $m_{R,e}$ as proposed by Bond [59] and given in Equation (39), in addition to setting

$$\Phi = \mu$$

$$\quad (40)$$

$$\Omega = -\beta$$

28

and under the condition

$$k = \frac{\pi^2 D}{(h)^2} \gg \gamma, \beta \qquad (41)$$

The mathematical similarity of the two models was noted by Bond [59], but the equivalency when the "diffusive absorption fraction" was set to $\frac{\beta}{\gamma+\beta}$ and the relaxation rate constant was set to $-\beta$ was unmentioned. In fact, the experimentally determined values of $\Phi$ and $\Omega$ reported by Bond for a carbon-fiber reinforced epoxy are consistent with the values of $\frac{\beta}{\gamma+\beta}$ and $-\beta$ reported elsewhere in the literature.

### (2.6) Three-Dimensional Effects and Material Anisotropy

One-dimensional moisture absorption models are widely used to characterize moisture diffusion behavior of polymeric composites. This approach, while valid in many cases, can introduce significant errors due to material anisotropy and finite sample dimensions. For example, Blikstad [60] found that in graphite/epoxy laminates it is possible for the diffusivity in the fiber direction to be more than ten times larger than the through-thickness diffusivity used in the one-dimensional Fickian model. In addition, Aronhime et al. studied the anisotropic moisture absorption behavior of unidirectional Kevlar/epoxy and found that the ratio of diffusion along the fiber to diffusion transverse to the fiber varied from 3 to over

100, depending on the fiber volume fraction [61]. The contribution of moisture absorption into the Kevlar fiber itself was assumed to play a role, and highlights the importance of three-dimensional and anisotropy considerations in moisture diffusion characterization, especially for Kevlar reinforced laminates.  In addition, Arao et al. report edge diffusivities between 2 and 4 times greater than through-thickness diffusivity for a woven carbon-fiber reinforced epoxy laminate [62]. Therefore, accurate modeling of the absorption process must take into account diffusion in all three dimensions in all cases except those in which the lateral dimensions are vastly greater than the thickness.  The existence of anisotropic three-dimensional diffusion in fiber-reinforced composites is well-documented and has been studied thoroughly [60-64].

### (2.7)  Three-Dimensional Anisotropic Fickian Diffusion Model

In principal material coordinates, the three-dimensional form of the anisotropic Fickian diffusion model is given by

$$\frac{\partial n}{dt} = D_x \frac{\partial^2 n}{dx^2} + D_y \frac{\partial^2 n}{dy^2} + D_z \frac{\partial^2 n}{dz^2} \tag{42}$$

where $D_x$, $D_y$, and $D_z$ are the spatially uniform diffusion coefficients in the $x$, $y$, and $z$ directions, respectively.

Assuming an initially dry slab of dimensions $h$ x $w$ x $l$, the boundary and initial

conditions become

$$n(x, y, z, 0) = 0 \quad \text{for} \quad |x| < \frac{l}{2}, \ |y| < \frac{w}{2}, \ |z| < \frac{h}{2}$$

and (43)

$$n\left(x, y, \frac{h}{2}, t\right) = n\left(x, y, -\frac{h}{2}, t\right) = 0 \quad \text{for all} \ t$$

$$n\left(x, \frac{w}{2}, z, t\right) = n^*\left(x, -\frac{w}{2}, z, t\right) = 0 \quad \text{for all} \ t$$

$$n\left(\frac{l}{2}, y, z, t\right) = n\left(-\frac{l}{2}, y, z, t\right) = 0 \quad \text{for all} \ t$$

The solution to the problem defined in Equations (42-43) for the spatial

concentration of mobile molecules in the specimen is given by

$$n(x, y, z, t) = n_\infty$$

$$- \frac{64 n_\infty}{\pi^3} \sum_{p=0}^{\infty} \sum_{q=0}^{\infty} \sum_{r=0}^{\infty} \frac{(-1)^{p+q+r}}{(2p + 1)(2q + 1)(2r + 1)}$$ (44)

$$\times \cos \frac{(2p + 1)\pi z}{h} \cos \frac{(2q + 1)\pi y}{w} \cos \frac{(2r + 1)\pi x}{l}$$

$$\times e^{-\alpha_{p,q,r} t}$$

where

$$\alpha_{p,q,r} = \pi^2 \left( \frac{D_z (2p + 1)^2}{h^2} + \frac{D_y (2q + 1)^2}{w^2} + \frac{D_x (2r + 1)^2}{l^2} \right)$$ (45)

The percent mass gain function for the three-dimensional Fickian model was found by integrating the solution to Equation (44) and is given by [64]

$$M(t) = M_\infty - \frac{512 M_\infty}{\pi^6} \sum_{p=0}^{\infty} \sum_{q=0}^{\infty} \sum_{r=0}^{\infty} \frac{1}{(2p+1)^2(2q+1)^2(2r+1)^2}$$
$$\times e^{-\pi^2 t \left( \frac{D_z \, (2p+1)^2}{h^2} + \frac{D_y \, (2q+1)^2}{w^2} + \frac{D_x \, (2r+1)^2}{l^2} \right)}$$

(46)

where $M(t)$ is the moisture weight percent at time $t$ and $M_\infty$ is the equilibrium moisture weight percent of a sample of dimensions $h$ x $w$ x $l$.

# Chapter 3: Development and Validation of Three-Dimensional Anisotropic Hindered Diffusion Model

The existing predictive models of moisture absorption proposed in the literature have been shown to be valid for specific cases, but a model that accurately encompasses both Fickian and non-Fickian absorption behavior while accounting for diffusion anisotropy in three-dimensional space does not exist. Developing a three-dimensional, anisotropic model is particularly important for the case of laminated composites since the moisture diffusivity along the fiber direction is expected to be much higher than the bulk diffusivity in other directions (i.e., through-the-thickness of a laminate). This anisotropy in fiber-reinforced composites may lead to much higher rates of absorption across the side surfaces; even when the side surface areas are much smaller than the planar surfaces. Hence, one-dimensional diffusion models that are typically applied in the through-the-thickness direction of thin parts are not necessarily applicable or accurate [64].

It should be noted that there may be applications in which the most basic one-dimensional Fickian model of moisture diffusion is sufficiently accurate. However, at  long times and in the case of significant material anisotropy, deviation of actual moisture absorption behavior from the commonly-used one-dimensional Fickian diffusion model would most likely yield erroneous

predictions of moisture content and associated mechanical and electrical performance.  Within this framework, the objective of this chapter is to establish and provide support for a comprehensive model of three-dimensional anisotropic moisture absorption which accounts for both the effect of hindered diffusion due to physical or molecular interactions at the microscale and anisotropic diffusion in three dimensions. The proposed model is believed to be capable of accurately predicting absorption behavior for polymeric composites throughout the complete moisture intake cycle which exhibit varying degrees of both simple (Fickian) and anomalous absorption behavior.

### (3.1)    Development of a Three-Dimensional Anisotropic Hindered Diffusion Model

The existence of non-Fickian absorption behavior that has been accurately captured by the "Langmuir-type" model coupled with the necessity of considering anisotropic diffusion in all three spatial dimensions led to the development of a new, comprehensive model. This model captures both the effect of hindered diffusion by physical or chemical interactions as well as anisotropic diffusion in three dimensions. Hindered diffusion, in which Fickian diffusion is impeded or slowed, has been observed for a variety of solutes diffusing through polymers [65-68].  This phenomenon has been attributed to the effect of micropores [66], mechanical loading [67], and chemical interactions between the solute and the

polymer [68]. The Fickian model assumes diffusion proceeds unimpeded by any interaction between the diffusing molecules and the polymer. In other words, the diffusion is not hindered physically due to non-homogeneity of the structure, or chemically due to molecular binding between water and polymer chains.  In the absence of anisotropy and finite sample dimensions, the proposed model reduces to the mathematical equivalent of the "Langmuir-type" model proposed by Carter and Kibler [52]. However, in the current development of this model, we prefer not to make any assumptions about the cause of the hindered diffusion, whether it is due to molecular binding, resin microvoids, or some other micro or nanoscale phenomenon. It is assumed only that sources and sinks of diffusing molecules exist within the resin from a phenomenological framework which hinders the Fickian diffusion process. The nature and extent of the impediment can be defined by probabilities of mobile molecules becoming bound and bound molecules becoming mobile.  To the best of our knowledge, this type of absorption governing equation for a three-dimensional, anisotropic domain and its solution has not been previously published. In the proposed anisotropic model, the concentration at time *t* and position *x, y,* and *z* satisfies the coupled pair of equations

$$D_x \frac{\partial^2 n}{\partial x^2} + D_y \frac{\partial^2 n}{\partial y^2} + D_z \frac{\partial^2 n}{\partial z^2} = \frac{\partial n}{\partial t} + \frac{\partial N}{\partial t}$$

(47)

$$\frac{\partial N}{\partial t} = \gamma n - \beta N$$

Assuming an initially dry slab of dimensions $h$ by $w$ by $l$, the boundary and initial conditions are

$$n(x, y, z, 0) = 0, \quad N(x, y, z, 0) = 0 \quad \text{for} \quad |x| < \frac{l}{2}, \ |y| < \frac{w}{2}, \ |z| < \frac{h}{2} \qquad (48)$$

and

$$n\left(x, y, \frac{h}{2}, t\right) = n\left(x, y, -\frac{h}{2}, t\right) = n_\infty \quad \text{for all} \ t$$

$$n\left(x, \frac{w}{2}, z, t\right) = n\left(x, -\frac{w}{2}, z, t\right) = n_\infty \quad \text{for all} \ t \qquad (49)$$

$$n\left(\frac{l}{2}, y, z, t\right) = n\left(-\frac{l}{2}, y, z, t\right) = n_\infty \quad \text{for all} \ t$$

### (3.2)   Analytical Solution of the Hindered Diffusion Model in One Dimension

An exact solution for the one-dimensional version of the governing equation for the hindered diffusion model can be found by means of Laplace transforms, similar to the process briefly outlined by Carter and Kibler [52]. The solution process using this method will be expanded and described here. The one-dimensional governing equation again is given by

$$D_z \frac{\partial^2 n}{\partial z^2} = \frac{\partial n}{\partial t} + \frac{\partial N}{\partial t} \tag{50}$$

$$\frac{\partial N}{\partial t} = \gamma n - \beta \tag{51}$$

subject to the following boundary and initial conditions

$$n(z, 0) = 0, \ \ N(z, 0) = 0 \ \ \ n\left(\frac{h}{2}, t\right) = n\left(-\frac{h}{2}, t\right) = n_\infty \tag{52}$$

The Laplace transform of Equation (50) can be expressed as

$$\mathcal{L}\left(D_z \frac{\partial^2 n}{\partial z^2}\right) = \mathcal{L}\left(\frac{\partial n}{\partial t}\right) + \mathcal{L}\left(\frac{\partial N}{\partial t}\right) \tag{53}$$

where the Laplace transforms (using the complex transform variable $p$) of the

individual terms in Equations (50) and (51) can be expressed as

$$\mathcal{L}\left(\frac{\partial n}{\partial t}\right) = p\bar{N} - n(0) \tag{54}$$

$$\mathcal{L}\left(\frac{\partial N}{\partial t}\right) = \mathcal{L}(\gamma n) - \mathcal{L}(\beta N) \tag{55}$$

$$\mathcal{L}\left(D_z \frac{\partial^2 n}{\partial z^2}\right) = D_z \frac{d^2 \bar{n}}{dz^2} \tag{56}$$

Equation (54) can then be rewritten as

$$p\bar{N} - \bar{N}(0) = \gamma\bar{n} - \beta\bar{N} \tag{57}$$

37

Taking into account that $N(z, 0) = 0$ from Equation (52), and solving Equation

(57) for $\overline{N}$ yields

$$\overline{N} = \frac{\gamma\bar{n}}{p + \beta} \tag{58}$$

Substituting into Equation (54) then yields

$$\mathcal{L}\left(\frac{\partial n}{\partial t}\right) = \bar{n}\left(\frac{p\gamma}{p + \beta}\right) \tag{59}$$

Therefore,

$$D_z \frac{d^2\bar{n}}{dz^2} = p\bar{n} - n(0) + \bar{n}\left(\frac{p\gamma}{p + \beta}\right) \tag{60}$$

Rearranging yields

$$\frac{d^2\bar{n}}{dz^2} = \bar{n}\left\{\frac{1}{D_z}\left(p + \frac{p\gamma}{p + \beta}\right)\right\} \tag{61}$$

which can be expressed as

$$\frac{d^2\bar{n}}{dz^2} - u^2\bar{n} = 0 \tag{62}$$

where

$$u^2 = \frac{1}{D_z}\left(p + \frac{p\gamma}{p + \beta}\right) \tag{63}$$

The transformed boundary conditions are expressed as

$$\bar{n}\left(-\frac{h}{2},p\right) = \bar{n}\left(\frac{h}{2},p\right) = \frac{n_\infty}{p}$$

<div align="right">(64)</div>

$$\frac{d\bar{n}}{dz}\left(-\frac{h}{2},p\right) = \frac{d\bar{n}}{dz}\left(\frac{h}{2},p\right) = 0$$

The characteristic equation for the differential equation expressed in Equations (62-64) is therefore

$$r^2 - u^2 = 0 \qquad (65)$$

Therefore,

$$r = \pm u \qquad (66)$$

and $\bar{n}$ is then

$$\bar{n} = c_1 e^{-uz} + c_2 e^{uz} \qquad (67)$$

Differentiation yields

$$\frac{d\bar{n}}{dz} = -uc_1 e^{-uz} + uc_2 e^{uz} \qquad (68)$$

When $z = 0$

$$\frac{d\bar{n}}{dz} = -uc_1 + uc_2 = 0 \qquad (69)$$

Therefore,

$$c_1 = c_2 \tag{70}$$

When $z = \delta$

$$\frac{n_\infty}{p} = c_1 e^{-u\delta} + c_2 e^{u\delta} \tag{71}$$

which is equivalent to

$$\frac{n_\infty}{p} = c_1 e^{-u\delta} + c_1 e^{u\delta} = c_1\left(e^{-u\delta} + e^{u\delta}\right) \tag{72}$$

Solving for $c_1$ and equating to $c_2$ yields

$$c_1 = \frac{n_\infty}{p}\frac{1}{e^{-u\delta} + e^{u\delta}} = c_2 \tag{73}$$

substituting into Equation (67) yields

$$\bar{n} = \frac{n_\infty}{p}\frac{(e^{-uz} + e^{uz})}{(e^{-u\delta} + e^{u\delta})} \tag{74}$$

and since

$$\cosh(x) = \frac{1}{2}(e^x + e^{-x}) \tag{75}$$

The solution for $\bar{n}$ can be written as

$$\bar{n} = \frac{n_\infty}{p}\frac{\cosh uz}{\cosh u\left(\frac{h}{2}\right)} \tag{76}$$

The solution for $\bar{\bar{N}}$ can be expressed as

$$\bar{\bar{N}} = \bar{\bar{n}} \frac{\gamma}{p + \beta} \tag{77}$$

Therefore,

$$\bar{N}(z, p) = \frac{n_\infty \gamma}{p(p + \beta)} \frac{\cosh uz}{\cosh u \left(\frac{h}{2}\right)} \tag{78}$$

The inversion of which is formally expressed as

$$N(z, t) = \frac{1}{2\pi j} \int_{C-j\infty}^{C+j\infty} \bar{N}(z, p) e^{tp} \, dp \tag{79}$$

where $C$ is chosen so that all singular points of the Laplace solution lie to the left

of the line $\text{Re}\{p\} = C$ in the complex $p$-plane.

Evaluation of Equation (79) is achieved using contour integration in the plane

defined by the complex transform variable $p$, which can be represented in terms of

real variables $r$ and $q$ as

$$p = r + iq \tag{80}$$

Based on Equations (63) and (78), it can be shown that $\bar{N}(z,p)$ is analytic and

single valued everywhere in the complex plane except at the points

$$[r = -(\gamma + \beta), \qquad q = 0]$$

$$[r = -\beta, \qquad q = 0]$$

$$[r = 0, \qquad q = 0]$$

and at two infinite sets of points                                                    (81)

$$[r = p_l, \qquad q = 0]$$

$$\left[r = p_j, \qquad q = 0\right]$$

where

$$p_l = \frac{1}{2}\left[-(kl^2 + \gamma + \beta) \pm \sqrt{(kl^2 + \gamma + \beta)^2 - 4k\beta l^2}\right] \qquad (82)$$

and

$$p_j = \frac{1}{2}\left[-(kj^2 + \gamma + \beta) \pm \sqrt{(kj^2 + \gamma + \beta)^2 - 4k\beta j^2}\right] \qquad (83)$$

where $j$ and $l$ are positive odd integers, and

$$k = \frac{\pi^2 D}{(h)^2} \qquad (84)$$

Therefore, $N(z,t)$ is the sum of the residues of $\bar{N}(z,p)e^{tp}$ at the singularities defined above. The spatial distribution of bound molecules can then be written as

$$N(z,t) = \frac{\gamma}{\beta} n_\infty \left\{ 1 - \frac{4}{\pi} \sum_{p=1}^{\infty(odd)} \frac{(-1)^{\frac{p-1}{2}}}{p(r_P^+ - r_P^-)} \right.$$

$$\left. \times [r_P^+ \exp(-r_P^- t) - r_P^- \exp(-r_P^+ t)] \cos \frac{p\pi z}{h} \right\} \qquad (85)$$

where

$$r_P^\pm = \frac{1}{2} \left[ (kp^2 + \gamma + \beta) \pm \sqrt{(kp^2 + \gamma + \beta)^2 - 4k\beta p^2} \right] \qquad (86)$$

Then from Equation (51), the spatial distribution of mobile molecules can be written as

$$n(z,t) = n_\infty \left\{ 1 - \frac{4}{\pi} \sum_{p=1}^{\infty(odd)} \frac{(-1)^{\frac{p-1}{2}}}{p(r_P^+ - r_P^-)} \right.$$

$$\times [r_P^+ \exp(-r_P^- t) - r_P^- \exp(-r_P^+ t)] \cos \frac{p\pi z}{h} \right\}$$

$$+ n_\infty \frac{4}{\pi\beta} \sum_{p=1}^{\infty(odd)} \frac{(-1)^{\frac{p-1}{2}}}{p(r_P^+ - r_P^-)} (r_P^+ r_P^-)[\exp(-r_P^- t) \qquad (87)$$

$$- \exp(-r_P^+ t)] \cos \frac{p\pi z}{h}$$

43

Integration over the thickness of the sample yields the mass gain function, which

is identical to the "Langmuir-type" model proposed by Carter and Kibler [52].

$$M(t) = M_\infty \left\{ \begin{array}{l} 1 - \dfrac{8}{\pi^2} \displaystyle\sum_{p=1}^{\infty(odd)} \dfrac{[r_P^+ \exp(-r_P^- t) - r_P^- \exp(-r_P^+ t)]}{p^2(r_P^+ - r_P^-)} + \\[3ex] \dfrac{8}{\pi^2}\left(\dfrac{k\beta}{\gamma + \beta}\right) \displaystyle\sum_{P=1}^{\infty(odd)} \dfrac{[\exp(-r_P^- t) - \exp(-r_P^+ t)]}{r_P^+ - r_P^-} \end{array} \right\} \qquad (88)$$

A similar solution process was followed in an attempt to arrive at an analytical

solution to the three-dimensional, anisotropic version of the hindered diffusion

model. The governing equation, repeated from Equations (47-49), is again given

by

$$D_x \frac{\partial^2 n}{\partial x^2} + D_y \frac{\partial^2 n}{\partial y^2} + D_z \frac{\partial^2 n}{\partial z^2} = \frac{\partial n}{\partial t} + \frac{\partial N}{\partial t}$$

$$(89)$$

$$\frac{\partial N}{\partial t} = \gamma n - \beta N$$

Assuming an initially dry slab of dimensions $h$ by $w$ by $l$, the boundary and initial

conditions are

$$n(x, y, z, 0) = 0, \quad N(x, y, z, 0) = 0 \quad \text{for} \quad |x| < \frac{l}{2}, \ |y| < \frac{w}{2}, \ |z| < \frac{h}{2} \qquad (90)$$

and

$$n\left(x, y, \frac{h}{2}, t\right) = n\left(x, y, -\frac{h}{2}, t\right) = n_\infty \quad \text{for all } t$$

$$n\left(x, \frac{w}{2}, z, t\right) = n\left(x, -\frac{w}{2}, z, t\right) = n_\infty \quad \text{for all } t \tag{91}$$

$$n\left(\frac{l}{2}, y, z, t\right) = n\left(-\frac{l}{2}, y, z, t\right) = n_\infty \quad \text{for all } t$$

Taking the Laplace transform of the individual terms in Equation (89)

$$\mathcal{L}\left(D_x \frac{\partial^2 n}{\partial x^2}\right) + \mathcal{L}\left(D_y \frac{\partial^2 n}{\partial y^2}\right) + \mathcal{L}\left(D_z \frac{\partial^2 n}{\partial z^2}\right) = \mathcal{L}\left(\frac{\partial n}{\partial t}\right) + \mathcal{L}\left(\frac{\partial N}{\partial t}\right) \tag{92}$$

where

$$\mathcal{L}\left(D_x \frac{\partial^2 n}{\partial x^2}\right) = D_x \frac{d^2 \bar{n}}{dx^2} \tag{93}$$

$$\mathcal{L}\left(D_y \frac{\partial^2 n}{\partial y^2}\right) = D_y \frac{d^2 \bar{n}}{dy^2} \tag{94}$$

$$\mathcal{L}\left(D_z \frac{\partial^2 n}{\partial z^2}\right) = D_z \frac{d^2 \bar{n}}{dz^2} \tag{95}$$

$$\mathcal{L}\left(\frac{\partial n}{\partial t}\right) = p\bar{N} - n(0) \tag{96}$$

$$\mathcal{L}\left(\frac{\partial N}{\partial t}\right) = \mathcal{L}(\gamma n) - \mathcal{L}(\beta N) \tag{97}$$

Equation (97) can then be rewritten as

$$p\bar{N} - \bar{N}(0) = \gamma\bar{n} - \beta\bar{N} \tag{98}$$

Taking into account that $N(x, y, z, 0) = 0$ from Equation (90), and solving

Equation (97) for $\overline{N}$ yields

$$\overline{N} = \frac{\gamma\bar{n}}{p + \beta} \tag{99}$$

Substituting into Equation (96) then yields

$$\mathcal{L}\left(\frac{\partial n}{\partial t}\right) = \bar{n}\left(\frac{p\gamma}{p + \beta}\right) \tag{100}$$

Therefore,

$$D_x\frac{\partial^2\bar{n}}{\partial x^2} + D_y\frac{\partial^2\bar{n}}{\partial y^2} + D_z\frac{d^2\bar{n}}{dz^2} = p\bar{n} - n(0) + \bar{n}\left(\frac{p\gamma}{p + \beta}\right) \tag{101}$$

Rearranging yields

$$D_x\frac{\partial^2\bar{n}}{\partial x^2} + D_y\frac{\partial^2\bar{n}}{\partial y^2} + D_z\frac{d^2\bar{n}}{dz^2} = \bar{n}\left(p + \frac{p\gamma}{p + \beta}\right) \tag{102}$$

which can be written as

$$D_x\frac{\partial^2\bar{n}}{\partial x^2} + D_y\frac{\partial^2\bar{n}}{\partial y^2} + D_z\frac{d^2\bar{n}}{dz^2} - u^2\bar{n} = 0 \tag{103}$$

where

$$u^2 = \left(p + \frac{p\gamma}{p + \beta}\right) \tag{104}$$

The transformed boundary conditions are expressed as

$$\bar{n}\left(x, y, -\frac{h}{2}, p\right) = \bar{n}\left(x, y, \frac{h}{2}, p\right) = \frac{n_\infty}{p}$$

$$\bar{n}\left(x, -\frac{w}{2}, z, p\right) = \bar{n}\left(x, \frac{w}{2}, z, p\right) = \frac{n_\infty}{p} \tag{105}$$

$$\bar{n}\left(-\frac{l}{2}, y, z, p\right) = \bar{n}\left(\frac{l}{2}, y, z, p\right) = \frac{n_\infty}{p}$$

The solution for $\bar{n}$ is then

$$\bar{n}(x, y, z, p) = \frac{n_\infty}{p}\left(D_z \frac{\cosh uz}{\cosh\left(u\frac{h}{2}\right)} + D_y \frac{\cosh uy}{\cosh\left(u\frac{w}{2}\right)} + D_x \frac{\cosh ux}{\cosh\left(u\frac{l}{2}\right)}\right) \tag{106}$$

Therefore,

$$\bar{N}(x, y, z, p) = \frac{n_\infty}{p}\frac{\gamma}{(p + \beta)}\left(D_z \frac{\cosh uz}{\cosh\left(u\frac{h}{2}\right)} + D_y \frac{\cosh uy}{\cosh\left(u\frac{w}{2}\right)}\right.$$
$$\left. + D_x \frac{\cosh ux}{\cosh\left(u\frac{l}{2}\right)}\right) \tag{107}$$

The inversion of which can be formally expressed as

$$N(x, y, z, t) = \frac{1}{2\pi j} \int_{C-j\infty}^{C+j\infty} \frac{n_\infty}{p} \frac{\gamma}{(p + \beta)} \times \left( D_z \frac{\cosh uz}{\cosh\left(u\frac{h}{2}\right)} \right.$$

$$\left. + D_y \frac{\cosh uy}{\cosh\left(u\frac{w}{2}\right)} + D_x \frac{\cosh ux}{\cosh\left(u\frac{l}{2}\right)} \right) \times e^{tp} dp \tag{108}$$

where $C$ is chosen so that all singular points of the Laplace solution lie to the left of the line $\text{Re}\{p\} = C$ in the complex $p$-plane.

The solution of the three-dimensional version of the hindered diffusion model in the Laplace domain is somewhat intractable, and not readily invertible to the real domain by analytical methods. Numerical inversion methods are common in engineering applications due to the difficulty associated with the inversion of some solutions. Hassanzadeh and Pooladi-Darvish [69] present four methods that are typically used for numerical inversion. Each method is based on the evaluation of the integral given by

$$f(t) = \frac{1}{2\pi j} \int_{C-j\infty}^{C+j\infty} F(p)e^{pt} dp \tag{109}$$

where $C$ is chosen so that all singular points of $F(p)$ lie to the left of the line $\text{Re}\{p\} = C$ in the complex $p$-plane. One such method is given by

$$f(t) = \frac{\ln 2}{t} \sum_{i=1}^{n} V_i F\left(\frac{\ln 2}{t} i\right) \tag{110}$$

where $V_i$ is given by the following equation:

$$V_i = (-1)^{\left(\frac{n}{2}+1\right)} \sum_{k=\left(\frac{i+1}{2}\right)}^{\min\left(i,\frac{n}{2}\right)} \frac{k^{\left(\frac{n}{2}+1\right)}(2k)!}{\left(\frac{n}{2}-k\right)! \, k! \, (i-k)! \, (2k-1)!} \tag{111}$$

The parameter $n$ is intended to be optimized by trial and error. According to Hassanzadeh and Pooladi-Darvish, increasing $n$ increases the accuracy of the result up to a point, and then the accuracy declines due to increasing round-off errors. Additionally, this method is most accurate when the time function is the form of $e^{-t}$. While easy to implement, the method leads to inaccurate results for some functions [69].

### (3.3)  Numerical Solution Method for 3D HDM

The complexity of the three-dimensional anisotropic model proposed here lends itself to the implementation of a numerical solution method.  The application of numerical methods to diffusion processes is well-established [70-74] as a viable approach as long as accuracy and stability criteria are considered. An explicit finite difference scheme was implemented by Youssef et al. [70] in solving a coupled hygro-mechanical diffusion model taking into account internal

mechanical states of a composite. The selection of the forward-time, centered-space (FTCS) explicit finite difference technique for this case was based on the relative simplicity, accuracy, and ease of implementation of the method. The FTCS discretization of the hindered diffusion model given in Equations (89-91) can be expressed by,

$$n_{i,j,k}^t = n_{i,j,k}^{t-1}\left(1 - 2s_x - 2s_y - 2s_z - \gamma \Delta t\right) + s_x\left[n_{i-1,j,k}^{t-1} + n_{i+1,j,k}^{t-1}\right] +$$

$$s_y\left[n_{i,j-1,k}^{t-1} + n_{i,j+1,k}^{t-1}\right] + s_z\left[n_{i,j,k-1}^{t-1} + n_{i,j,k+1}^{t-1}\right] + N_{i,j,k}^{t-1}[1-\beta]$$

$$(112)$$

$$N_{i,j,k}^t = \gamma \Delta t n_{i,j,k}^{t-1} - N_{i,j,k}^{t-1}[1-\beta]$$

and

$$s_x = D_x \frac{\Delta t}{\Delta x^2} \qquad s_y = D_y \frac{\Delta t}{\Delta y^2} \qquad s_z = D_z \frac{\Delta t}{\Delta z^2} \qquad (113)$$

where $i,j,k$ represent the spatial nodes, $\Delta t$ is the size of the time step, and $\Delta x, \Delta y,$ and $\Delta z$ represent the size of the spatial steps.

For this three-dimensional anisotropic model, using implicit finite difference methods such as the backward-time centered-space (BTCS) method and the Crank-Nicholson method would not be computationally feasible due to the

excessive CPU times required. In a study of numerical solution methods for the three-dimensional advection-diffusion equation, Dehgan [71] found that the solution of the system of linear algebraic equations inherent in the implicit finite difference methods required approximately 21 times more CPU time than the explicit methods. Furthermore, CPU time for fully implicit techniques cannot be reduced through parallel processing. CPU time for explicit methods can be drastically reduced by implementing the scheme in parallel on multiple processors. Although relatively quick to implement and requiring less CPU time than implicit solution methods, the FTCS method is susceptible to numerical instability. The restriction of the size of the time step due to stability requirements is a common feature of explicit finite difference methods [71], and careful analysis is required to select a sufficiently small time step to ensure accuracy and stability of the solution. In the FTCS scheme of the proposed model, satisfaction of the following equation is required for stability.

$$s_x + s_y + s_z \leq \frac{1}{2} \tag{114}$$

In addition, the accuracy of the solution depends on the spatial grid-spacing. A sufficient number of spatial nodes are required for the numerical solution to converge to the actual solution. The numerical error associated with the FTCS method is proportional to the square of the space step [71]:

$$O\{(\Delta x)^2, (\Delta y)^2, (\Delta z)^2\} \qquad\qquad (115)$$

In order to ensure the accuracy of the numerical solution, $\Delta x$, $\Delta y$, and $\Delta z$ are decreased until changes in the moisture content at a specific exposure time are limited to less than 1 x $10^{-4}$ % with further decreases in the size of the spatial steps. In some cases, 5 x $10^7$ discrete spatial nodes (the product of spatial grid points in the $x$, $y$, and $z$ dimensions) were required to achieve this level of convergence. The FTCS scheme was implemented in Matlab$^®$ to solve Equation (89-91) for the concentration of bound and mobile molecules. Numerical integration of the solution over the volume of the sample produced the total weight gain due to absorbed moisture. Simpson's rule was used to perform the numerical integration in Matlab$^{®.}$ The discrete points used as the spatial nodes in the FTCS scheme were also used in the implementation of the numerical integration. Thus, the accuracy of the numerical integration of the concentration is dependent on the size of the spatial steps as well. As the number of spatial nodes increases, the error associated with the numerical integration decreases more quickly than the error from the finite difference scheme. Therefore, convergence of the solution for mobile and bound molecule concentration indicates convergence of the numerical integration scheme as well.

## (3.4)    Validation of Three-Dimensional Anisotropic HDM

The specific cases of the model proposed here were compared to existing analytical solutions of the three-dimensional anisotropic Fickian model and the one-dimensional "Langmuir-type" diffusion model in order to verify the accuracy of the numerical solution method.  As the probability of a mobile molecule becoming bound approaches zero (i.e., $\gamma \rightarrow 0$), the moisture absorption behavior of the proposed model should reduce to three-dimensional anisotropic Fickian behavior.  The zero probability of a mobile molecule becoming bound precludes the existence of any molecules in the bound phase, thus the diffusion of mobile molecules is unhindered and Fickian in nature.  This reduction to Fickian diffusion and the consequent ability to capture Fickian behavior is one of the best arguments for the use of this type of hindered diffusion model for polymer absorption characterization. This type of model can accurately predict the moisture weight gain of polymers exhibiting either Fickian or non-Fickian behavior. Binding and unbinding probabilities determined from experimental moisture absorption data of a polymer that conforms to Fickian diffusion theory should yield a binding probability very near zero. Therefore, the model is applicable to a range of diffusion behavior from purely Fickian to highly anomalous.

Diffusivity and equilibrium moisture content values used by Pierron et al. [63] in a procedure for identification of 3D moisture diffusion parameters were used to validate the numerical solution of the model proposed here by reducing it to the three-dimensional Fickian model. These parameters (i.e., $D_x$, $D_y = 1.8$ x $10^{-3}$ mm$^2$hr$^{-1}$, $D_z = 7.2$ x $10^{-4}$mm$^2$hr$^{-1}$, $M_\infty = 0.8\%$, $w$, $l = 20$ mm, $h = 1$ mm) are typical values for a balanced woven glass/epoxy composite [63]. The probability of a bound molecule becoming unbound, $\beta$, was held at $1.5$ x $10^{-3}$ hr$^{-1}$, a typical value from the literature. As shown in Figure 4, the moisture absorption behavior of the proposed model approaches the analytical solution of the three-dimensional Fickian model given in Equation (46) as the probability of binding approaches zero. While a zero probability of binding guarantees reduction to Fickian diffusion behavior, a similar effect can be achieved by greatly increasing the probability of unbinding with respect to binding. As $\beta$ becomes much larger than $\gamma$, the number of mobile molecules that become bound and remain bound long enough to hinder the diffusion process becomes very small. Therefore, the absorption behavior appears Fickian in nature.

In order to further verify the accuracy of the numerical solution, theoretical sample dimensions were increased in the two planar dimensions ($x$ and $y$) while the thickness dimension ($z$) was held constant. As the sample size becomes semi-infinite in the two planar dimensions, the diffusion process becomes essentially one-dimensional. Moisture ingress through the edges of the theoretical sample

becomes negligible compared to ingress in the through-thickness direction as the edge surface area becomes very small compared to overall surface area. Consequently, the model reduces to the one-dimensional model proposed by Carter and Kibler [52] as the sample becomes a semi-infinite plate.
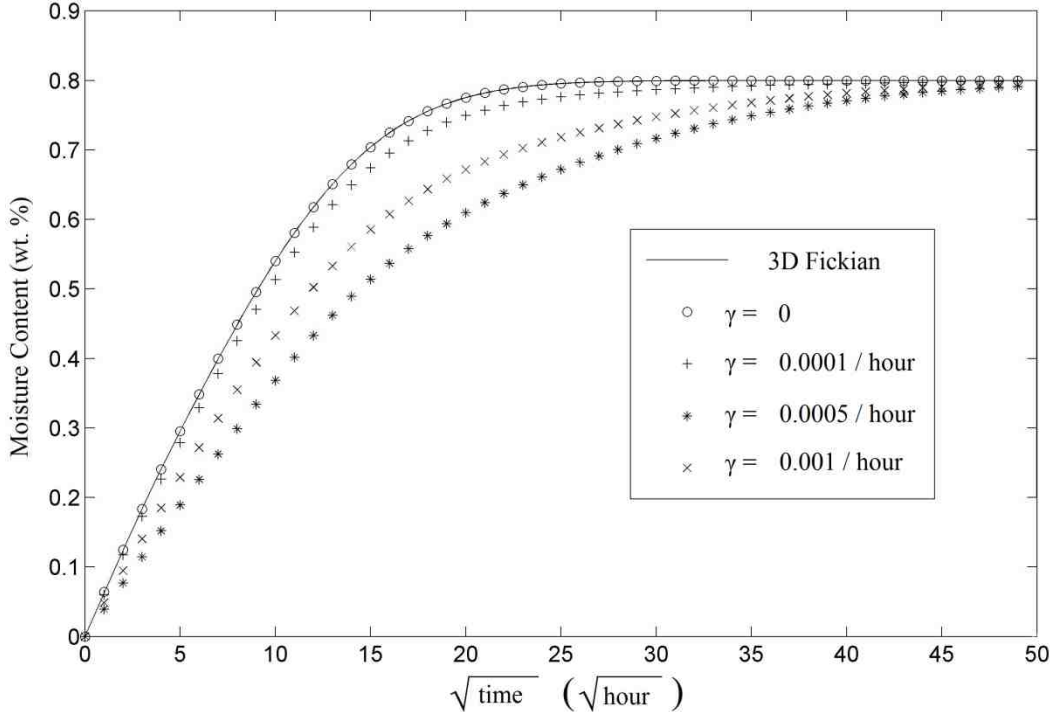


**Figure 4 - Reduction of the proposed three-dimensional anisotropic hindered diffusion model to the three-dimensional Fickian model with decreasing values of $\gamma$. Diffusion parameters: $D_x$, $D_y$ = 1.8 x 10$^{-3}$ mm$^2$hr$^{-1}$, $D_z$ = 7.2 x 10$^{-4}$mm$^2$hr$^{-1}$, $M_\infty$ = 0.8%, $\beta$ = 1.5 x 10$^{-3}$ hr$^{-1}$ $w$, $l$= 20 mm, $h$ = 1 mm [63].**

Figure 5 illustrates the moisture absorption behavior predicted by the numerical solution of the proposed model for square samples of increasing ratio of side

length to thickness. Sample $x$ and $y$ dimensions of 2, 10, 20, 40, 100, 200, and 1000 mm were used while thickness was maintained at 2 mm.  Diffusivity values in the $x$ and $y$ directions of 9.29 x $10^{-2}$ mm$^2$/hour, in the $z$ direction of 9.29 x $10^{-4}$ mm$^2$/hour, equilibrium moisture content of 5.2%, binding probability of 1 x $10^{-4}$ hr$^{-1}$, and unbinding probability of 2 x $10^{-4}$ hr$^{-1}$ were used to produce the results. Diffusivity in the $x$ and $y$ directions was set at 100 times the through-thickness diffusivity in order to exaggerate the effect of absorption through the edges. This serves to more clearly demonstrate the effect of edge diffusion and to ensure that the numerical solution approaches the one-dimensional "Langmuir-type" analytical solution in what might be considered a worst-case scenario. The equilibrium moisture content of 5.2% is an experimentally determined value for a fully-immersed bismaleimide resin at 70°C from Ref. [75].  Diffusivities, $\gamma$ and $\beta$ are typical values from the literature.  As expected, predicted moisture absorption behavior approaches the analytical solution of the one-dimensional "Langmuir-type" model of diffusion given in Equation (32) as the length and width of the 2 mm thick sample increases.
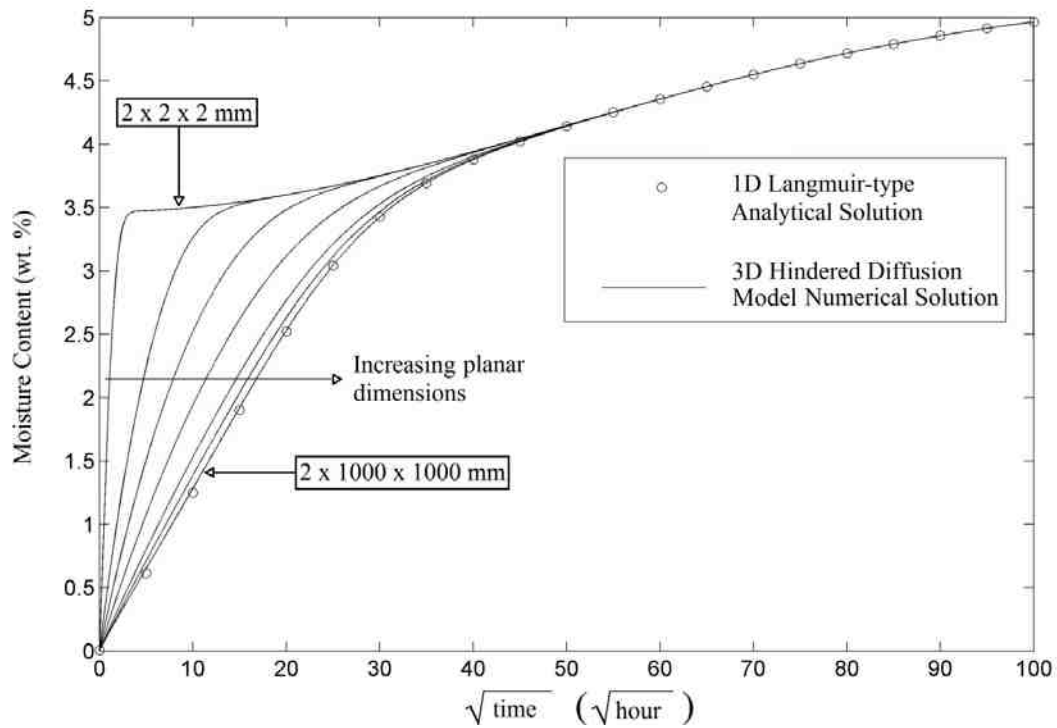
**Figure 5 - Reduction of the proposed three-dimensional anisotropic hindered diffusion model to the one-dimensional "Langmuir-type" model of diffusion with increasing planar sample dimensions. Model parameters: $D_x$, $D_y$ = 9.29 x 10$^{-2}$ mm$^2$/hour , $D_z$ = 9.29 x 10$^{-4}$ mm$^2$/hour, $\gamma$ = 1 x 10$^{-4}$ hr$^{-1}$, $\beta$ = 2 x 10$^{-4}$ hr$^{-1}$, M$_\infty$= 5.2% .**

### (3.5)  Effects of Anisotropy and Binding / Unbinding Probability on Model Behavior

The moisture absorption behavior of three-dimensional anisotropic polymer composites predicted by the proposed hindered diffusion model can be roughly

divided into two segments. The initial, relatively fast absorption process typically exhibits linear behavior in $\sqrt{t}$ as $t \to 0$ and depends heavily on the diffusion coefficients. In the three-dimensional Fickian model, the slope of this segment of the uptake curve is entirely dependent on the values of the diffusion coefficients. In the model proposed here, variations in the probabilities of binding and unbinding of diffusing molecules produce changes in the slope of the initial moisture uptake, though it is dominated in most cases by diffusion of mobile molecules. The effect of these variations in binding and unbinding probabilities on the initial slope of the moisture uptake curve is an important consideration when comparing the proposed model to the classical Fickian model. In order to illustrate these variations, examples of the short-time diffusion behavior predicted by the proposed hindered diffusion model for an anisotropic sample with varying binding probability are shown in Figure 6. The through-thickness diffusivity of 9.29 x $10^{-3}$ mm$^2$/hr and equilibrium moisture content of 5.2% from Ref. [75] are employed again in this example. Diffusion coefficients in the $x$ and $y$ directions are 4.645 x $10^{-2}$ mm$^2$/hr and 9.29 x $10^{-2}$ mm$^2$/hr (5 and 10 times the through-thickness diffusivity). The probability that a bound molecule will become free to diffuse is held constant at 5 x $10^{-3}$ hr$^{-1}$, while binding probability ranges from 0 to 0.01 hr$^{-1}$.
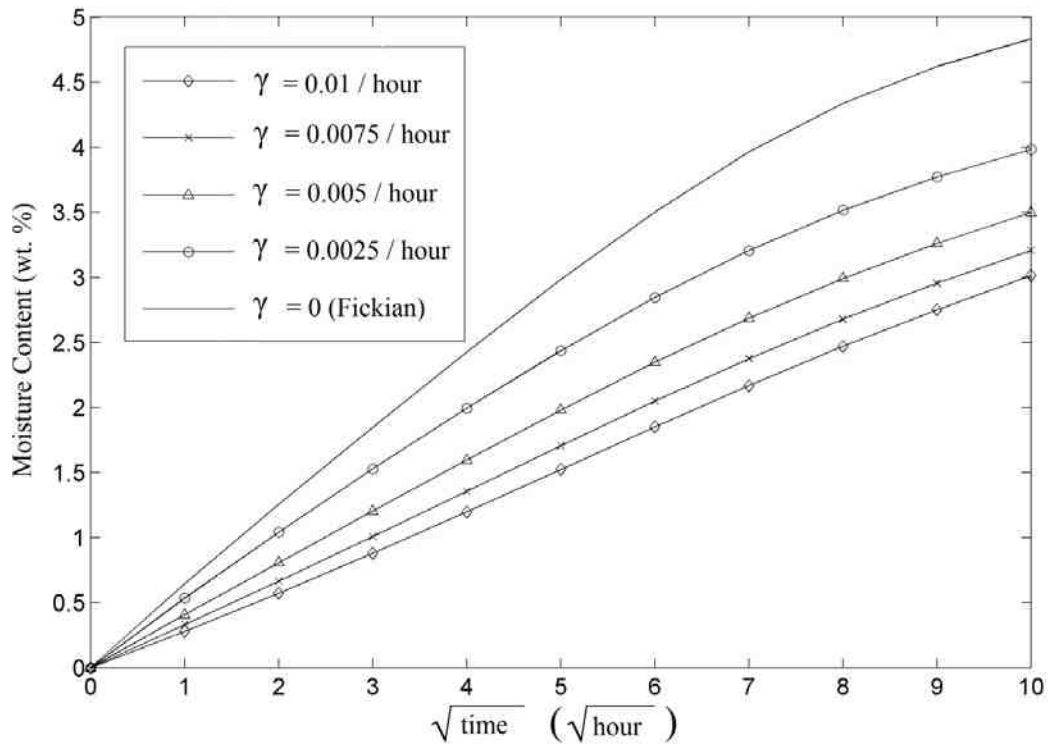
**Figure 6 - Example of the change in the slope of the initial portion of the moisture absorption curve with changing binding probability. Model parameters: $D_x = 4.645 \times 10^{-2}$ mm$^2$/hour, $D_y = 9.29 \times 10^{-2}$ mm$^2$/hour, $D_z = 9.29 \times 10^{-3}$ mm$^2$/hour, $M_\infty = 5.2\%$ [75], $\beta = 5 \times 10^{-3}$ hr$^{-1}$.**

Figure 6 depicts that as $\gamma$ increases, the moisture uptake process is hindered due to the higher probability that a mobile molecule will become bound rather than being free to diffuse. A relatively wide range of binding probabilities have been reported for the one-dimensional "Langmuir-type" diffusion model applied to experimental data for various polymer/fiber combinations and exposure

conditions. For example, Kumosa et al. [26] report a probability of binding of 1.1 x $10^{-5}$ $hr^{-1}$ for a glass/epoxy laminate exposed to 80% relative humidity at 50°C, while Popineau et al. [46] report a probability of binding of 3.6 x $10^{-3}$ $hr^{-1}$, over 300 times higher, for a neat epoxy fully immersed in distilled water at 90°C.

After the initial, Fickian-dominated moisture uptake, the second segment of the hindered moisture absorption curve begins at a point where Fickian theory predicts an equilibrium moisture content plateau. This second segment is much slower, and the rate at which moisture content approaches equilibrium is dependent on the probabilities of binding and unbinding of diffusing molecules. Variations in the binding and unbinding probabilities produce a wide range of curve shapes in this second portion of the curve, which further exemplifies the comprehensive nature of the model and its ability to capture many types of diffusion behavior.

Examples of the long-time moisture absorption behavior predicted by the proposed model for varying values of $\gamma$ and $\beta$ are shown in Figure 7 in an effort to illustrate the wide range of diffusion behavior the model is capable of capturing. Diffusivity values and equilibrium moisture content are again based on experimental data from Ref. [75]. Isotropic three-dimensional diffusion is assumed, with diffusivity in all three principal directions set at 9.29 x$10^{-3}$ $mm^2$/hr. The figure presents moisture absorption behavior for nine different combinations

of $\gamma$ and $\beta$ grouped into three ratios of binding ($\gamma$) to unbinding ($\beta$) probability. The probabilities of binding within each of these three groups are 5 x $10^{-3}$ $hr^{-1}$, 5 x $10^{-4}$ $hr^{-1}$, and 5 x $10^{-5}$ $hr^{-1}$. The probability of unbinding is adjusted to match the three $\gamma/\beta$ ratios. In general, Figure 7 shows a delay in moisture uptake as the $\gamma$ to $\beta$ ratio is increased. In addition, Figure 7 illustrates that increasing the magnitude of $\beta$ while maintaining the same $\gamma$ to $\beta$ ratio can significantly accelerate the diffusion process.  The point in the diffusion process at which the moisture uptake curve deviates from the initial linear portion changes according to the ratio of binding probability to unbinding probability. Additionally, the shape of the second portion of the curve varies widely within these ratios for changing values of $\gamma$ and $\beta$. The point in the moisture absorption process at which the relatively fast initial diffusion begins to slow and the second, slower diffusion process becomes dominant is sometimes referred to as Fickian pseudo-equilibrium. The initial slope of the second portion of the moisture absorption curve can be very low (see, for example, the case of $\gamma/\beta = 0.5$ and $\beta = 5$ x $10^{-5}$ $hr^{-1}$ in Figure 7), and the potential exists for composites with specific values of $\gamma$ and $\beta$ to prematurely exhibit moisture uptake behavior similar to a composite that has reached Fickian equilibrium.  As demonstrated in Figure 7, higher ratios of $\gamma$ to $\beta$ produce curves with a greater difference between Fickian pseudo-equilibrium and actual equilibrium, which could lead to significant errors in experimental determination of maximum moisture content.
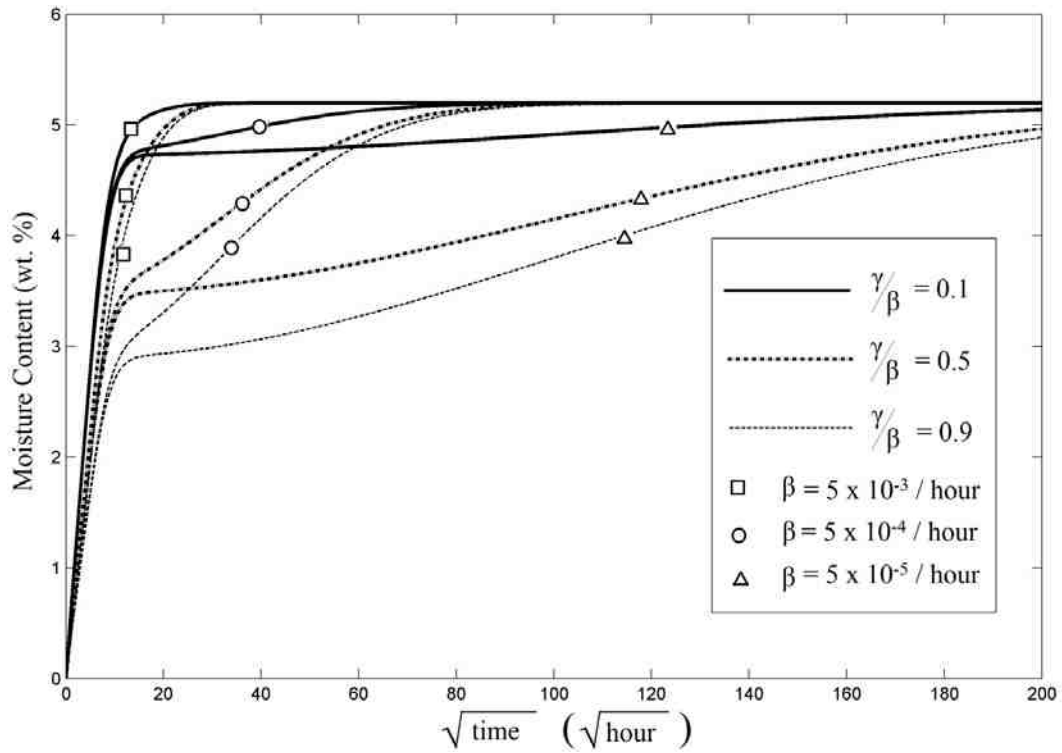
**Figure 7 - Examples of changes in long-time diffusion behavior for varying ratios of γ to β for samples of equivalent size (25 x 25 x 2 mm) and diffusion coefficients. $D_x, D_y, D_z = 9.29 \times 10^{-3}$ mm²/hour, $M_\infty = 5.2\%$ [75].**


### (3.6)  Model Application to Published Experimental Data


The proposed hindered diffusion model is capable of capturing a wide range of diffusion behavior as shown in Figures 6 and 7. In order to further demonstrate the utility of the model, it is applied to experimental data reproduced from three different studies previously published on moisture absorption in polymers and their composites.

*(3.6.1) Application of the Hindered Diffusion Model to Capture*

*Anomalous Thickness Effects in Epoxy Specimens*

In the first study, the moisture absorption results published by Wong and

Broutman [48] are used to demonstrate the utility of the hindered diffusion model.

Wong and Broutman observed an anomaly in the moisture absorption behavior of

an isotropic epoxy resin due to the thickness of the specimen. Multiple samples

of varying thickness dimensions were immersed in deionized water at 90°C and

the gravimetric data over time recorded. The moisture absorption curves were

scaled according to thickness of the sample, with the expectation that moisture

uptake curves would therefore be identical regardless of sample thickness.

However, gravimetric experiments indicated that there was a critical thickness

below which the diffusion process was no longer as predicted by Fickian

diffusion. Wong and Broutman suggested that this anomalous behavior was due

to the long relaxation times associated with large scale cooperative motion of

polymer chain segments resulting from the introduction of a penetrant. The

authors further proposed that at a given fractional distance through a polymer

specimen, changes in concentration would occur more slowly than at an

equivalent fractional distance in thinner samples. Thus, thicker specimens would

allow more time for the molecular rearrangement of the polymer network due to

the penetrant. Accordingly, changes in the polymer network of thicker specimens

would be complete prior to the sample reaching equilibrium moisture content, and the moisture absorption behavior appears Fickian in nature.

Experimental data reported by Wong and Broutman was reconstructed in an effort to assess the ability of the hindered diffusion model to capture the reported thickness anomaly. Eleven data points from each specimen thickness were used in a least-squares curve fit to the hindered diffusion model. The one-dimensional version of the model was selected for the curve fit due to sample geometry and isotropy of the material. The diffusion parameters which yielded the best fit to the experimental data are shown in Table 1. The best fit was produced for a binding probability of $1.64 \times 10^{-3}$ hr$^{-1}$ and an unbinding probability of $2.18 \times 10^{-2}$ hr$^{-1}$.

**Table 1 - Parameters of one-dimensional isotropic version of the hindered diffusion model recovered from least-squares curve fit to reconstructed experimental moisture absorption data for an isotropic epoxy resin from Ref. [48].**

| | |
|---|---|
| $D$ | $2.11 \times 10^{-5}$ in$^2$/hr |
| $\gamma$ | $1.64 \times 10^{-3}$ hr$^{-1}$ |
| $\beta$ | $2.18 \times 10^{-2}$ hr$^{-1}$ |
| $M_\infty$ (%) | 3.43 |

Figure 8 depicts the results of the hindered diffusion model together with the gravimetric data reported by Wong and Broutman. The thickness-scaled absorption curves very closely match the non-Fickian behavior of the samples of three different thicknesses. The root mean squared (RMS) error for each sample thickness was calculated as a measure of the effectiveness of the model, and to highlight the approximately equivalent agreement with all three data sets.
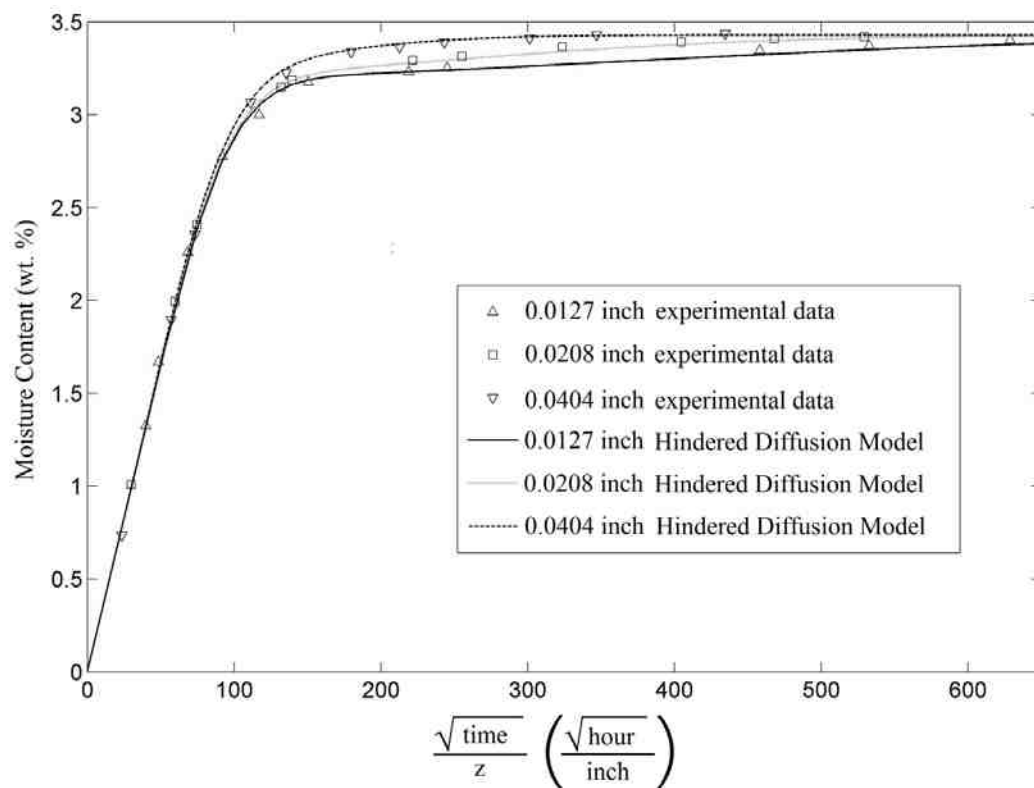


**Figure 8 - Application of least-squares curve fit of one-dimensional isotropic version of the proposed hindered diffusion model to reconstructed experimental moisture absorption data for an isotropic epoxy resin of varying thickness as reported by Wong and Broutman [48].**

The RMS error values, reported in Table 2, were relatively small and similar.

Thus, the appearance of Fickian behavior in the thickness-scaled absorption

curves as the specimen thickness increases, which the authors attributed to

molecular rearrangement of the polymer network, is an inherent characteristic of

this type of hindered diffusion model.  That is, for sufficiently small specimen

thickness, the thickness-scaled moisture absorption curves are non-Fickian in

appearance.  As the thickness increases, the thickness-scaled absorption curves

predicted by the hindered diffusion model approach what would be considered

Fickian moisture absorption behavior even as $\gamma$ and $\beta$ remain the same.

**Table 2 - Error associated with least-squares curve fit to reconstructed experimental moisture absorption data for an isotropic epoxy resin from Ref. [48].**

| Thickness (in.) | Data Points | Root Mean Squared Error (%) |
|---|---|---|
| 0.0127 | 11 | 0.0329 |
| 0.0208 | 11 | 0.0159 |
| 0.0404 | 11 | 0.0225 |

The explanation for this behavior when assuming hindered diffusion due to binding/unbinding of diffusing molecules, while physically different than that proposed by Wong and Broutman, yields similar moisture absorption curves. As described previously, when the presence of bound molecules is precluded by a zero probability of becoming bound, the absorption process is unhindered and Fickian in nature. The non-Fickian contribution associated with the binding and unbinding of diffusing molecules results in a gradual increase in total absorbed molecules after the relatively fast initial moisture uptake. The contribution of the unbinding of bound molecules, which are then free to diffuse, continues until the relationship in Equation (26) is satisfied. That is, equilibrium moisture concentration is not reached until the number of bound molecules becoming unbound in unit time is equal to the number of unbound molecules becoming bound in the same time. This process is generally longer-term than the diffusion of mobile molecules, much like the suggested rearrangement of the polymer network due to the presence of diffusing molecules proposed by Wong and Broutman. The behavior exhibited will be similar in that the diffusion process is essentially complete prior to the achievement of equilibrium between bound molecules becoming unbound and unbound molecules becoming bound, just as the polymer network rearrangement is ongoing after diffusion is complete for thin samples in the explanation proposed by Wong and Broutman. The ability of this type of hindered diffusion model to accurately capture the experimental gravimetric absorption data and also predict the "thickness anomaly" that Wong

and Broutman attributed to polymer network rearrangement is a strong indication that the diffusion behavior of polymers is driven by a process such as that described mathematically by the proposed hindered diffusion model.

*(3.6.2) Application of the 3D Hindered Diffusion Model to*

*Orthotropic Absorption in a Glass-Reinforced Polymer*

In the second study considered, Kumosa et al. [26] investigated the moisture absorption characteristics of unidirectional glass reinforced polymer composites exposed to a moist environment of 80% relative humidity at 50°C. Although glass-reinforced polymer composites are used as an alternative to porcelain as high voltage insulators, moisture ingress in these composites can lead to electrical failures [26]. In Ref. [26], particular attention was paid to the effects of specimen geometry and material properties as each relates to moisture absorption behavior. The composite specimens used in the experiment were cut from pultruded plates, and diffusion occurred parallel to the unidirectional fibers along two edges and perpendicular to the fibers along the other four surfaces (i.e., two edges and top and bottom faces). Gravimetric data was recorded and presented for various sample geometries, allowing the use of this data for the determination of diffusion coefficients in multiple directions. Orthotropic Fickian diffusion in three dimensions was considered and was modeled numerically using finite element techniques. In addition, the one-dimensional "Langmuir-type" model was applied

to the gravimetric data for each geometry. The authors did acknowledge the effect of three-dimensional diffusion and anisotropy based on the dimensions of the sample, which fail to meet the nominal-length-of-one-side to thickness ratio of 100:1 called for by ASTM D5229 [76].  However, the lack of a three-dimensional anisotropic hindered diffusion model necessitated the use of the one-dimensional "Langmuir-type" model for the curve-fitting process by Kumosa et al.   The authors suggested a correlation between probabilities of molecular binding and unbinding and the geometry of the sample.  Kumosa et al. proposed that values of $\gamma$ and $\beta$ should be proportionally smaller as specimen thickness increases, and fitting of the experimental data to the one-dimensional "Langmuir-type" model supports this claim based on the quality of the fit shown in Ref. [26].

Instead of assuming geometry or anisotropy dependent values for $\gamma$ and $\beta$ as proposed by the authors of Ref. [26], we postulated that what was perceived as a proportional decrease in $\gamma$ and $\beta$ may be accounted for by the increasing contributions of three-dimensional anisotropic diffusion as specimen thickness increases.  To corroborate this hypothesis, all three moisture uptake curves were fit simultaneously to determine diffusion coefficients, $\gamma$, $\beta$, and equilibrium moisture content regardless of sample thickness. For our purposes, gravimetric data was reconstructed for an E-glass/epoxy composite with thicknesses of 1, 2, and 4 mm and lateral dimensions of 50 mm by 50 mm as given in Ref. [26]. Based on Figure 3b of Ref. [26], moisture content at 11 points was estimated for

each specimen geometry. These 33 gravimetric data points were used in a least-squares curve fit of the proposed hindered diffusion model. In an effort to enforce the orthotropy of the sample and reduce the computational time required, diffusion coefficients in the $y$ and $z$ directions were assumed to be equivalent. Equilibrium moisture content for these specific samples was not reached during the experimental time frame; therefore equilibrium moisture content was treated as a variable during the least-squares fit. The moisture uptake curve fit results are shown in Figure 9, and can be seen to match the data with reasonable accuracy. The recovered diffusion coefficients, binding and unbinding probabilities, and equilibrium moisture content are shown in Table 3. A maximum moisture content of 0.375% was recovered, which is slightly higher than the value of 0.35% assumed by Kumosa et al. based on prior experiments carried out on different samples of the same material.

The use of different pairs of $\gamma$ and $\beta$ values based on sample thickness, as in Ref. [26], would likely yield moisture uptake curves that more closely fit the experimental data. However, if one accepts that the moisture absorption behavior should be entirely governed by the intrinsic material properties and thus should be geometrically scalable, then one can argue that the $\gamma$, $\beta$ and anisotropic diffusivity constants should not be influenced by the sample size. Although the material properties governing the hindered or unhindered diffusion are expected to be independent of the sample size, the possibility that values of $\gamma$ and $\beta$ are

influenced by the anisotropy of the samples should not be discounted, particularly

in the case of fiber-reinforced polymers. It is almost certain that the error

associated with the fitting process would decrease further if the probabilities of

binding and unbinding were not assumed to be the same in all diffusion

directions. A notable but unmentioned result from the work of Kumosa et al. in

the determination of thickness-dependent probabilities of binding and unbinding

is that, in each thickness case, the ratio of $\gamma$ to $\beta$ remains at approximately 0.6

though the values of each parameter change.  Further study is needed to determine

if anisotropy needs to be extended to the binding and unbinding probabilities of

the absorbed molecules.

**Table 3 - Parameters of three-dimensional anisotropic hindered diffusion model recovered from least-squares curve fit to reconstructed experimental moisture absorption data for three sample sizes of glass-reinforced polymer composite plate from Ref. [26].**

| | |
|---|---|
| $D_x$ | 11.2 x $10^{-7}$ mm$^2$/s |
| $D_y$ | 4.1 x $10^{-7}$ mm$^2$/s |
| $D_z$ | 4.1 x $10^{-7}$ mm$^2$/s |
| $\gamma$ | 1.04 x $10^{-8}$ s$^{-1}$ |
| $\beta$ | 1.36 x $10^{-8}$ s$^{-1}$ |
| $M_\infty$ (%) | 0.375 |
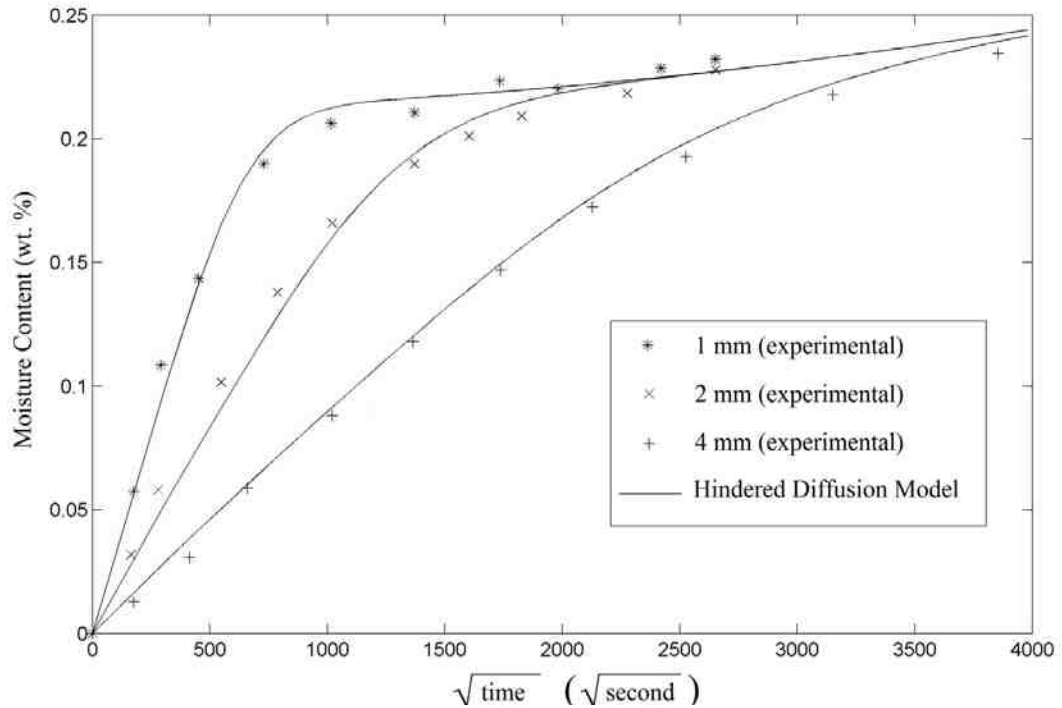
**Figure 9 - Application of three-dimensional anisotropic hindered diffusion model to reconstructed experimental moisture absorption data for three sample sizes of glass-reinforced polymer composite plate as reported by Kumosa et al. [26].**

*(3.6.3)    Comparison of Hindered Diffusion Model to a Two-Stage Model for Long-term Moisture Absorption in a BMI/Carbon Fiber Composite*

In the third study considered, Bao and Yee [37, 38] investigated moisture absorption and hygrothermal aging in bismaleimide-carbon fiber composites. Experimental gravimetric data indicated that the diffusion behavior was

72

anomalous, but could be reproduced well with the implementation of a two-stage model in which the first and second stages were diffusion and relaxation controlled, respectively. The two-stage model was applied to experimental data from a fully-immersed 3-ply carbon fiber reinforced bismaleimide at 70ºC gathered prior to one year of moisture exposure. The two-stage model was able to capture the weight gain behavior with reasonable accuracy. However, three measurements were taken after one year of exposure which showed significant deviation from the two-stage model. Furthermore, these three data points indicated that the second stage weight gain behavior was distinctly non-linear. The second, low-slope stage in the two-stage diffusion process corresponds to the second stage of the model proposed in this work. Bao and Yee postulate that the slope of the second-stage absorption is related to the rate of relaxation of the polymer, and thus exhibits significant temperature dependence. Similar temperature dependence has been observed in the application of the "Langmuir-type model" of diffusion, in which the probabilities of binding and unbinding of diffusing molecules vary with temperature [46].

The experimental data reported by Bao and Yee was only presented for one specimen geometry, thereby severely restricting the possibility of recovering anisotropic diffusivities by the use of the fully anisotropic hindered diffusion model. Therefore, the one dimensional isotropic version was implemented in a least-squares curve fit to data reconstructed from Figure 3 of Ref. [38]. The

objective is to demonstrate the ability of the hindered diffusion model to capture deviations in the long term weight gain behavior that are not predicted by the two-stage model or any model with a strictly linear second stage beyond the Fickian plateau.

The curve fit of the one-dimensional version of the hindered diffusion model to the experimental data is shown in Figure 10. Unlike the two-stage model, the hindered diffusion model was able to capture the weight gain behavior prior to one year in addition to the three data points that deviate from the linear second-stage with excellent agreement.  The reproduced data points and the two-stage curve fit which excluded the last three data points beyond one year of exposure are also shown in Figure 10.

Table 4 lists the parameters found by fitting the reproduced data points to the hindered diffusion model using the least-squares method.  A notable result of the recovery of these parameters is that the value of $\beta$ is slightly lower than that of $\gamma$, which is not the case for the other two hindered model applications presented earlier in this section. The physical meaning of this result is that at the equilibrium condition given in Equation (26) more absorbed molecules exist in the bound phase than in the mobile phase.
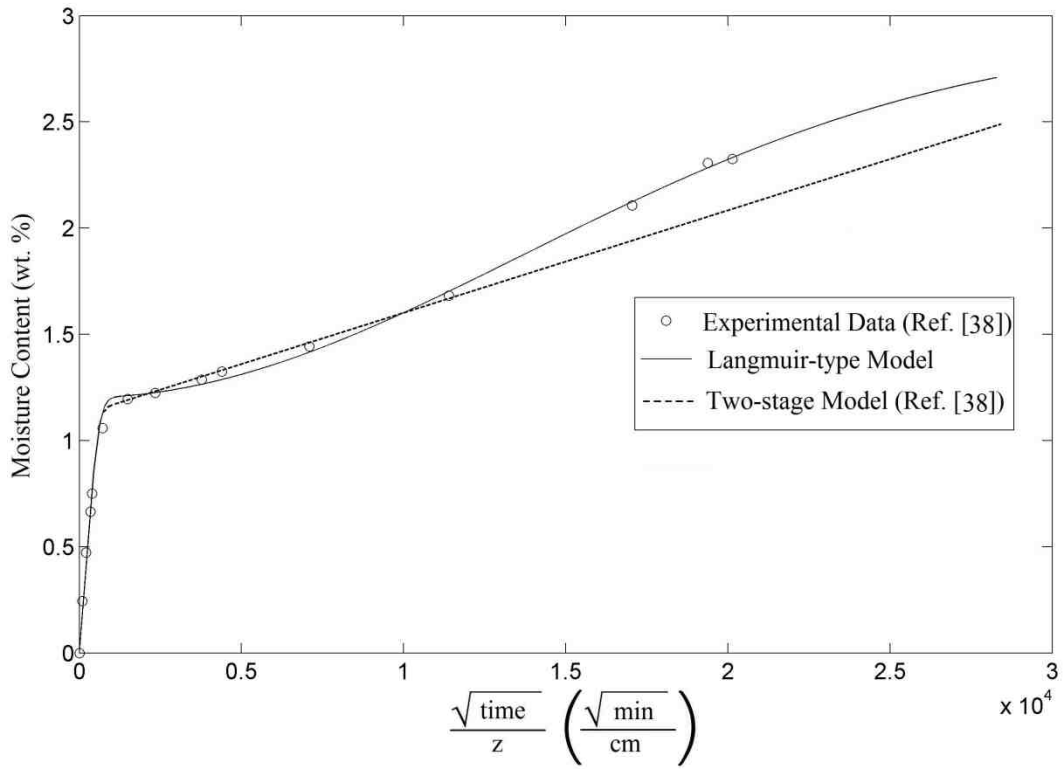
**Figure 10 - Verification of the long-term anomalous diffusion modeling capability of the proposed model through application to reconstructed experimental moisture absorption data for a woven 3-ply bismaleimide/carbon fiber composite and comparison to a two-stage model of diffusion as used in Ref. [38].**

**Table 4 - Parameters one-dimensional isotropic version of the hindered diffusion model recovered from least-squares curve fit to reconstructed experimental moisture absorption data for woven 3-ply bismaleimide/carbon fiber composite from Ref. [38].**

| | |
|---|---|
| $D_z$ | $5.25 \times 10^{-7}$ cm$^2$/min |
| $\gamma$ | $1.52 \times 10^{-6}$ min$^{-1}$ |
| $\beta$ | $1.065 \times 10^{-6}$ min$^{-1}$ |
| $M_\infty$ (%) | 2.915 |

### (3.7)    Conclusions

Existing literature illustrates a wide range of absorption behavior observed for various types of polymer/fiber combinations, environmental conditions, and specimen geometries.  In some cases, moisture absorption follows a purely one-dimensional Fickian moisture absorption curve. However, there are numerous applications in which geometry, material anisotropy, and anomalous diffusion behavior necessitate the use of a more comprehensive and accurate model of diffusion.  The three-dimensional anisotropic hindered diffusion model developed in this paper is capable of capturing simple Fickian diffusion as well as a wide variety of anomalous diffusion behavior through inclusion of polymer/diffusing molecule interaction. This interaction, which impedes the Fickian diffusion

process, is represented by the probability of a mobile molecule becoming bound and a bound molecule becoming free to diffuse. In addition, the model captures the effects of material anisotropy and specimen geometry on moisture absorption. The accuracy and stability of the numerical solution of the proposed model was successfully verified by comparing simplified specific cases to existing analytical solutions of the three-dimensional anisotropic Fickian model and the one-dimensional "Langmuir-type" diffusion model. The effect of binding probability on the initial slope of the moisture absorption curve and the wide range of diffusion behavior that can be captured by the proposed model was demonstrated.

To further demonstrate the utility of the hindered diffusion model, it was applied to experimental gravimetric moisture absorption data for three different polymers and their reinforcements. First, the one-dimensional isotropic version of the hindered diffusion model accurately captured the anomalous absorption results obtained from epoxy resin samples of various thicknesses. Second, good agreement with reconstructed experimental moisture absorption data for a unidirectional glass-reinforced composite was achieved by applying a least-squares curve fit of the three-dimensional version of the proposed model. In the third example, the hindered diffusion model was shown to be capable of capturing both short- and long-term moisture absorption behavior of a bismaleimide/carbon fiber composite more accurately than a two-stage model.

# Chapter 4:  Characterization of Anisotropic Moisture Absorption in Polymeric Composites Using Hindered Diffusion Model

## (4.1)    Development of the 3D HDM Analytical Mass Gain Function

The moisture concentration profile predicted by the 3D HDM can be determined through the use of the forward-time, centered-space (FTCS) finite difference technique as Chapter 3.  The primary limitation of the FTCS method is the computational effort required to achieve convergence. As a method to illustrate the moisture absorption behavior with known diffusion properties, the mass gain profile determined by the FTCS scheme is useful and effective.  If the model parameters are known, using the numerical solution to predict the time-dependent moisture gain profile is practical, albeit time-consuming. However, the utility of the full numerical solution decreases significantly when the numerical solution needs to be used repeatedly in conjunction with experimental data to recover actual diffusion parameters. Clearly, a time-marching, explicit numerical solution method such as the FTCS method requires significant computational time. In addition, the iterative nature of parameter recovery using least-squares regression or a similar matching method further increases the required computational time. Therefore, the development of an analytical version of the mass gain function

would increase the practicality of using the 3D HDM to determine the actual diffusion properties.

The analytical solution to the one-dimensional version of the hindered diffusion model is outlined in [52] and is given by Equations (28-31). The parameter $k$, which determines the rate of saturation in a particular direction, is given by Equation (30). When $\gamma$ and $\beta$ are both small compared to this parameter, the analytical mass gain function of the hindered diffusion model can be greatly simplified. Algebraic manipulation of this simplification yields the following:

$$M(t) = \frac{\beta}{\gamma + \beta}[M_F(t)] + M_\infty \left(1 - \frac{\gamma}{\gamma + \beta}e^{-\beta t} - \frac{\beta}{\gamma + \beta}\right) \tag{116}$$

where, $M_F(t)$ is the mass gain function of the Fickian diffusion model which, in one-dimensional cases is given by

$$M_F(t) = M_\infty - \frac{8M_\infty}{\pi^2}\sum_{P=0}^{\infty}\frac{1}{(2P+1)^2}\, e^{-\pi^2 t\left(\frac{D_x\,(2P+1)^2}{h^2}\right)} \tag{117}$$

Equations (116) and (117) imply that the judicious approximation of the mass gain function for the hindered diffusion model can be considered a linear superposition of the Fickian mass gain function and hindrance effects expressed by the second term in Equation (116). The extent of the modification is directly proportional to the values of $\gamma$ and $\beta$. The terms that effectively hinder the Fickian diffusion process ($\gamma$ and $\beta$) are independent of absorption direction, and

serve only to modify the Fickian mass gain function, $M_F(t)$. As a result, one can arrive at a three-dimensional approximation to the hindered diffusion model by substituting the three-dimensional Fickian mass gain function into Equation (116). The mass gain function for the three-dimensional Fickian model, shown again here for simplicity, was found by integrating the solution to Equation (42) and is given by [64]

$$M_F(t) = M_\infty - \frac{512M_\infty}{\pi^6} \sum_{P=0}^{\infty} \sum_{Q=0}^{\infty} \sum_{R=0}^{\infty} \frac{1}{(2P+1)^2 (2Q+1)^2 (2R+1)^2} e^{-\alpha t}$$

where, (118)

$$\alpha = \pi^2 \left( \frac{D_x (2P+1)^2}{h^2} + \frac{D_y (2Q+1)^2}{w^2} + \frac{D_z (2R+1)^2}{l^2} \right)$$

In Equation (118), $M_F(t)$ is the moisture weight percent at time $t$ and $M_\infty$ is the equilibrium moisture weight percent of a sample of dimensions $h$ x $w$ x $l$. Within this framework, the analytical solution of the 3D HDM can be rewritten as:

$$M^* = 1 - \frac{512\mu}{\pi^6} \sum_{P=0}^{\infty} \sum_{Q=0}^{\infty} \sum_{R=0}^{\infty} \frac{1}{(2P+1)^2 (2Q+1)^2 (2R+1)^2} e^{-\alpha t^*}$$
$$- (1-\mu)e^{-t^*}$$

(119)

where,

$$\alpha = (A_1(2P+1)^2 + A_2(2Q+1)^2 A_3(2R+1)^2)$$

$$M^* = \frac{M(t)}{M_\infty} \qquad t^* = \beta t \qquad \mu = \frac{\beta}{\gamma + \beta}$$

$$\text{(120)}$$

$$A_1 = \frac{\pi^2 D_x}{\beta l^2} \qquad A_2 = \frac{\pi^2 D_y}{\beta w^2} \qquad A_3 = \frac{\pi^2 D_z}{\beta h^2}$$

It is interesting to note that the non-dimensional mass gain solution given in Equation (119) uses four non-dimensional material properties, including three diffusion parameters, $A_1, A_2, A_3$. The fourth parameter, $\mu$, governs the extent of diffusion hindrance due to physical and chemical interactions, and is referred to as the diffusion hindrance coefficient. This coefficient was previously described in the introduction of the one-dimensional "Langmuir-type" dual-mode sorption model and the diffusion-relaxation model. Again, the importance of the ratio given by $\mu$ and the value of $\beta$ is apparent. As in the one-dimensional version, the parameter that determines the rate of saturation of the sample must be much larger than the values of $\gamma$ and $\beta$. In the three-dimensional case, this can be expressed as:

$$k = k_x + k_y + k_z \gg \gamma, \beta$$

where, $\qquad\qquad\qquad\qquad\qquad\qquad\qquad\qquad\qquad\qquad\qquad\qquad\qquad$ (121)

$$k_x = \frac{\pi^2 D_x}{(l)^2}, \quad k_y = \frac{\pi^2 D_y}{(w)^2}, \quad k_z = \frac{\pi^2 D_z}{(h)^2}$$

## (4.2)    Method for Recovery of 3D HDM Parameters

Recovery of the 3D HDM parameters from experimental gravimetric data can be accomplished using least-squares regression in conjunction with a gradient optimization method, similar to the procedure used by Aktas et al. [64]. The goal of the least-square curve fitting procedure is the minimization of the following function:

$$E(t) = \sum_i^n \left[ M_i(t) - M_{\text{exp}_i}(t) \right]^2 \qquad (122)$$

where $M(t)$ is the theoretical and $M_{\text{exp}}(t)$ is the experimentally determined moisture content at a given time.

The six model parameters (i.e., $D_x$, $D_y$, $D_z$, $\gamma$, $\beta$, $M_\infty$) that minimize the function given in Equation (122) are determined by using a slightly modified version of the method of steepest descent, or Cauchy's method. The method is based on the fact that the gradient vector of the function $E(t)$ points toward the direction of steepest ascent. Therefore, in order to minimize the function the model parameters are adjusted in the opposite direction of the gradient according to

$$x^{(k+1)} = x^k - \hat{n}\rho x^k \qquad (123)$$

where $x$ is the vector of model parameters, $\rho$ is a vector of parameters chosen to minimize $E(t)$ evaluated at $x^{(k+1)}$, and $\hat{n}$ is the normalized gradient vector given by

$$\hat{n} = \frac{\left[\frac{\partial E(t)}{\partial D_x} \quad \frac{\partial E(t)}{\partial D_y} \quad \frac{\partial E(t)}{\partial D_z} \quad \frac{\partial E(t)}{\partial M_\infty} \quad \frac{\partial E(t)}{\partial \gamma} \quad \frac{\partial E(t)}{\partial \beta}\right]}{\sqrt{\left[\left(\frac{\partial E(t)}{\partial D_x}\right)^2 + \left(\frac{\partial E(t)}{\partial D_y}\right)^2 + \left(\frac{\partial E(t)}{\partial D_z}\right)^2 + \left(\frac{\partial E(t)}{\partial M_\infty}\right)^2 + \left(\frac{\partial E(t)}{\partial \gamma}\right)^2 + \left(\frac{\partial E(t)}{\partial \beta}\right)^2\right]}} \quad (124)$$

The use of the vector $\rho$ serves to increase the speed with which the function is minimized. The components of $\rho$ are chosen according to the model parameter that is being adjusted in each iteration, due to the fact that each model parameter produces a different change in the magnitude of the time-dependent moisture concentration. The value of $M_\infty$, for example, is adjusted more quickly than the other parameters due to the large effect it has on $E(t)$ relative to other parameters.

In order to illustrate this effect more clearly, all six model parameters are separately increased by 50% while maintaining the other parameters at their original value. Initially, the through thickness diffusivity and diffusivity through one edge, $D_z$ and $D_x$, are 0.73103 x $10^{-9}$ m$^2$/hour and the diffusivity in the fiber direction, $D_y$, is higher at 1.125 x $10^{-9}$ m$^2$/hour, which are typical values for a unidirectional fiber-reinforced epoxy from Ref. [64]. Equilibrium moisture content was normalized at 1, while $\gamma$ was set at 1 x $10^{-6}$ / hour and $\beta$ at 5 x $10^{-6}$ / hour. These parameters are increased by 50%, one at a time. The root-mean

squared (RMS) deviation associated with each adjustment compared to the

original parameters is shown in Table 5. Increasing the value of $M_\infty$ by 50%

causes an RMS deviation of 52.8 x $10^{-2}$ compared to the original data, which

indicates that the typical change in any data point would be 52.8% for this case.

Therefore, $M_\infty$ can be viewed as the most critical parameter to the accuracy of any

predictive model of diffusion behavior. Accordingly, the adjustment of the value

of $M_\infty$ (the corresponding component of $\rho$) must be greater than the adjustment to

other parameters at each iteration. In order to further illustrate the importance of

$M_\infty$, the moisture uptake curve given by initial parameter estimates is shown in

Figure 11 alongside curves for a 50% increase in $M_\infty$, $\gamma$, and $\beta$. The slight change

in the slope of the initial, linear section of the moisture uptake profile caused by a

50% increase in diffusivity values is difficult to discern, and hence, is omitted

from Figure 11 for clarity.

**Table 5 - Deviation associated with 50% increase in individual model parameters, quantified as root-mean squared deviation.**

| Adjusted Parameter (50% increase) | RMS Deviation |
|:---:|:---:|
| $D_x$ | 8.54 x $10^{-2}$ |
| $D_y$ | 8.54 x $10^{-2}$ |
| $D_z$ | 7.92 x $10^{-2}$ |
| $\gamma$ | 7.21 x $10^{-2}$ |
| $\beta$ | 8.12 x $10^{-2}$ |
| $M_\infty$ (%) | 52.8 x $10^{-2}$ |
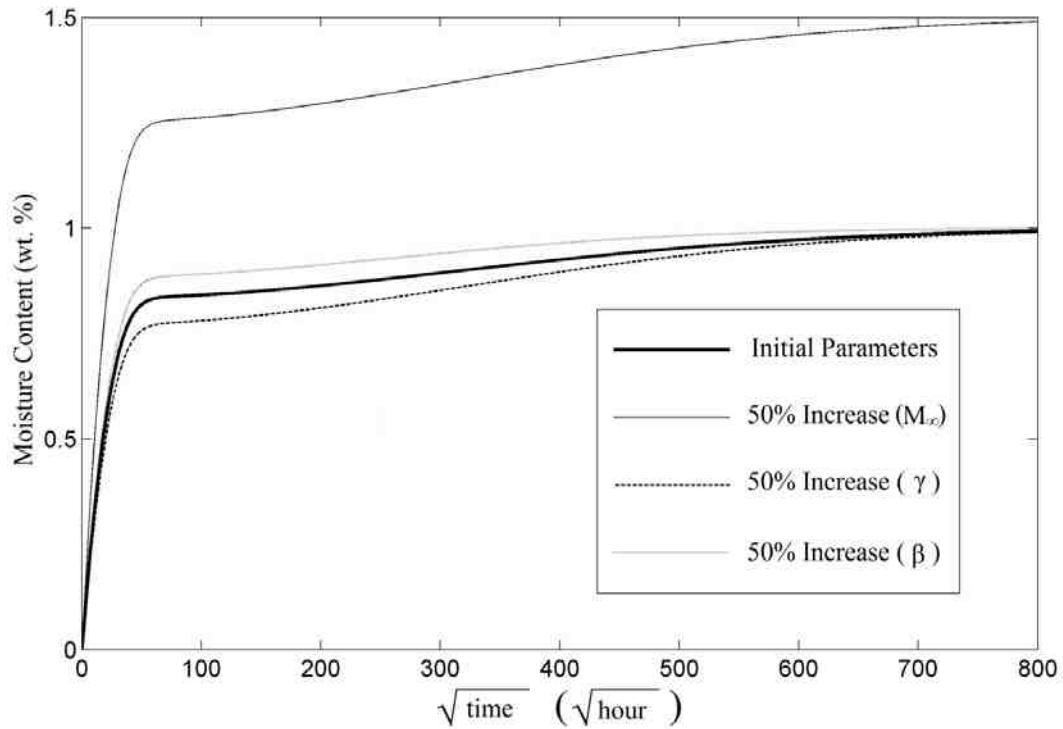
**Figure 11 - Effect of 50% increase in individual model parameters, $M_\infty$, $\gamma$, and $\beta$. Initial parameters: $D_x = D_z = 0.73103 \times 10^{-9}$ m$^2$/hour, $D_y = 1.125 \times 10^{-9}$ m$^2$/hour, $\gamma = 1 \times 10^{-6}$ / hour, $\beta = 5 \times 10^{-6}$ / hour.**

The primary goal of the analytical version of the 3D HDM mass gain function is to increase its practical applicability in recovering model parameters from experimental data. The extent to which the condition described in Equation (121) is met affects the error between the exact solution and the analytical approximation. Adherence to this condition is not known prior to model parameter recovery using experimental data. Therefore, diffusion properties can be used to check if Equation (121) is satisfied after they are recovered using the analytical solution. Another alternative is to use the recovered model parameters

85

to generate an accurate numerical solution, which can then be compared to the experimental data.  In this manner, any error induced by the approximation can be quantified. However, based on experimental results reported in the literature, Equation (121) is satisfied for the vast majority of composite systems.

**(4.3)    Recovering 3D HDM Parameters from**

**Synthetic Moisture Absorption Data**

In order to demonstrate the utility of the parameter recovery method when applied to experimental data, synthetic moisture absorption data was generated for both Fickian and non-Fickian absorption scenarios. In each case, a moisture weight percent value was generated at 24 exposure times for three different sample geometries. Successful recovery of diffusion properties will serve to validate the parameter recovery method, as well as the analytical approximation to the 3D HDM.

*(4.3.1)  Synthetic Fickian Moisture Absorption Data*

Generating synthetic Fickian moisture absorption data was accomplished using the three-dimensional Fickian mass gain function given in Equation (118).  The expectation is that the least-squares curve fitting process of the 3D HDM will

yield diffusivities approximately equivalent to the Fickian diffusivities used to produce the synthetic data.  In addition, it is expected that the hindrance coefficient should be very near unity, thereby indicating that the absorption is Fickian. In this case, diffusivity values and sample geometries are taken from Ref. [64] and are representative of a fiber-reinforced epoxy with a 50% fiber volume fraction. The theoretical sample contains unidirectional fiber reinforcement, and therefore has equivalent diffusivity values in the two directions perpendicular to the fibers. The through thickness diffusivity and diffusivity through one edge, $D_z$ and $D_x$, are 0.73103 x $10^{-9}$ m$^2$/hour.  The diffusivity in the fiber direction, $D_y$, is higher at 1.125 x $10^{-9}$ m$^2$/hour. Theoretical sample thickness for all three geometries is 2 mm. Planar dimensions for the three different sample sizes are 40 x 40 mm, 20 x 20 mm, and 4 x 8 mm.

The least-square regression of the HDM solution led to the recovery of the orthotropic diffusivities and equilibrium moisture content with less than 1% error each.  The recovered values of $\gamma$ and $\beta$ exhibited a dependence on the initial estimates. However, the hindrance coefficient was consistently recovered within one percent of unity, which further reinforces the importance of this parameter. The implication is that $\gamma$ is not required to be very near zero for the process to be essentially Fickian in nature, provided $\beta$ is sufficiently large.  The non-dimensional hindrance coefficient $\mu$, therefore, is a more accurate indication of

conformance to Fickian diffusion behavior.  Actual and recovered diffusivities

and $M_\infty$ are shown in Table 6 along with associated error.

**Table 6 - Actual and recovered absorption parameters obtained by applying the analytical 3D HDM solution to synthetic Fickian moisture absorption data and associated error.**

|  | Actual | Recovered | Error |
|---|---|---|---|
| $D_x$ (m$^2$/hour) | 0.73103 x 10$^{-9}$ | 0.7376 x 10$^{-9}$ | 0.661% |
| $D_y$ (m$^2$/hour) | 1.1250 x 10$^{-9}$ | 1.1272 x 10$^{-9}$ | 0.644% |
| $D_z$ (m$^2$/hour) | 0.73103 x 10$^{-9}$ | 0.7357 x 10$^{-9}$ | 0.193% |
| $M_\infty$ (%) | 1 | 0.998 | 0.2% |
| $\mu$ | 1 | 1.003 | 0.3% |

The discrete data points generated using the analytical 3D Fickian  mass gain

function are shown in Figure 12 along with the moisture absorption curve

generated using the recovered parameters applied to the 3D HDM numerical

solution. Only the curves for the 4 x 8 mm sample are shown for clarity. The

nature of the optimization method used to minimize the function in Equation

(122) allows a relatively quick convergence regardless of the error in the initial

estimates of the model parameters. In order to illustrate the fact that initial

estimates need not be close to the actual values, the moisture absorption curve

generated by applying the initial parameter estimates to the 3D HDM is also shown in Figure 12 for reference. Approximately 6000 parameter iterations are required in this specific case to achieve convergence.
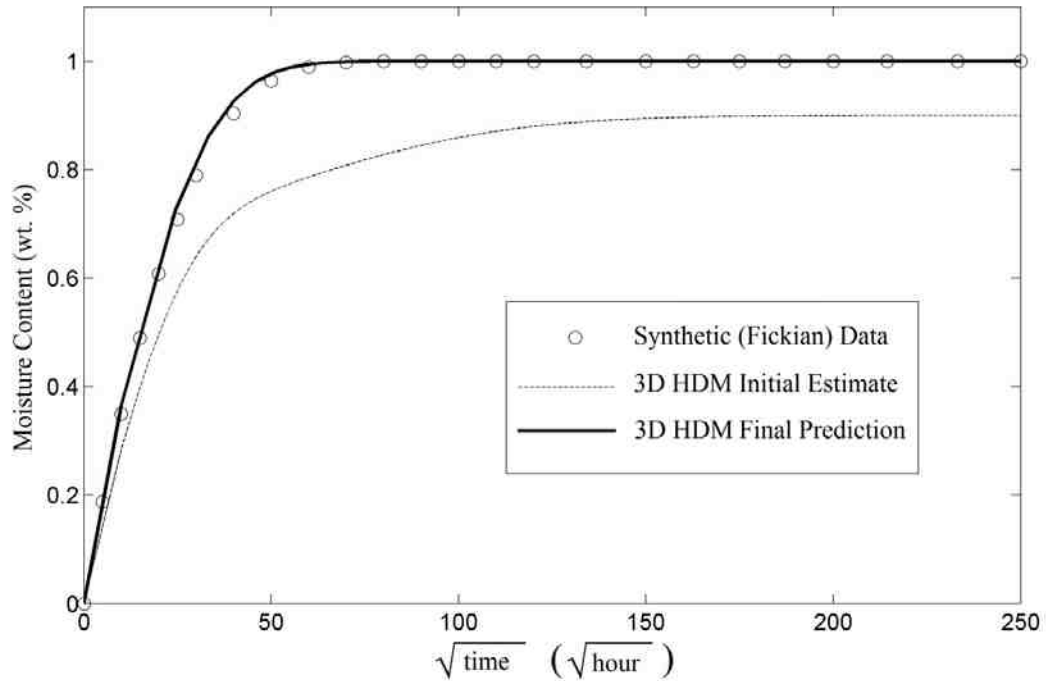


**Figure 12 - Recovery of 3D HDM parameters using analytical solution from synthetic three-dimensional Fickian moisture absorption data.**

*(4.3.2)    Synthetic Non-Fickian Moisture Absorption Data*

In order to further demonstrate the utility of the proposed analytical solution to the 3D HDM, synthetic data typical of anomalous absorption behavior was generated using the numerical solution to the 3D HDM developed in Chapter 3. The values of $\gamma$ and $\beta$ used to generate the synthetic data are based on experimental results reported in Ref. [52] for a 5208 epoxy resin immersed in

24ºC water for a period of two years.  Diffusivity values are again based on Ref. [64] and are 0.73103 x $10^{-9}$ $m^2$/hour in the through thickness ($z$) direction, and 1.125 x $10^{-9}$ $m^2$/hour through the smaller side surfaces. Sample dimensions are 4 x 8 mm, 8 x 10 mm, and 20 x 20 mm. Sample thickness is constant at 2 mm.  The parameter that determines saturation rate $k$, given in Equation (121), is at a *minimum* 21 times larger than β and 124 times larger than γ for all three sample geometries. Therefore, the conditions are met for the use of the analytical solution.

The recovered moisture uptake curve shows excellent agreement with the synthetic data as shown in Figure 13. The model parameters were recovered using the dimensionless 3D HDM approximation proposed in this article with less than 1% error for all three diffusivities and $M_\infty$.  The parameters applied to the numerical solution to generate the synthetic data, the parameters recovered using the analytical solution and the associated error are shown in Table 7.

The values of γ and β were not recovered as accurately as the other parameters, although error for both was less than 3%.  However, the diffusion hindrance coefficient was recovered with approximately 0.12% error. This further highlights the importance of the hindrance coefficient to the diffusion behavior predicted by the 3D HDM.   The value of these parameters individually does play a role in the absorption behavior, thought it is less pronounced than the hindrance coefficient.

Slight changes in γ or β cause very little change in the uptake curve, provided the

hindrance coefficient remains constant. The discrete data points generated using

the full numerical solution are shown in Figure 13 along with the moisture

absorption curve generated using the recovered parameters. Only the curves for

the 10 x 8 mm sample are shown for clarity. The moisture absorption curve

generated by applying the initial parameter estimates to the 3D HDM is also

shown for reference.

**Table 7 - Actual and recovered parameters of proposed analytical 3D HDM solution applied to synthetic anomalous moisture absorption data and associated error.**

| Model Parameter | Actual | Recovered | Error |
|---|---|---|---|
| $D_x$ (m$^2$/hour) | $1.125 \times 10^{-9}$ | $1.116 \times 10^{-9}$ | 0.80 % |
| $D_y$ (m$^2$/hour) | $1.125 \times 10^{-9}$ | $1.130 \times 10^{-9}$ | 0.48 % |
| $D_z$ (m$^2$/hour) | $7.3103 \times 10^{-10}$ | $7.2660 \times 10^{-10}$ | 0.61% |
| $\gamma$ (hour$^{-1}$) | $1.45 \times 10^{-5}$ | $1.41 \times 10^{-5}$ | 2.76 % |
| $\beta$ (hour$^{-1}$) | $8.5 \times 10^{-5}$ | $8.3 \times 10^{-5}$ | 2.35 % |
| $M_\infty$ (%) | 5 | 5.006 | 0.11 % |
| $\mu$ | 0.854 | 0.855 | 0.12 % |
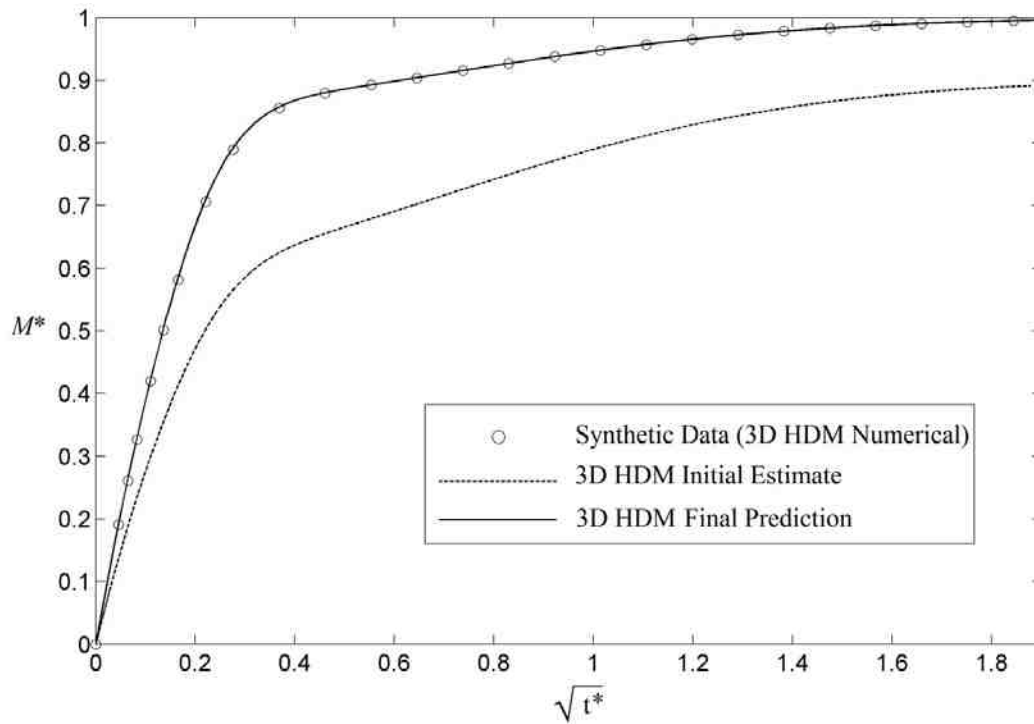
**Figure 13 - Recovery of 3D HDM parameters using proposed analytical approximation applied to synthetic anomalous moisture absorption data.**

The synthetic data represents the exact solution to the three-dimensional anisotropic hindered diffusion model. Therefore, accurate recovery of the parameters using a least-squares curve fit to an approximate analytical solution serves to validate both the analytical solution as well as its implementation in the least-squares curve fit. Additionally, the large difference between the initial guess and the actual parameters demonstrates that the method is capable of recovering the parameters with excellent agreement even when the initial guess is far from the actual values. Again in this case, approximately 6000 parameter iterations during the curve fit process are required to achieve convergence.

## (4.4)    Predicting Equilibrium Moisture Content

## Prior to Experimental Equilibrium

The prediction of equilibrium moisture content in polymer composites is of
particular importance. Equilibrium moisture content of a composite material is
typically determined experimentally. Full saturation is assumed to be reached
after consecutive gravimetric measurements show no further significant weight
gain (i.e., less than 0.01% as suggested by ASTM D 5229). It is important to note
that in polymeric composites moisture absorption can be roughly divided into two
sections:  before and after "pseudo-equilibrium."  We refer to "pseudo-
equilibrium" as the point in the absorption process at which the rate of moisture
uptake slows dramatically (see Figure 14).  The first section is essentially linear
and relatively rapid in both Fickian and non-Fickian absorption cases when
plotted versus the square root of time.  In Fickian diffusion, moisture content does
not increase in the second section, and "pseudo-equilibrium" is the actual
equilibrium moisture content. In polymer composites subject to hindered
diffusion, however, the approach to $M_\infty$ continues and can be very slow after
pseudo-equilibrium. Therefore, experimental determination of $M_\infty$ may require
very long exposure times. In addition, the very slow moisture uptake rate may
lead to premature assumption of Fickian diffusion behavior, and thus to incorrect
determination of equilibrium moisture content.
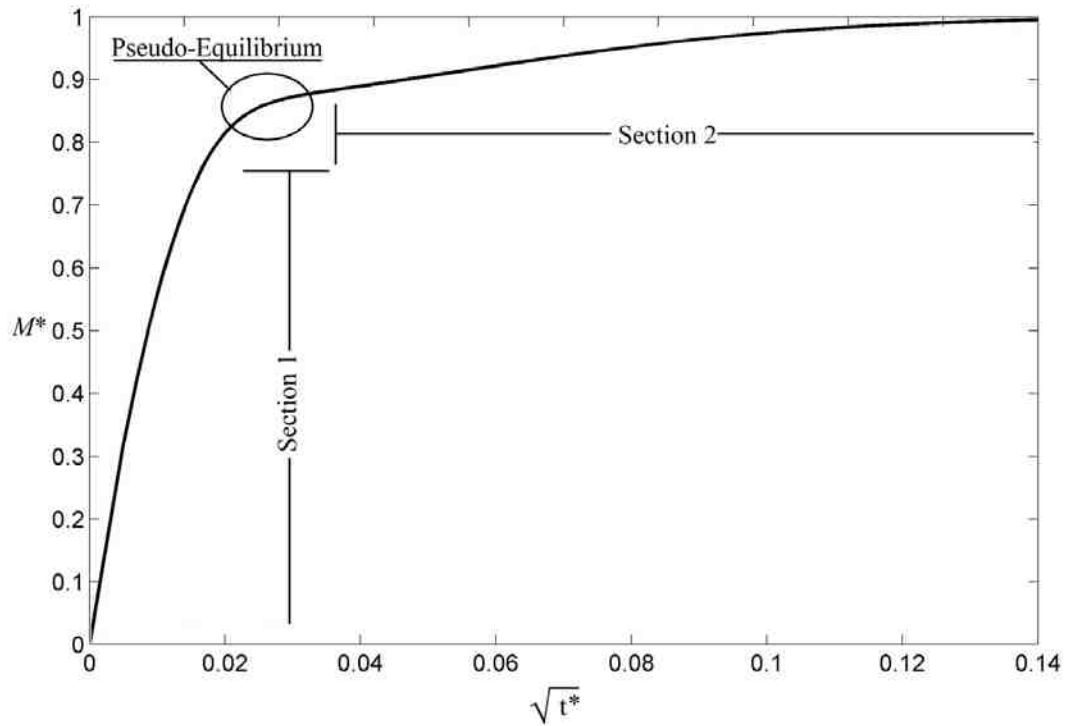
**Figure 14 - Typical moisture absorption profile of hindered diffusion divided into two sections to illustrate "pseudo equilibrium."**

In a study on the effect of weave microstructure on moisture diffusion behavior in polymer composites, Tang et al. [77] collected gravimetric data on 3-ply samples of carbon-fiber reinforced bismaleimide fully immersed in distilled water. The authors applied the one-dimensional Fickian diffusion model to the collected data. The reproduced moisture absorption data and the Fickian curve fit are shown in Figure 15. The accuracy of the fit for short times was excellent, though the authors acknowledged that recorded gravimetric measurements at longer times deviated from Fickian predictions. The application of the hindered diffusion model to the reproduced experimental data yields an excellent fit for all recorded

data points, as shown in Figure 15. However, because the data was limited due to the experimental time frame, a range of $M_\infty$ may produce equally well-fitting moisture absorption curves with approximately equivalent RMS error. In this case, a good fit is achieved for $M_\infty$ values between 1.85% and 3.87%, which represent full saturation at 4.5 and 16 years exposure time, respectively. Both of these curves are shown in Figure 15. The implication of these equivalent fits, which could yield a wide range of $M_\infty$, is that the two-month long gravimetric experiments may be insufficient to allow accurate prediction of equilibrium moisture content. The slow approach to equilibrium moisture content, which is typical of hindered diffusion, proceeds at such a rate that reaching full saturation may potentially take many years. It is clear from this case that additional data collection is necessary, though achieving full saturation may take several more years. Therefore, accurate prediction of $M_\infty$ prior to experimentally reaching equilibrium saturation would greatly reduce experimental time and effort.
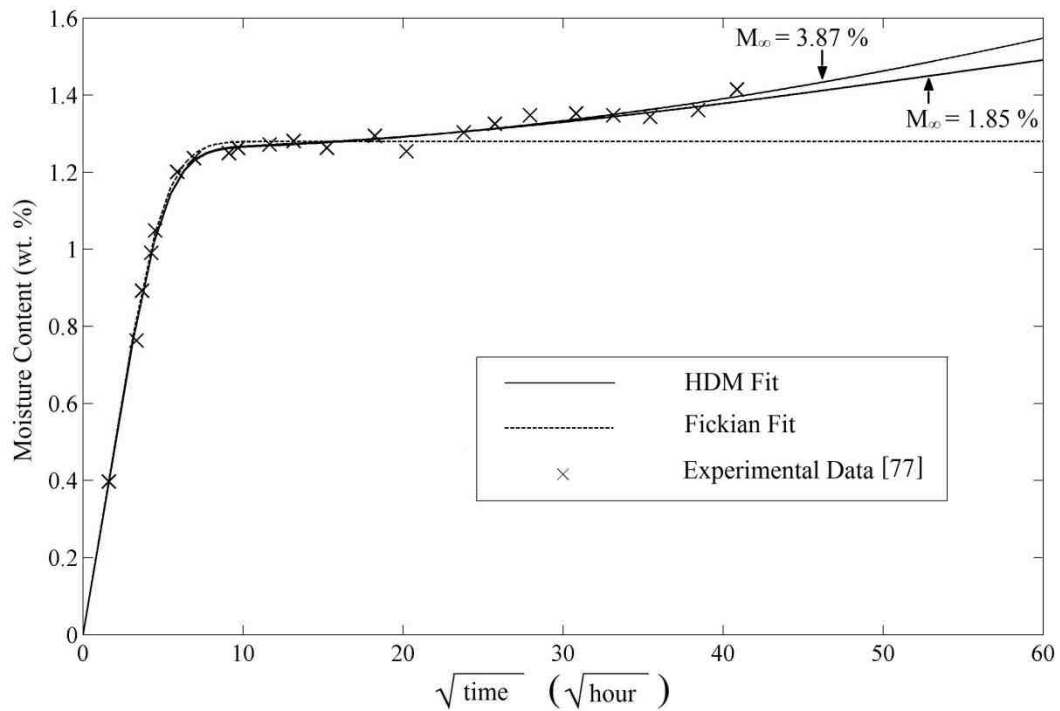
**Figure 15 - Application of the hindered diffusion model to reproduced experimental data from Ref. [77].**

During moisture absorption experiments, the parameter recovery method described above can be applied to collected data in an attempt to recover $M_\infty$ with the addition of each measurement. It is expected that $M_\infty$ can be accurately determined at some point in this process prior to equilibrium saturation. In order to validate this hypothesis, synthetic moisture absorption data was generated using the numerical solution of the 3D HDM. A total of 32 data points were generated for three different geometries, representing 32 measurements taken at equal time intervals throughout the 6 years required to experimentally reach equilibrium saturation. Binding and unbinding probabilities were set at 1.45 x

$10^{-5}$ hr$^{-1}$ and 8.5 x $10^{-5}$ hr$^{-1}$, respectively, based on Ref. [52]. The through thickness diffusivity, $D_z$, was set at 9 x$10^{-9}$ m$^2$/h. Planar diffusivities, $D_y$, and $D_x$, are 1.8 x $10^{-8}$ and 4.5 x $10^{-8}$ m$^2$/h, respectively two and five times the through-thickness diffusivity. Theoretical sample thickness for all three geometries is 2 mm. Planar dimensions are 20 x 40 mm, 10 x 10 mm, and 4 x 8 mm. Equilibrium moisture content is set at 5% by weight. The dimensionless parameters for this case are shown in Table 8. The conditions for applicability of the analytical solution are met for all three sample geometries.

**Table 8 - Dimensionless parameters used in the investigation of 3D HDM parameter recovery using incomplete experimental data and the proposed analytical solution.**

|        | Sample 1 | Sample 2 | Sample 3 |
|--------|----------|----------|----------|
| $A_1$  | 263.87   | 263.87   | 263.87   |
| $A_2$  | 5.23     | 20.90    | 130.63   |
| $A_3$  | 3.27     | 52.25    | 81.64    |
| M*     | 1        | 1        | 1        |
| μ      | 0.8543   | 0.8543   | 0.8543   |

As expected, the least-squares curve fit process was able to recover $M_\infty$ with less than 1% error shortly after pseudo-equilibrium, at approximately 11 months exposure time. The total time required to reach 99% of equilibrium moisture content is more than 4 years, with full equilibrium reached at approximately 6

years. In this case, the time required to predict equilibrium moisture content is markedly less than the time required to reach equilibrium experimentally.

*(4.4.1) Effect of Measurement Error on Equilibrium*

*Moisture Content Prediction*

In actual experiments, varying amounts of measurement error are introduced during the data collection process. It is expected that the presence and magnitude of measurement error will affect the ability to recover $M_\infty$ using incomplete experimental data. Artificially generated random error was applied to the synthetic data in order to investigate the effect of measurement error on the experimental time required to determine equilibrium moisture content. The magnitude of the induced measurement error is expressed as the RMS error of the altered versus unaltered synthetic data. The RMS error represents the typical magnitude of the artificially generated error associated with each measurement. Two magnitudes of measurement error were applied to the data, one representing an RMS error of 0.005 and the other an RMS error of 0.02. The RMS error of 0.005 indicates that the recorded value of $M_\infty$ at a given time is typically 0.5% from the actual value. For example, if a composite sample contains 100 mg of absorbed water at a given time, the measured value would typically be 99.5 mg or 100.5 mg.

The equilibrium moisture content was recovered with less than 1% error at approximately 1.64 years for RMS measurement error of 0.005, and approximately 2.24 years for RMS measurement error of 0.02. These results validate the hypothesis that more accurate measurement of moisture content throughout the experiment leads to a decrease in the experimental time required to predict $M_\infty$. However, even when a recorded measurement is 2% above or below the actual value for a typical measurement, equilibrium moisture content can be predicted approximately 1.75 years prior to experimentally achieving 99% saturation.

*(4.4.2) Effect of Measurement Frequency on Equilibrium*

*Moisture Content Prediction*

In addition to measurement error, the frequency of measurements will likely affect the accuracy of parameter recovery. In an effort to determine the effect of measurement frequency on the accurate recovery of $M_\infty$, the time interval between each measurement was decreased by 50%, doubling the number of generated data points to 64. Interestingly, when the number of data points was doubled, $M_\infty$ was recovered with less than 1% error more than 4 months earlier at approximately 6.7 months. A similar decrease in required experimental time was observed for cases with artificially induced measurement error. Typical induced measurement error of 0.5% for 64 data points yielded a required experimental time of 0.92 years, and

measurement error of 2 % yielded a required experimental time of 1.64 years.

Therefore, a marked decrease in the time required to predict $M_\infty$ can be realized

by increasing the frequency of measurements, despite measurement error.

The six cases and the equilibrium moisture content recovery results are

summarized in Table 9. The data points simulating measurement error are shown

in Figure 16 for experimental data with 32 measurements and in Figure 17 for 64

measurements. The moisture absorption curve without measurement error is

shown in both figures. Only data for the 2 x 4 x 8 mm sample size is shown for

clarity. The time at which the equilibrium moisture content can be predicted

within 1% error is also annotated in both figures.

**Table 9 - Description of each case used for investigation of 3D HDM**

**parameter recovery using incomplete data.**

| Measurement RMS Error | Data Points | $M_\infty$ Recovery Time (years) | M* at Recovery |
|---|---|---|---|
| 0 | 32 | 0.92 | 0.927 |
| 0.005 | 32 | 1.64 | 0.957 |
| 0.02 | 32 | 2.24 | 0.973 |
| 0 | 64 | 0.56 | 0.903 |
| 0.005 | 64 | 0.92 | 0.927 |
| 0.02 | 64 | 1.64 | 0.957 |
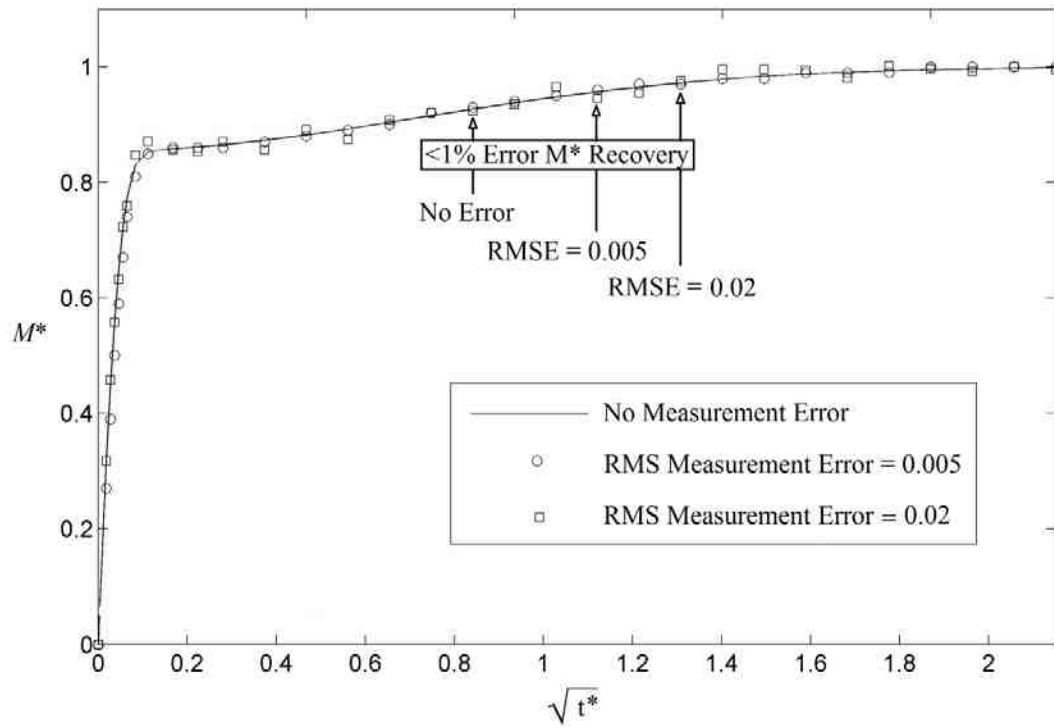
**Figure 16 - Recovery of equilibrium moisture content based on incomplete experimental data with and without artificial measurement error. 32 total measurements.**
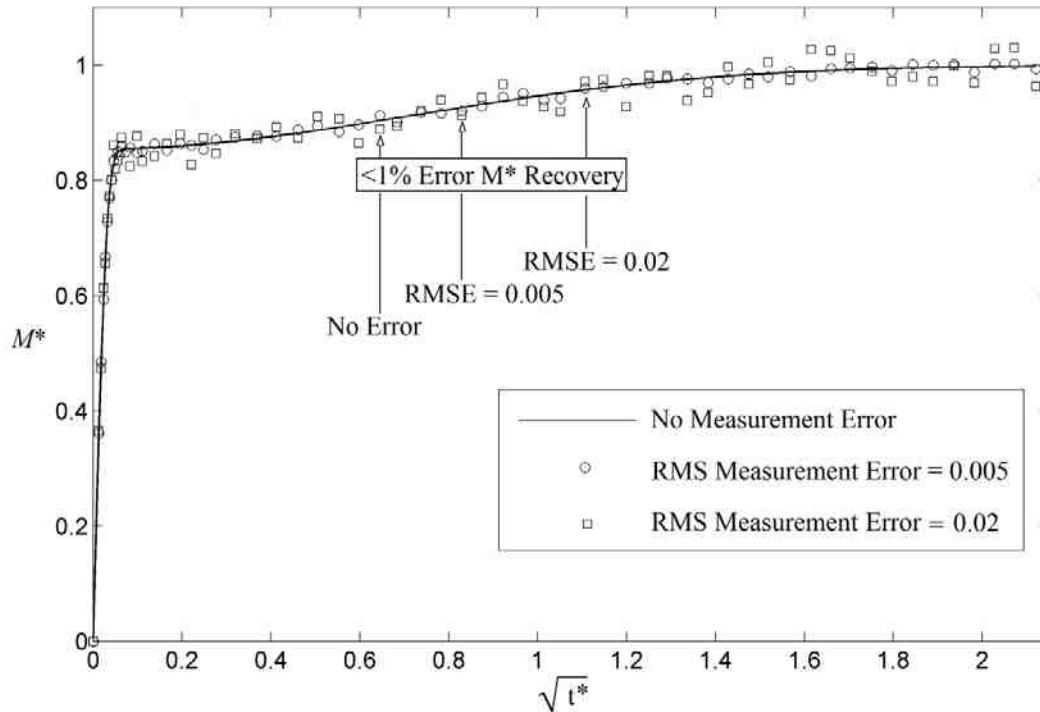
**Figure 17 - Recovery of equilibrium moisture content based on incomplete experimental data with and without artificial measurement error. 64 total measurements.**

**(4.5)    Conclusions**

The development of a predictive moisture absorption model for a specific composite material requires experimental determination of diffusion properties. An analytical solution to the three-dimensional anisotropic hindered diffusion model was developed in order to increase the utility of the model in recovering these diffusion properties based on experimental data.  A parameter recovery method employing the analytical solution of the 3D HDM and least-squares regression was presented. The recovery method was applied successfully to

synthetic moisture absorption data generated using both the 3D Fickian mass gain function and the numerical solution to the 3D HDM.  Anisotropic diffusivities and equilibrium moisture content, $M_\infty$ were recovered with less than 1% error for both cases. The hindrance coefficient, $\mu$, which is dependent on the values of $\gamma$ and $\beta$, was consistently recovered with less than 1% error for both Fickian and non-Fickian synthetic data regardless of initial estimates.  The ability to accurately recover $M_\infty$ using experimental data prior to reaching equilibrium moisture saturation was investigated with varying amounts of artificially induced measurement error.  Accurate recovery of $M_\infty$ is possible long before it is reached experimentally, though the time required is dependent on measurement error and frequency. The results indicated that increased measurement error lengthens the experimental time required to accurately predict equilibrium moisture content. A typical measurement error of 2 % was shown to increase the required experimental time frame by nearly 150% compared to data collected with no error.  In addition, collecting experimental gravimetric measurements twice as often may decrease the time required to recover $M_\infty$ by as much as 40%.

# Chapter 5: Three-Dimensional Hindered Diffusion in Quartz-Fiber-Reinforced Bismaleimide Laminate

## (5.1)  Bismaleimide Uses and Properties

Bismaleimide (BMI) is often used as the matrix material in composites expected to operate in extreme environmental conditions, such as high temperature, thermal cycling, and high humidity.  Bismaleimide polymers are a type of polyimide class which can be thermally polymerized without the formation of volatile byproducts. This provides a considerable advantage in processing over conventional condensation-type polyimides while maintaining the high-temperature capabilities of polyimides.  Bismaleimides are constructed of two maleimide groups connected by a main chain of varying construction, as shown in Figure 18 [78].



Bismaleimide

Maleimide [ $H_2C_2(CO)_2NH$ ]
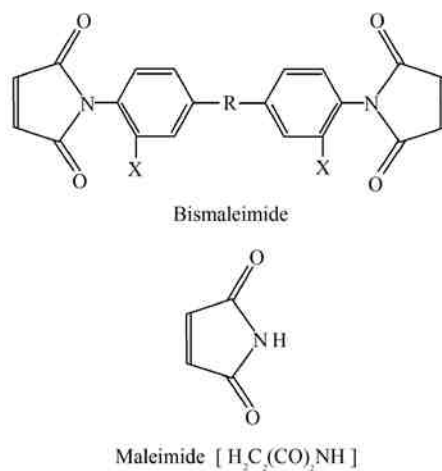
**Figure 18 - Representation of typical bismaleimide construction, with a maleimide group at each end [78].**

BMI resins have a densely cross-linked molecular structure, and are therefore inherently brittle [78]. However, BMI resins are widely used in high-performance composites due to their excellent corrosion resistance, high glass transition temperature, and excellent mechanical property retention in hygrothermal conditions [79]. In addition, BMI resins exhibit good flame, radiation, and chemical resistance [78]. Further, BMI resins are often used in the electronic and aerospace industries due to their excellent dielectric properties, relatively low susceptibility to moisture absorption, and high thermal stability. The applications of BMI composites are many and varied, though BMI systems are typically used where retention of mechanical and electrical properties in high temperature, thermal cycling, or high humidity environments is critical. These properties of BMI resins enable their use in high temperature applications such as multi-layer printed circuit boards, large-scale computers, advanced composites for the aerospace industry, and structural adhesives [78]. In addition, BMI resins have been considered for use in cryogenic environments where resistance to thermal cycling is critical. For example, Ju and Morgan investigated the suitability of carbon fiber-reinforced BMI as the cryogenic fuel containment structure for single stage to orbit launch vehicles [79]. In addition, BMI is an ideal matrix material for quartz fiber reinforcement as part of the radar protecting structure, or radome, on commercial and military aircraft. Liang et al. [80] investigated the suitability of BMI based composites for radome structures on aircraft. In this application,

electrical properties in the form of radar transparency are critical in all environmental conditions.

## (5.2)    Moisture Absorption in Bismaleimide

The moisture absorption behavior and associated degradation of fiber-reinforced epoxy composites has been investigated thoroughly [28, 30-36, 40, 43, 46-48, 50, 54, 60].  Research into the moisture absorption characteristics of bismaleimide resin and its composites is not as extensive, though the topic has been addressed directly [37-39, 44, 75] or indirectly [80, 81] by several articles. In addition, a few articles have addressed the moisture absorption behavior of epoxy resins modified with BMI [82, 45].  The broader popularity of epoxy resin compared to the more specialized BMI is the likely cause for the relative lack of moisture absorption studies.  The studies available in the literature, to the best of our knowledge, address only one-dimensional isotropic diffusion behavior. Further, the lack of extensive moisture absorption studies on fiber-reinforced bismaleimides prevents a consensus from being drawn regarding the general moisture uptake behavior. The few available studies that directly address the moisture absorption behavior of BMI indicate non-Fickian moisture absorption, which is compared to a two-stage model [39], a dual-diffusivity model [38], and the one-dimensional "Langmuir-type" model [75].

In a study of the moisture absorption behavior of a carbon-fiber reinforced BMI, Bao and Yee [38] observed non-Fickian diffusion moisture uptake as evidenced by deviation from the Fickian equilibrium plateau at long times. The authors suggest that the gradual increase in moisture content is due to the long-range cooperative motion of polymer chains. This cooperative motion occurs at an appreciable rate due to the relatively large amount of moisture in the matrix, which contributes to plasticization of the matrix, lower glass transition temperature, and dramatically enhanced segmental mobility in the network. In summary, the authors suggest that the second-stage of moisture absorption, in which a gradual increase in moisture content is observed, is controlled by the rate of polymer network rearrangement. The first-stage was assumed to be Fickian in nature, and the one-dimensional diffusivity of the composite under full immersion in liquid water was reported for various temperatures. Diffusivity is reported as 1.1 $mm^2$/hour at 35°C, 4.8 $mm^2$/hour at 70°C, and 10.6 $mm^2$/hour at 90°C. The increase in diffusivity as temperature increases is typical of moisture diffusion in polymer composites. Bao and Yee also observed that a combination of high temperature and moisture is especially damaging to the fiber-matrix interface. Numerous moisture induced interfacial cracks were observed after prolonged exposure at 90°C, whereas no cracks were observed at 50°C.

In a second study on the moisture absorption behavior of carbon fiber-reinforced BMI, Bao and Yee [39] investigated the effect of fiber architecture, specifically

woven and woven/uni-weave reinforcement. Unlike in the initial study, short term diffusion behavior was found to be non-Fickian. The authors developed a dual-diffusivity model that was able to successfully describe the experimental weight gain curves. The one-dimensional model describes two independent diffusion processes with very different diffusivities. The first process is associated with diffusion in cure-induced cracks and voids, and proceeds relatively quickly. The second, slower process is attributed to the diffusion of mobile molecules in the resin due to random molecular motions, as in the Fickian model. At 70°C, the slower diffusivity was reported as $1.66 \times 10^{-3}$ mm$^2$/hour. The diffusivity of the fast process, attributed to diffusion in voids and cracks, was nearly two orders of magnitude higher at 0.151 mm$^2$/hour. Equilibrium moisture content of the fiber-reinforced BMI was found to be approximately 1.3%.

Liang et al. [80] studied a BMI resin system modified for improved impact strength and processing characteristics by the addition of epoxy to the matrix. The excellent mechanical and electrical properties of BMI resins at high temperature and high moisture or a combination of both are one of the primary advantages of BMI systems. Therefore, the authors investigated the hot-wet resistance of the modified BMI reinforced with glass or quartz fabric. The dielectric constant and dielectric loss of the composites were consistent and low through the test frequency range of 1GHz to 20GHz. The loss tangent (tan $\delta$) at 10 GHz of the neat resin is reported to be 0.012, while the dielectric constant is 3.14 at the same

frequency. The electrical properties after hygrothermal aging were not reported. However, the mechanical properties showed only slight decreases after 100 hours in boiling distilled water. The moisture content of the composites, measured as the weight percent of the sample, was measured at less than 1.1% for both glass and quartz-reinforced resins. Flexural strength was retained at 85% of its original value, while shear strength was retained at 90%.

Li et al. [75] studied the moisture diffusion behavior of a neat bismaleimide resin subject to hygrothermal aging conditions. The nature of the diffusion process was investigated using Fourier transform infrared spectroscopy and swelling experiments. The moisture absorption behavior was modeled successfully using the one-dimensional version of the hindered diffusion model (as developed by Carter and Kibler [52]). According to the authors, the widely used Fick's law is not appealing in this case due to the fact that it does not account for the interaction between water and polar groups in thermoset polymers. The BMI resin used in this study, like most BMI resins, contains polar groups such as hydroxyl groups, which can form hydrogen bonds with water during the diffusion process. In an effort to quantify the interaction between the polymer and the diffusing molecules, two different cure schedules were used to prepare BMI resins with different network structures. The specimens were referred to as L-BMI (lower temperature post-cure, 218°C), and H-BMI (higher temperature post-cure, 230°C). Specimens were exposed to 100% relative humidity at 70°C and 100°C.

The recovered parameters used in one-dimensional hindered diffusion model fit are shown in Tables 10 and 11, which are reproduced from Ref. [75].

**Table 10 - One-dimensional hindered diffusion parameters recovered from experimental moisture absorption data of a neat bismaleimide resin at 100% relative humidity as reported by Li et al. [75].**

| Temperature | Specimen | $\beta$ ($10^{-4}$ hr$^{-1}$) | $\gamma$ ($10^{-4}$ hr$^{-1}$) | $M_\infty$ (%) |
|---|---|---|---|---|
| 70°C | L-BMI | 2.0 | 0.5 | 5.2 |
| | H-BMI | 7.0 | 2.0 | 5.3 |
| 100°C | L-BMI | 20 | 4.0 | 4.2 |
| | H-BMI | 30 | 4.0 | 4.8 |

**Table 11 - Fickian diffusion parameters recovered from experimental moisture absorption data of a neat bismaleimide resin at 100% relative humidity as reported by Li et al. [75].**

| Specimen | Diffusivity ($10^{-6}$ mm$^2$/s) | | $M_f^a$ | |
|---|---|---|---|---|
| | 70°C | 100°C | 70°C | 100°C |
| **L-BMI** | 2.58 | 6.00 | 4.06 | 3.50 |
| **H-BMI** | 2.80 | 6.50 | 4.20 | 4.35 |

The 12°C difference in post-cure temperature appears to have an effect on all parameters of the model, including diffusivity, probability of molecular binding and unbinding, and equilibrium moisture content. It should be noted that the diffusivities reported in Table 11 are calculated assuming Fickian diffusion. In addition, the equilibrium moisture content $M_f^a$ is the apparent Fickian equilibrium, referred to as "pseudo-equilibrium" previously in this work. The actual moisture content continues to increase after this point, as shown in Table 10.  The hindrance coefficient associated with the reported values of γ and β are given in Table 12.

**Table 12 - Hindrance coefficient recovered from experimental moisture absorption data of a neat bismaleimide resin at 100% relative humidity as reported by Li et al. [75].**

| Temperature | Specimen | Hindrance Coefficient (μ) |
|---|---|---|
| 70 | L-BMI | 0.80 |
|  | H-BMI | 0.78 |
| 100 | L-BMI | 0.83 |
|  | H-BMI | 0.88 |

The existing studies that attempt to characterize moisture absorption behavior in BMI resins and their composites assume only one-dimensional moisture diffusion

[37-39,44,75] or fail to consider non-Fickian behavior [80,81]. The effects of three-dimensional anisotropic diffusion and non-Fickian absorption behavior are crucial to accurate moisture absorption characterization. Therefore, the objective of this chapter is to address the three-dimensional anisotropic moisture absorption behavior of a quartz-fiber-reinforced bismaleimide laminate. Three-dimensional effects are particularly important for this material.  Quartz-reinforced BMI laminates up to 40-ply are known to be used as the radar-enclosing structure on some aircraft, providing significant edge surface area for moisture ingress. As a result, one-dimensional through-thickness diffusion models may not be applicable or accurate.  To the best of our knowledge, three-dimensional anisotropic moisture absorption studies have not been carried out for a bismaleimide resin or its composites.

### (5.3)    Experimental Procedure

#### (5.3.1)    Material Properties

The material used in this study is a bismaleimide resin, trade name HexPly$^{\circledR}$ F650, reinforced with an eight-harness satin weave quartz fabric, style 581, per AMS3849B.   The reported equilibrium moisture content for the neat resin, without reinforcement, is 4.3% and the specific gravity is 1.27 [83]. The material properties of the laminate, reported by the manufacturer in Ref. [83] are given in

Table 13.  The dielectric properties of the dry laminate at 9.375 GHz (within the

X-band radar frequency range) are given in Table 14. The reported laminate

physical properties are 55.4% fiber volume, 31.4% resin by weight, 0.7% void

content and specific gravity of 1.78.  Based on these laminate properties and the

reported equilibrium moisture content of 4.3% for the neat resin, the expected

equilibrium moisture content of the laminate is 1.38%.

**Table 13 - Material properties of BMI/Quartz Laminate as reported by the**

**manufacturer [83].**

|  | Room Temp. | 350°F (177°C) | 450°F (232°C) |
|---|---|---|---|
| **Tension** |  |  |  |
| Strength, ksi (MPa) | 77.10 (531.6) | 66.60 (459.2) | 62.80 (433.0) |
| Modulus, msi (GPa) | 3.90 (26.9) | 3.60 (24.8) | - |
| **Compression** |  |  |  |
| Strength, ksi (MPa) | 73.20 (504.7) | 54.50 (375.8) | 42.40 (292.3) |
| Modulus, msi (GPa) | 4.06 (28.0) | 3.85 (26.5) | - |
| **Short Beam Shear** |  |  |  |
| Strength, ksi (MPa) | 8.80 (60.7) | 7.20 (49.6) | 6.10 (42.1) |

**Table 14 - BMI/Quartz laminate dielectric properties as reported by the**

**manufacturer [83].**

| **Temperature** | **Dielectric Constant** | **Loss Tangent** |
|---|---|---|
| 75°F (24°C) | 3.31 | .003 |
| 300°F (149°C) | 3.33 | .004 |
| 450°F (232°C) at 9.375 GHz | 3.34 | .005 |

*(5.3.2)   Fabrication*

Test panels were constructed of six, twelve, and forty plies with dimensions of 36, 36, and 18 inches square, respectively.  The layup assembly is depicted in Figure 19 and is according to the manufacturer's recommendations [83]. Test panels were cured in an autoclave at 375°F for four hours, followed by a four hour postcure at 475°F, also according to the manufacturer's recommendations. The cure procedure was as follows [83]:

A.  Apply vacuum, 22 in. Hg (74 kPa), and 85 psi (586 kPa)  autoclave pressure at ambient temperature.

B.  Hold at 80-100°F (27-38°C) for 30 minutes, then vent vacuum.

C.  Raise temperature to "option."

   a.   375°F at 1-5°F (191°C at 0.6-3°C) per minute, hold for four hours.

   b.   350°F at 1-5°F (191°C at 0.6-3°C) per minute, hold for six hours.

D.  Cool and remove from autoclave.

E.  Postcure four hours at 475°F (232°C). Raise temperature from ambient to 375°F (191°C) at a rate of 5-10°F (3-6°C) per minute and a rate not to exceed 3.3°F (2°C) per minute above 375°F (191°C).
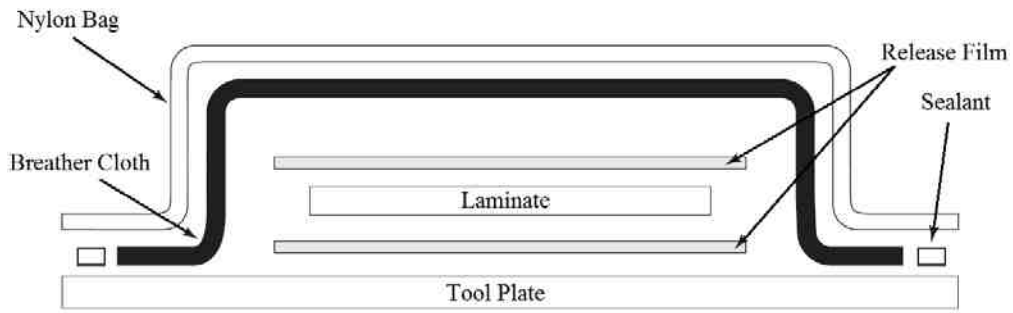
**Figure 19 - Layup assembly used during fabrication of BMI/Quartz laminate test panels.**

A graphical representation of the cure process suggested by the manufacturer, including temperature and pressure, is shown in Figure 20.
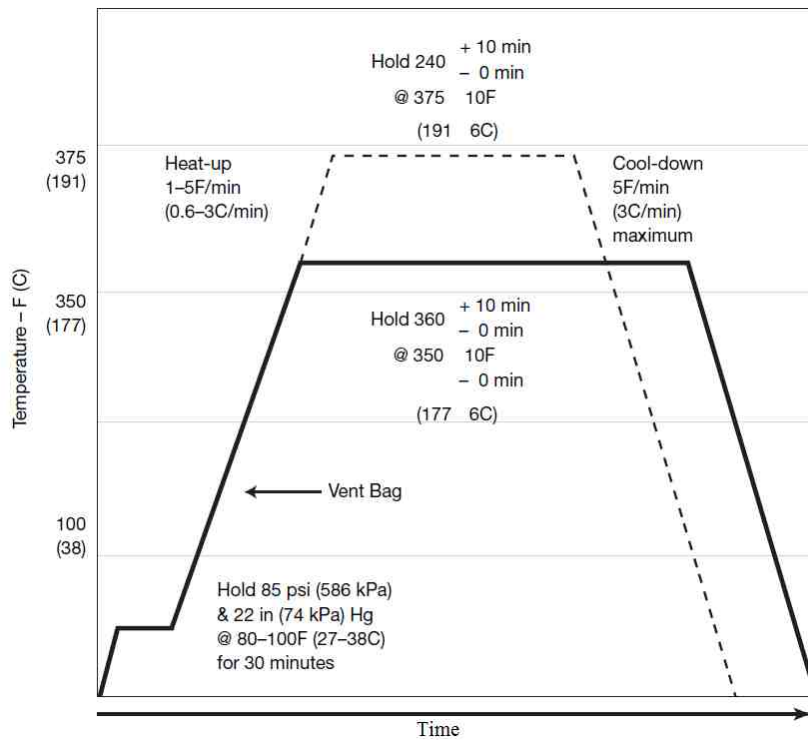


**Figure 20 - Graphical representation of the cure process suggested by the manufacturer.**

The total cycle programmed into the autoclave, including cure and post-cure processing temperature and pressure is shown in Figure 21. The actual temperature and pressure data of the autoclave during the cure process is shown in Figure 22.
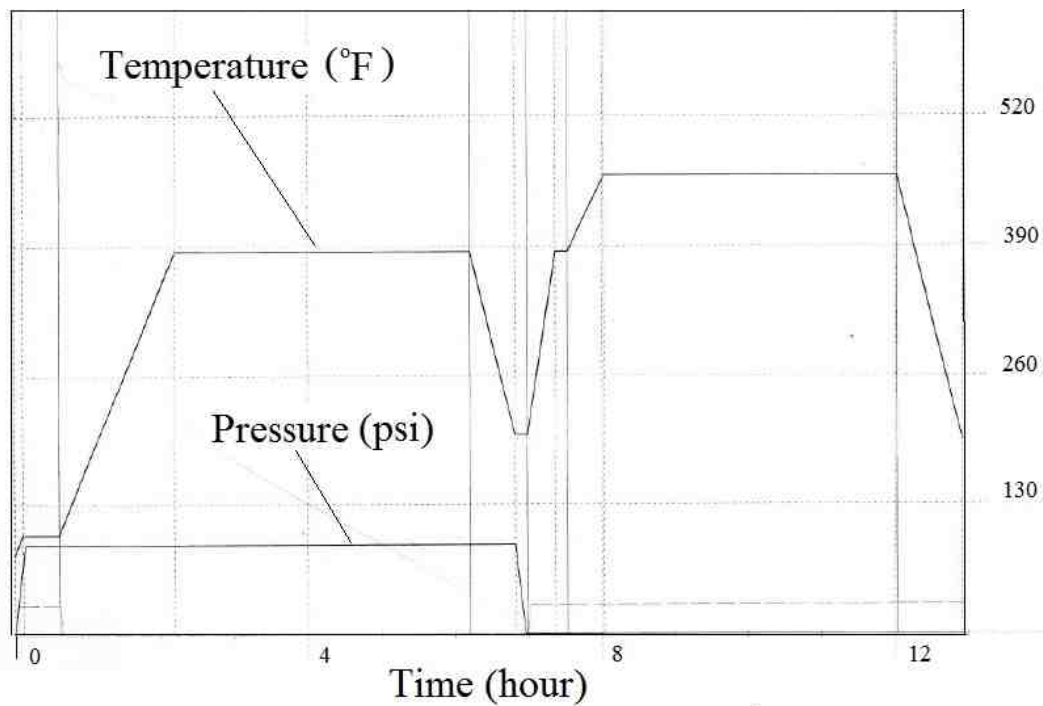


**Figure 21 - Graphical representation of the cure and postcure process programmed into the autoclave.**
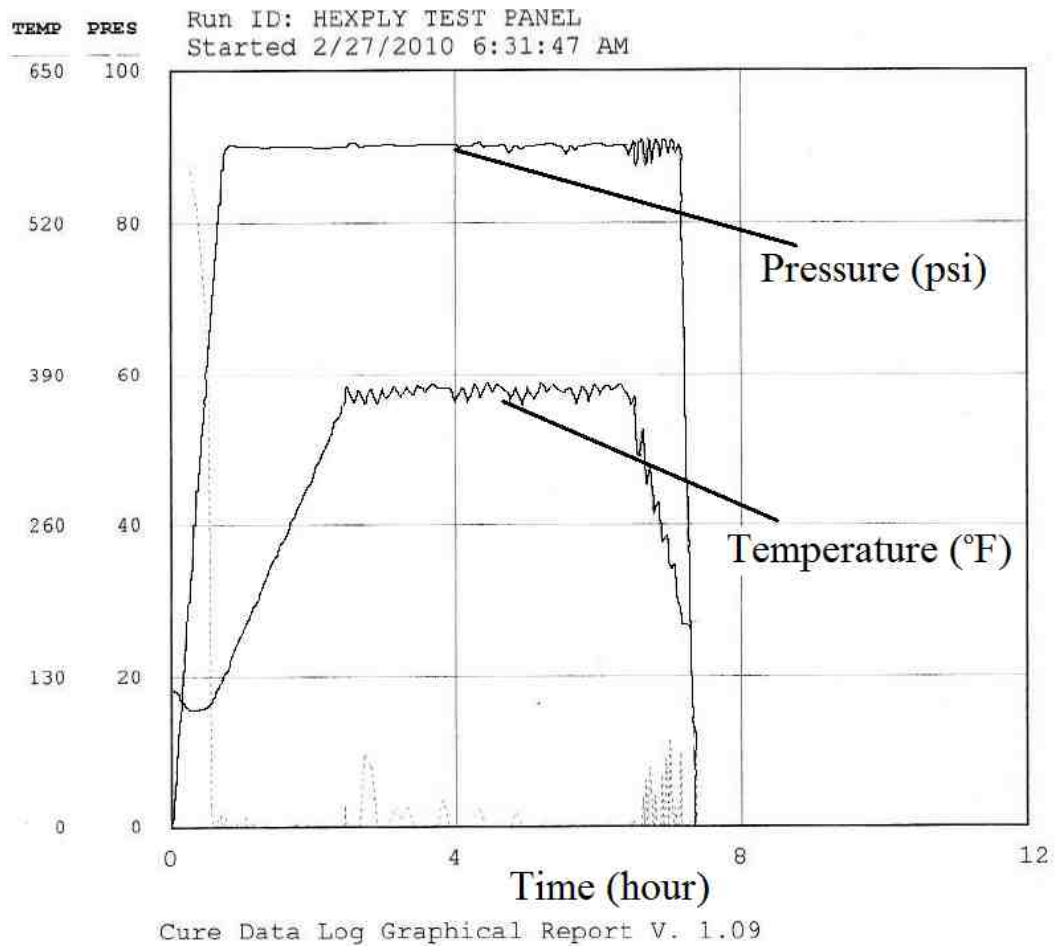
**Figure 22 - Actual temperature and pressure data recorded during the cure process of BMI/Quartz laminates.**

The full-size BMI/Quartz test panels are shown in Figure 23. At this point, the layup assembly has been completed and the panels are under vacuum prior to being placed in the autoclave.
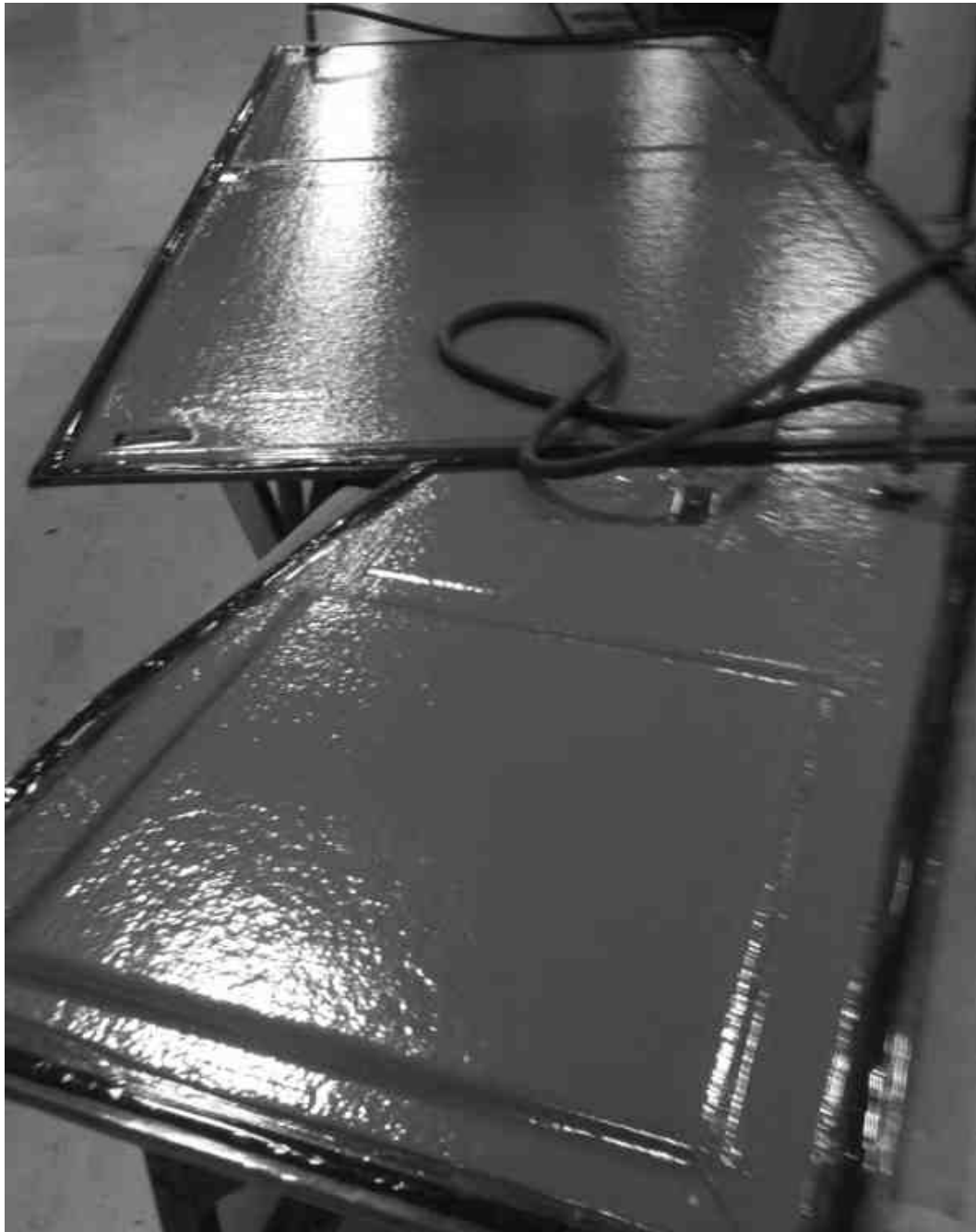
**Figure 23 - The original BMI/Quartz test panels under vacuum prior to being placed in the autoclave.**

*(5.3.3)      Sample Preparation*


 Individual test samples of multiple dimensions were cut from the original test

panels using a wet diamond saw, which is a typical machining method in a

composite manufacturing setting.  In order to more accurately quantify the

anisotropic diffusion characteristics of this material, samples of different planar

dimensions were machined from the original test panels. The approximate

dimensions of each sample used in this study are shown in Table 15. Once

machined to their final size, samples were marked according to the naming

convention *ply.aspect ratio.sample.* For example, the twelve-ply, 30 x 30 mm

samples were labeled *12.1.1* through *12.1.5.*  The twelve-ply, 30 x 30 mm and 40

x 20 mm samples are shown in Figure 24 after labeling and prior to environmental

conditioning.  A total of 20 six-ply samples, 15 twelve-ply samples, and 10 forty-

ply samples were machined. The six and twelve-ply samples are shown in Figure

25 prior to conditioning.
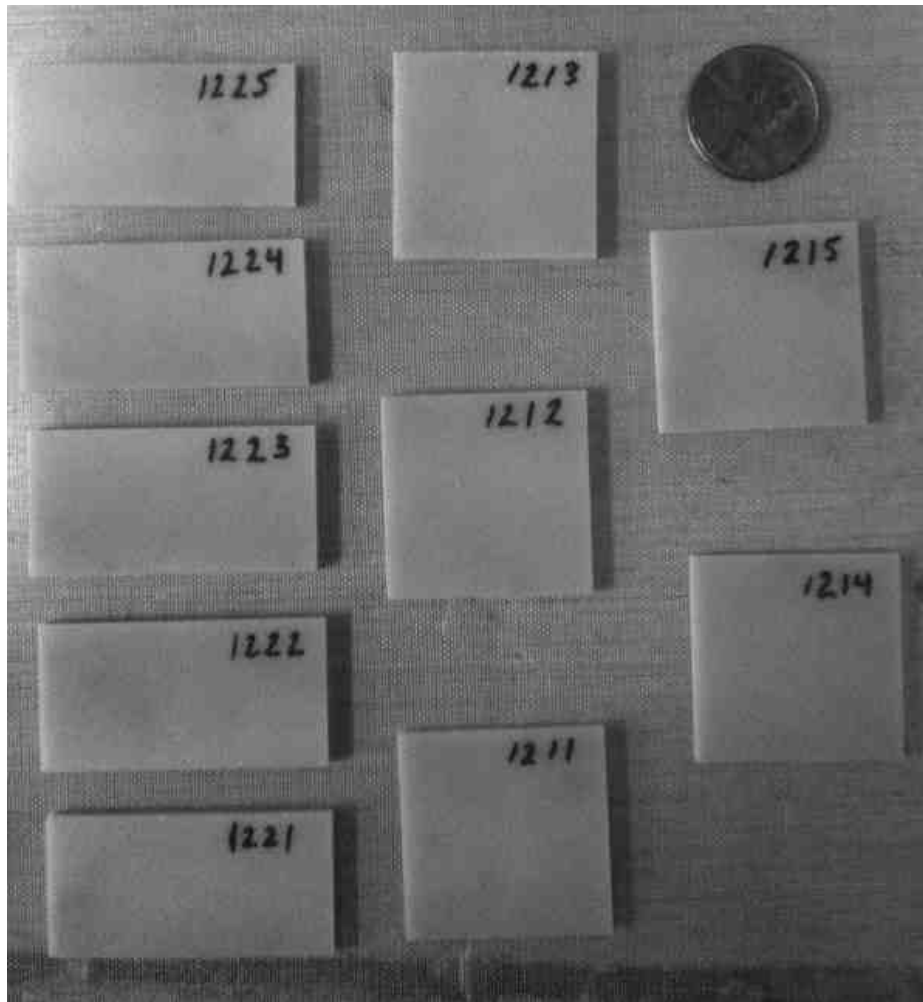
**Figure 24 - Twelve-ply samples used in gravimetric moisture absorption experiments. Sample dimensions of 40 x 20 mm and 30 x 30 mm are shown.**

**Figure 25 - Six and twelve-ply samples prior to moisture conditioning.**

**Sample dimensions shown, from left: six-ply 40 x 10 mm, six-ply**

**45 x 15 mm, six-ply 40 x 20 mm, six-ply 30 x 30 mm, twelve-ply 40**

**x 10 mm, twelve-ply 40 x 20 mm, and twelve-ply 30 x 30 mm.**

**Table 15 - Dimensions, ply-counts, and per-ply thickness of laminate samples**

**used in this study.**

|  | Planar Dimensions (mm) | | |
| --- | --- | --- | --- |
| Aspect Ratio | Six-ply | Twelve-ply | Forty-ply |
| 4 | 40 x 10 | 40 x 10 | 40 x 10 |
| 3 | 45 x 15 | - | - |
| 2 | 40 x 20 | 40 x 20 | - |
| 1 | 30 x 30 | 30 x 30 | 30 x 30 |
| Total Thickness | 1.34 | 2.63 | 10.6 |
| Per-ply Thickness | 0.223 | 0.219 | 0.264 |

Scanning electron microscopy (SEM) was used to investigate the structure of the laminates prior to moisture conditioning. The bundles of 9-micron quartz fibers are clearly visible under relatively low magnification.  The woven structure of the eight-harness satin weave is easily distinguishable in the curvature of the fiber bundle parallel to the edge as it travels over a fiber bundle perpendicular to the edge of the sample. This curvature is visible on the left side of the image shown in Figure 26, which depicts of the edge of a six-ply sample prior to immersion. All six plies are clearly visible in the image. In a similar manner, the fiber bundles perpendicular to the edge of the twelve-ply laminate are clearly visible under low magnification in Figure 27.

The darker areas in Figures 26 and 27 represent areas occupied solely by bismaleimide resin. In the six and twelve-ply laminates, these areas are relatively small and difficult to distinguish, which is indicative of lower resin content. In contrast, SEM images of the edges of the forty-ply laminates show a significantly higher ratio of resin-rich areas to fiber-reinforced areas. This is indicative of higher resin content, likely due to less compaction and resin flow during the cure process.
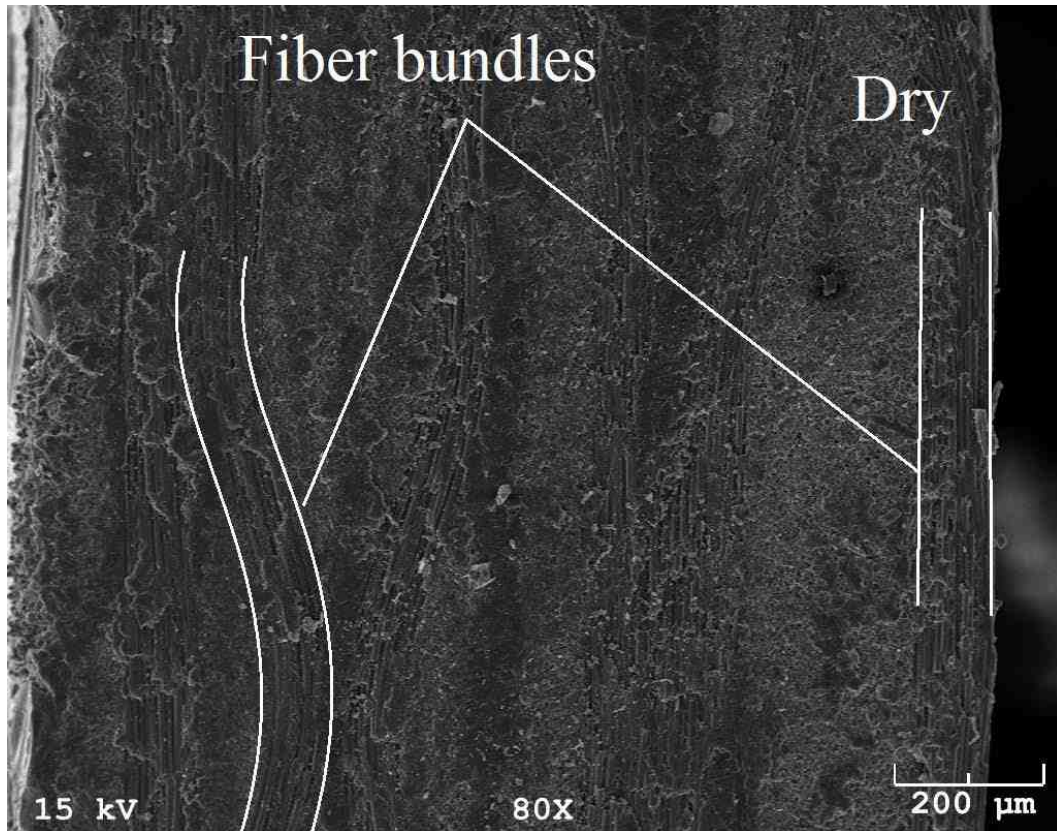
**Figure 26 - SEM image of edge of six-ply laminate prior to immersion,**

**illustrating fiber bundles parallel to laminate edge and**

**characteristic eight-harness satin weave structure.**
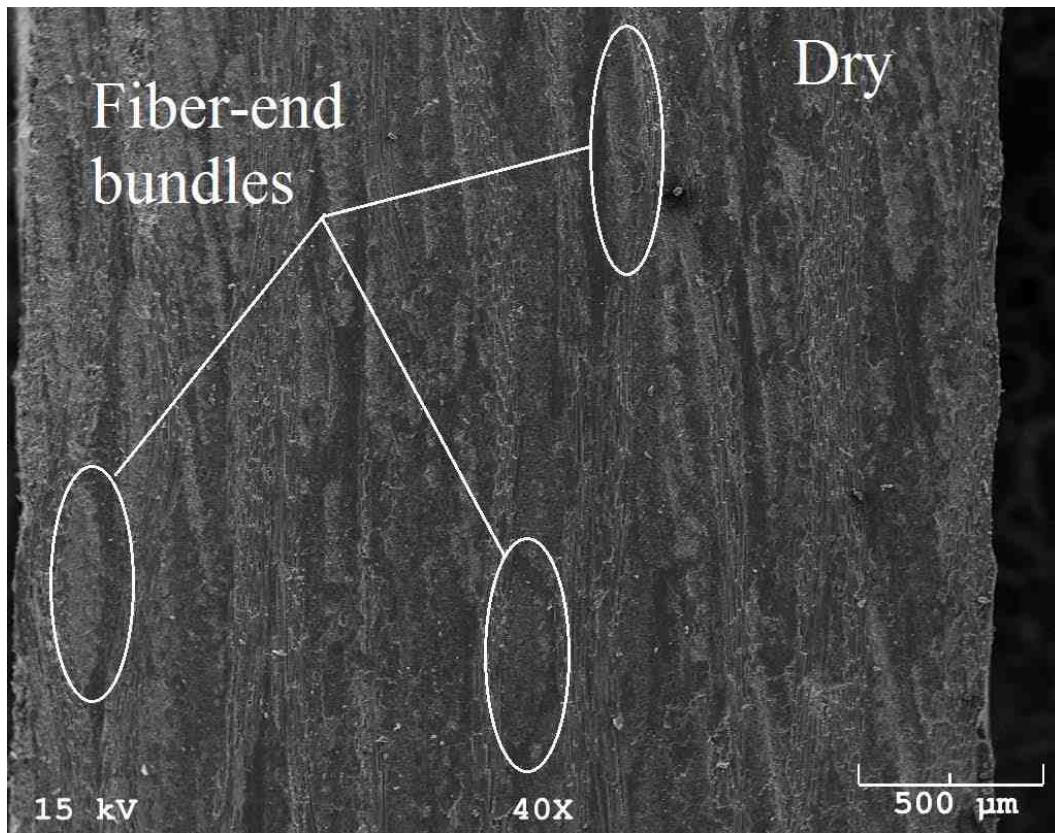
**Figure 27 – SEM image of edge of twelve-ply laminate prior to immersion, illustrating fiber end bundles perpendicular to laminate edge.**

Figure 29 illustrates a higher magnification image of the edge of a fiber bundle prior to immersion. While somewhat difficult to distinguish, the circular fiber ends are identifiable by their lighter color relative to the surrounding resin.
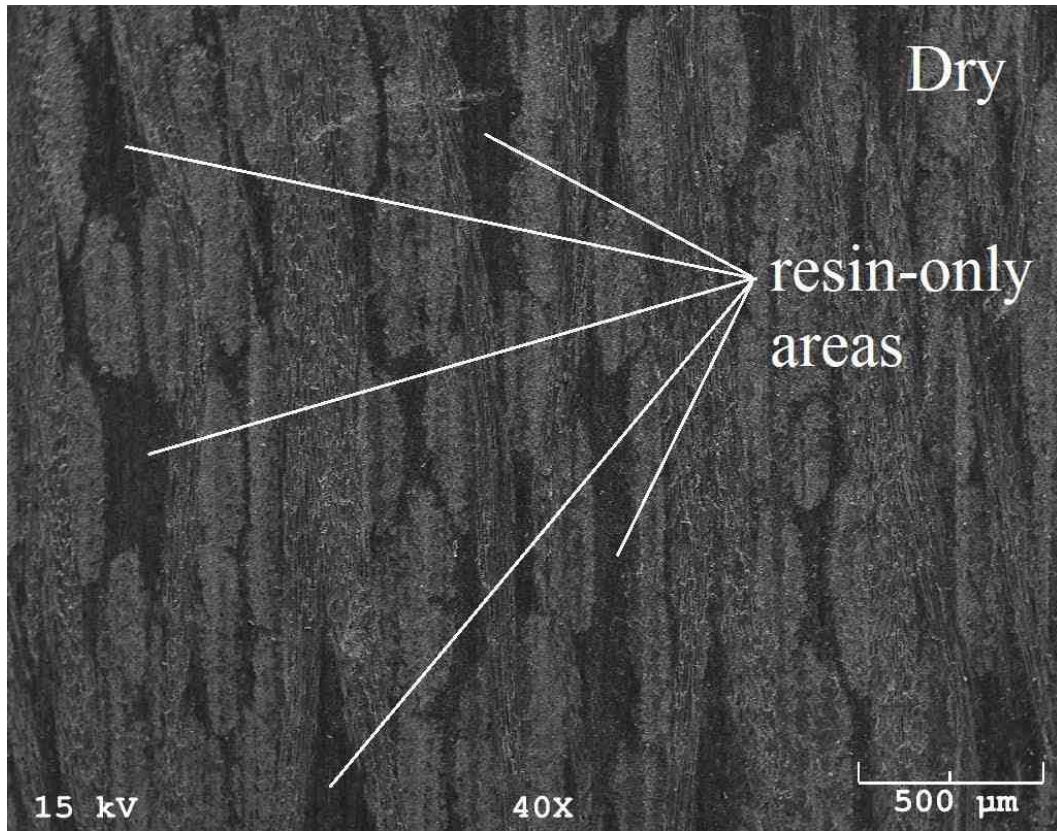
**Figure 28 – SEM image of edge of forty-ply laminate prior to immersion,**

**illustrating significant resin-rich areas without fiber**

**reinforcement.**
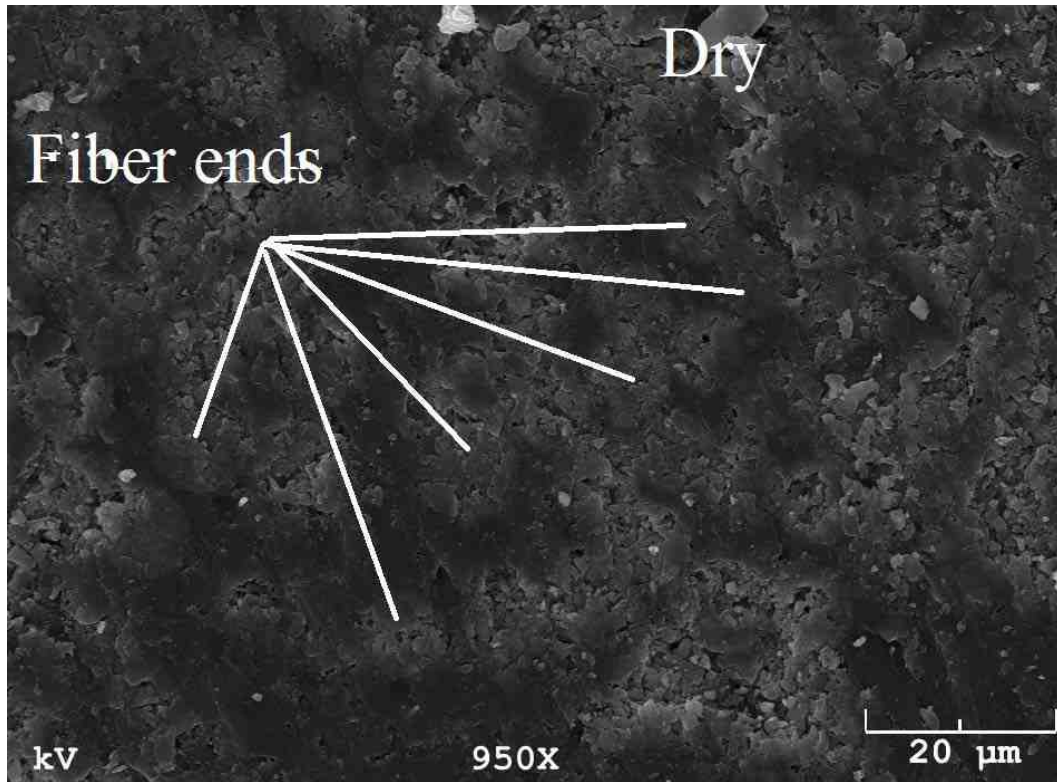
**Figure 29 – Fiber-end bundles of six-ply laminate prior to immersion at 950x magnification.**

*(5.3.4) Gravimetric Test Procedure*

Once machined to their final size, samples were dried in an oven at 90°C until a constant weight was achieved. Samples were then placed in an environmental chamber and maintained at 25°C and 100% relative humidity by full immersion in distilled water. Each of the 45 samples was immersed in an individual container in order to ensure full exposure to the distilled water on all sides. Samples were

removed from immersion, dried with a non-linting cloth to remove residual surface water, exposed to room temperature air for five minutes to allow for evaporation of any remaining surface water, and weighed with a high-precision analytical balance. The time required to dry and weigh the samples was subtracted from the moisture exposure time, and five samples were used for each specimen size in order to increase accuracy.  The weight change of each sample was calculated according to:

$$\frac{W - W_i}{W_i} \times 100\% \tag{125}$$

where $W$ is the weight of the specimen after absorption and $W_i$ is the initial, dry weight after desorption in the oven.

All gravimetric data reported in this study for a specific sample size is an average of all five samples with uncertainty levels calculated using 95% confidence interval. All average gravimetric data and the complete data from all five samples of a particular planar dimension are presented in graphical format in Appendix A.

### (5.3.5)  *Moisture Induced Damage*

SEM images of the edge of the laminate samples after 21 months of exposure to full immersion in 25°C water show slight evidence of material degradation in the

form of delamination and interfacial debonding. Surface microcracks were not observed in the samples viewed under the SEM. Inspection of the edge of the six-ply sample after 21 months showed no conclusive material degradation due to immersion.



Immersed

15 kV                    80X                    200 µm
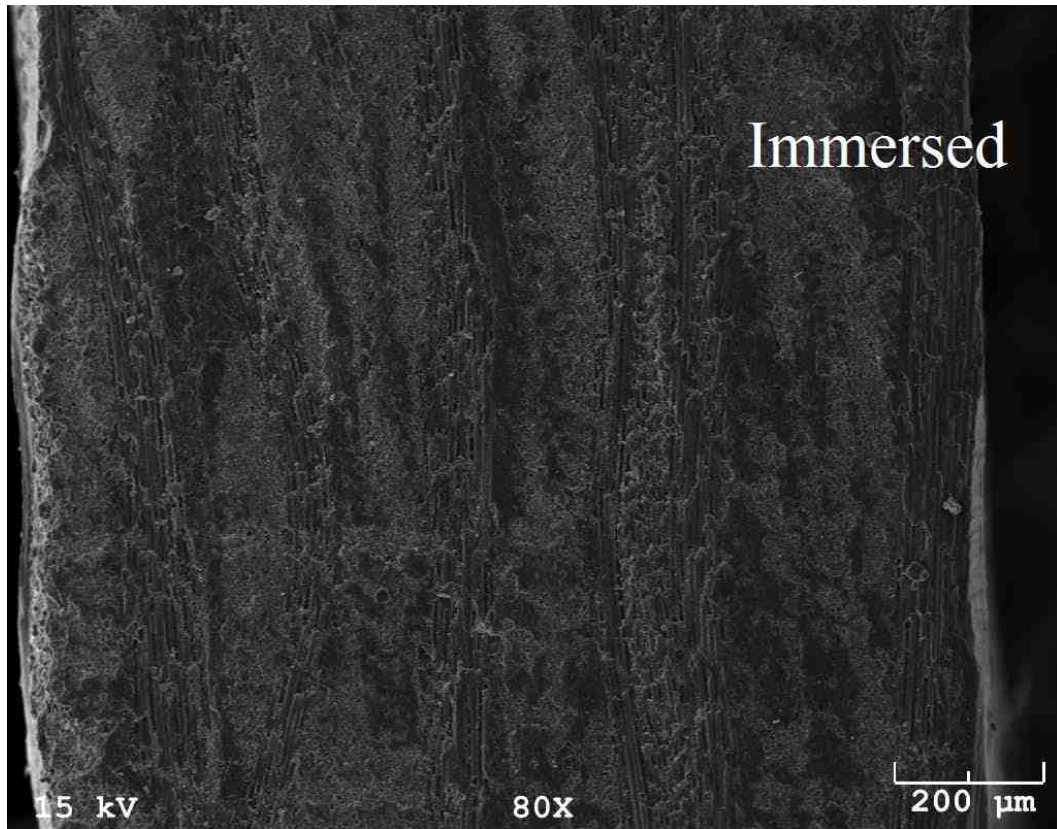
**Figure 29 – SEM image of six-ply laminate edge after 21 months of moisture exposure.**

The edge of a twelve-ply sample after immersion showed no obvious signs of microcracking or significant delamination. No visible gaps between plies were

observed, though some potential swelling of the resin-rich areas between plies seems to be visible on the right side of the sample in Figure 31.
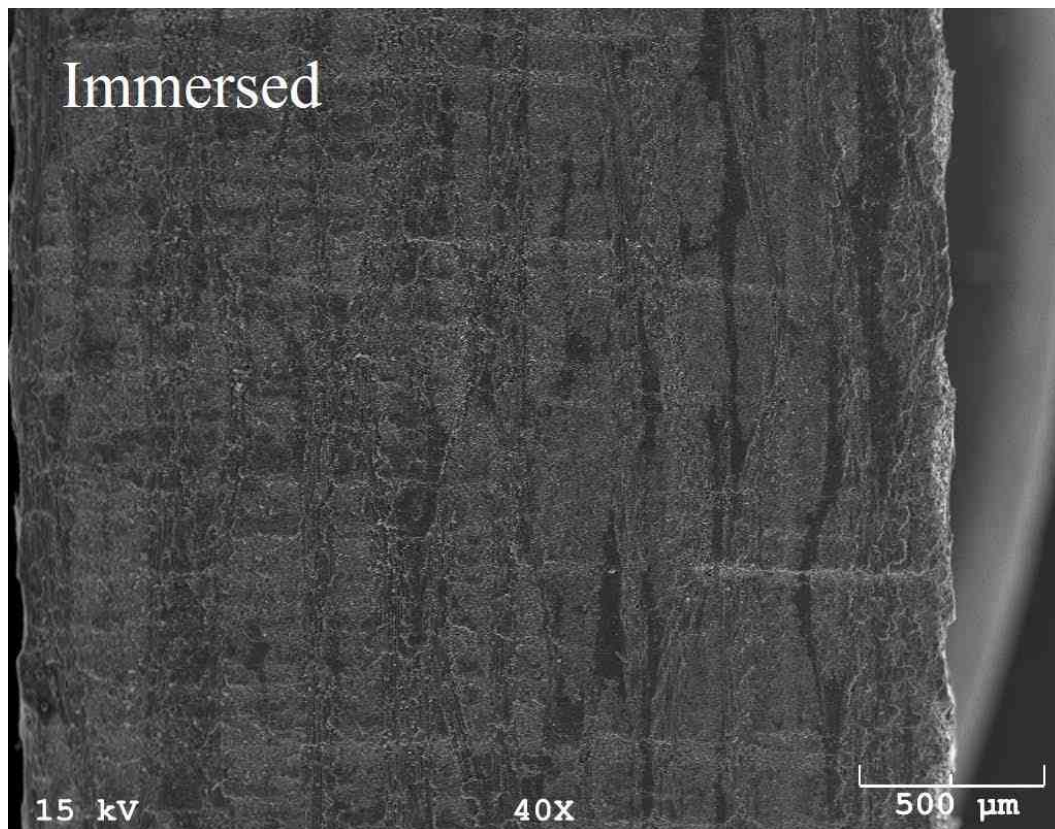


**Figure 31 - SEM image of twelve-ply laminate edge after 21 months of moisture exposure.**

The lower resin flow observed in the 40-ply samples, as evidenced by the increased resin content and per-ply thickness, likely caused a less cohesive bond between some of the individual plies. As a result, two separate forty-ply samples showed evidence of slight delamination in the resin-rich area between plies. This

can be seen in the form of a darker line, which is a gap between plies, in Figures

32 and 33.
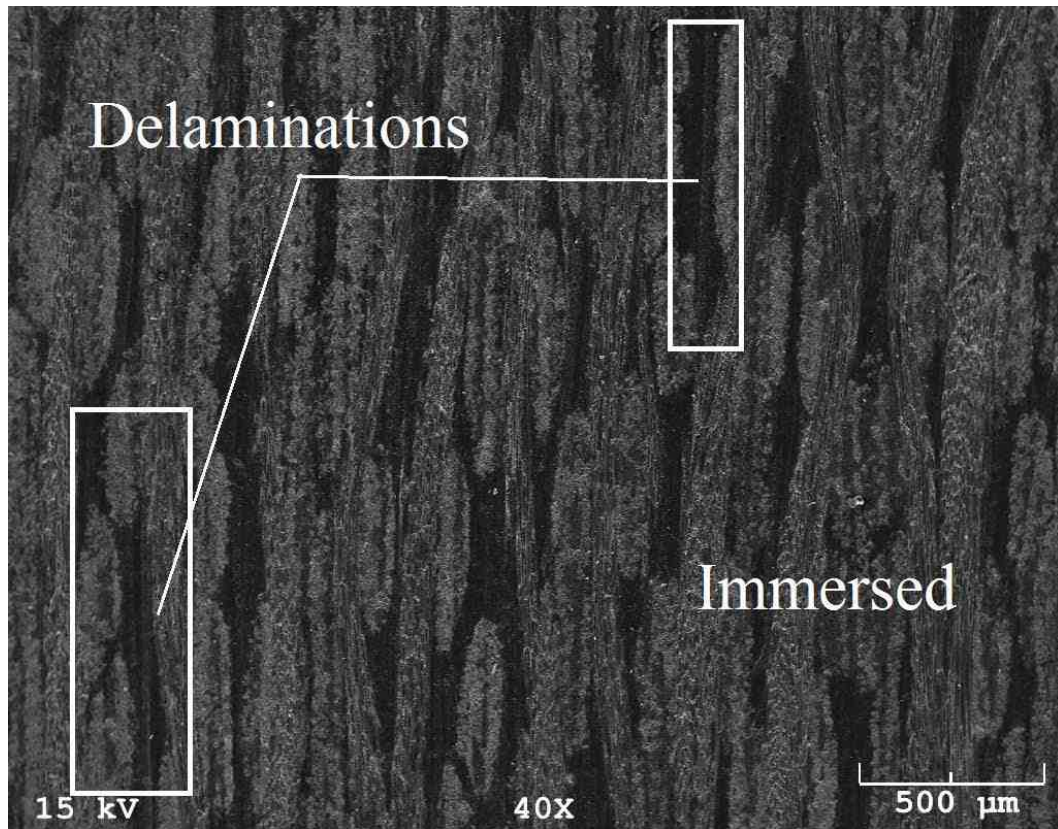


**Figure 32 - SEM image of forty-ply laminate edge after 21 months of**

**moisture exposure, showing evidence of slight delamination**
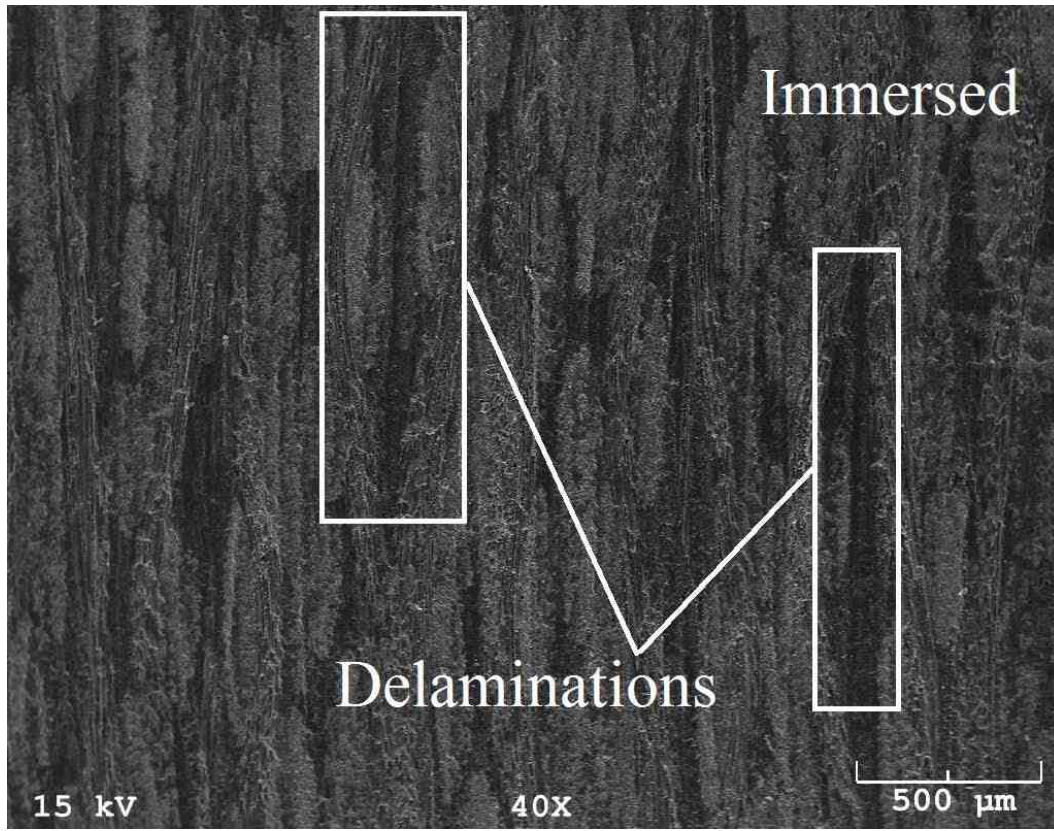
**between plies.**

**Figure 33 - SEM image of additional forty-ply laminate edge after 21 months of moisture exposure, showing further evidence of slight delamination between plies.**

A higher magnification image of the fiber ends of the twelve-ply sample after immersion appears to suggest some interfacial debonding. It is difficult to conclusively correlate the gap between fiber and matrix with immersion in water, as the cutting and polishing process may produce similar artifacts. It is worth nothing, however, that similar interfacial debonding was not observed in the dry samples. Additionally, debonding does not appear to be directional in this high-magnification image, which would be indicative of cut or polish-induced artifacts.

In other words, debonding is visible around the entire circumference of the fibers, much like the SEM images of fiber/matrix debond in Ref. [23].
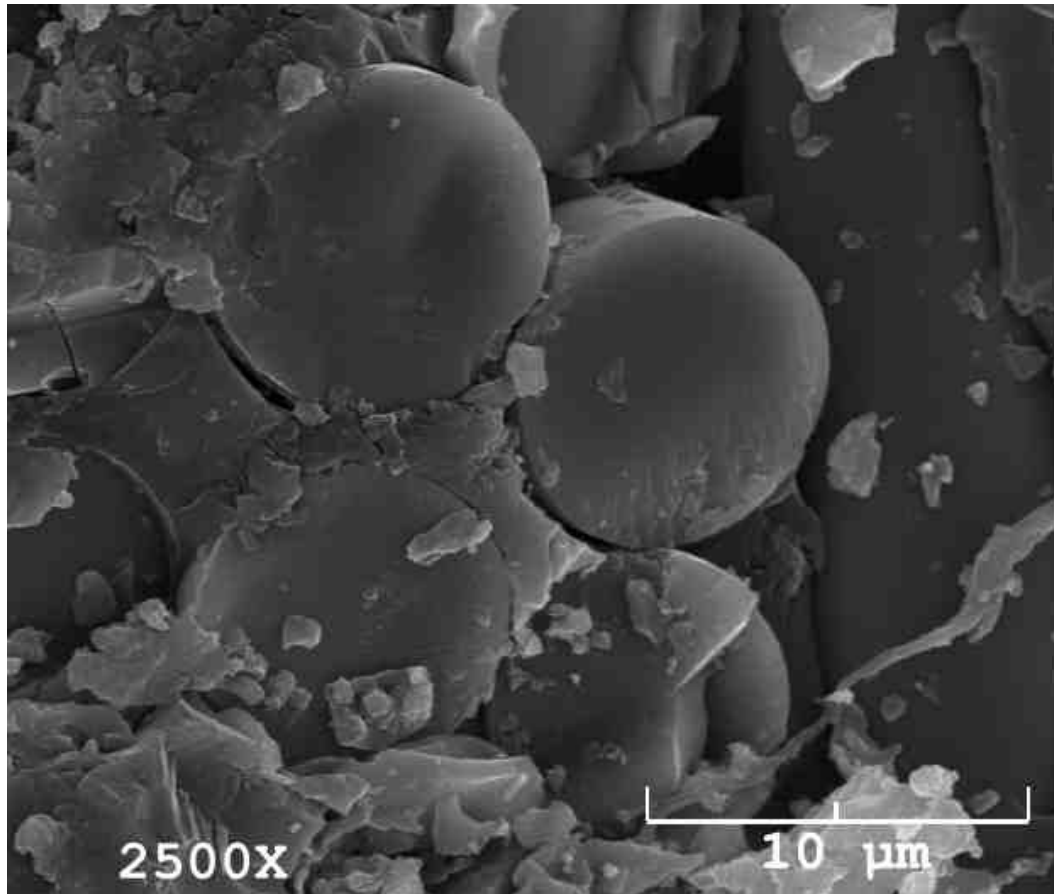


**Figure 34 – SEM image of fiber ends of twelve-ply laminate edge at 2500x magnification showing debond between fiber and matrix, potentially as a result of moisture exposure.**

### (5.4)   Modeling BMI/Quartz Laminate

### Moisture Absorption Behavior

Based on existing BMI moisture absorption studies, the moisture absorption behavior was not expected to conform to typical Fickian diffusion behavior [38-39, 44]. Therefore, the three-dimensional anisotropic hindered diffusion model (3D HDM) developed in Chapter 3 was chosen to represent the moisture absorption behavior. The 3D HDM is a comprehensive model that has the capability to predict three-dimensional anisotropic moisture diffusion while incorporating varying degrees of Fickian or non-Fickian behavior.  In this model, the concentration at time $t$ and position $x$, $y$, and $z$ satisfies the coupled pair of equations

$$D_x \frac{\partial^2 n}{\partial x^2} + D_y \frac{\partial^2 n}{\partial y^2} + D_z \frac{\partial^2 n}{\partial z^2} = \frac{\partial n}{\partial t} + \frac{\partial N}{\partial t}$$

(126)

$$\frac{\partial N}{\partial t} = \gamma n - \beta N$$

where $n$ represents the mobile molecules per unit volume, $N$ represents the bound molecules per unit volume, $\gamma$ is the probability per unit time that a mobile molecule will become bound, $\beta$ is the probability per unit time that a bound molecule will become mobile, and $D_x$, $D_y$, $D_z$ are diffusivities in the three principal directions.

Assuming an initially dry slab of dimensions $h$ x $w$ x $l$, the boundary and initial conditions are given by Equations (48-49) in Chapter 3. The analytical mass gain function of the 3D HDM developed in Chapter 4 is given by

$$\frac{M(t)}{M_\infty} = 1 - \frac{512\mu}{\pi^6} \sum_{P=0}^{\infty} \sum_{Q=0}^{\infty} \sum_{R=0}^{\infty} \frac{1}{(2P+1)^2 \, (2Q+1)^2 \, (2R+1)^2} e^{-\alpha t}$$

$$- (1-\mu)e^{-\beta t}$$

where,                                                                                                          (127)

$$\alpha = \pi^2 \left( \frac{D_x}{l^2} (2P+1)^2 + \frac{D_y}{w^2} (2Q+1)^2 + \frac{D_z}{h^2} (2R+1)^2 \right)$$

$$\mu = \frac{\beta}{\gamma + \beta}$$

where $M(t)$ is the weight of absorbed moisture at time $t$ given an equilibrium moisture weight percent, $M_\infty$, and $\mu$ is the diffusion hindrance coefficient. The analytical mass gain function is subject to the condition given in Equation (121), which is satisfied for most polymeric composites.

The 3D HDM was applied to the experimental data using least-squares regression, which involved the minimization of

$$E(t) = \sum_i^n \left[ M_i(t) - M_{\text{exp}_i}(t) \right]^2$$                                              (128)

where $M(t)$ is the theoretical moisture content predicted by the 3D HDM and $M_{\exp}(t)$ is the experimentally determined moisture content. The six model parameters (i.e., $D_x$, $D_y$, $D_z$, $\gamma$, $\beta$, $M_\infty$) that minimize the function given in Equation (128) are determined by using a slightly modified version of the method of steepest descent as in Chapter 4.

In order to compared the accuracy of the 3D HDM to the 3D Fickian model as applied to the experimental data, both are shown in Figure 35. The experimental moisture absorption data exhibits a definite "pseudo-equilibrium" at which moisture weight percent does not deviate more than 0.01% for over 100 days. Such behavior has the potential to cause premature termination of gravimetric measurements, on the assumption that the moisture absorption is Fickian in nature and equilibrium has been reached. In fact, the experimental gravimetric data easily meets the requirements for equilibrium as defined in ASTM D5229 [76]. The ASTM specification requires two consecutive measurements within a maximum time period of seven days which do not change by more than 0.01% moisture weight percent. In this case, seven consecutive measurements over more than 100 days conform to this requirement. Moisture equilibrium determination per ASTM D5229, therefore, yields a maximum moisture content of 1.38% as shown in Figure 35.
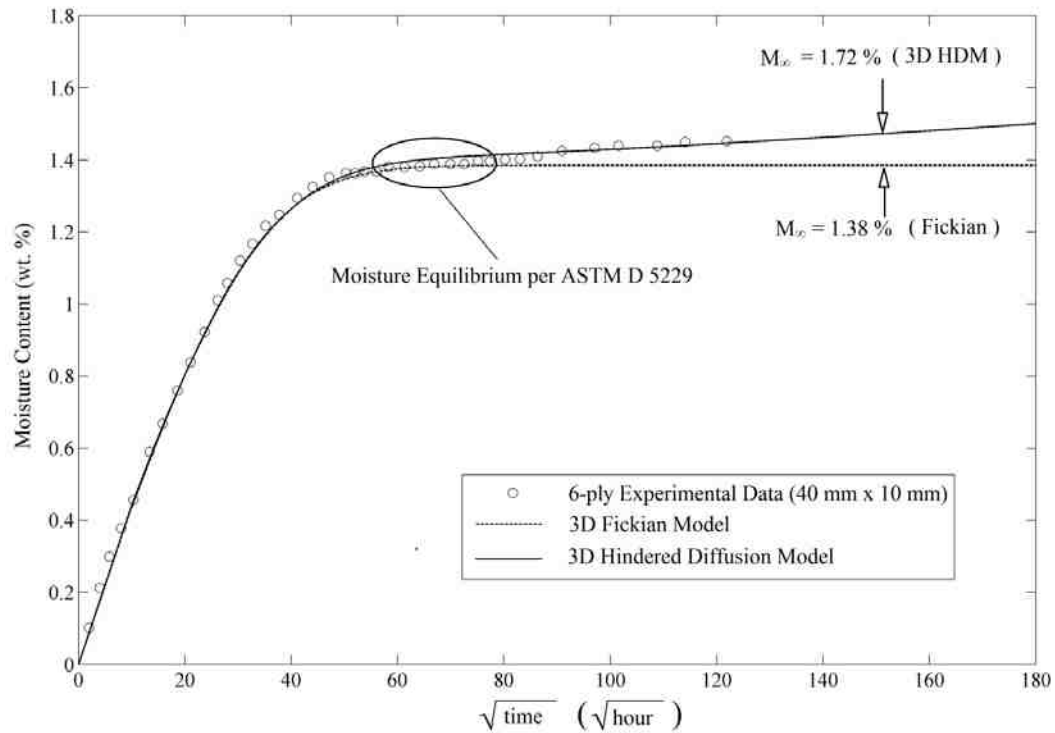
**Figure 35 – Applicability of three-dimensional hindered diffusion model to experimental data, compared to Fickian equilibrium as defined by ASTM D5229.**

### (5.5)    Recovering 3D HDM Parameters from Experimental Data

In an effort to predict the diffusion properties of the BMI/quartz laminate, three separate sets of gravimetric data were used to recover the 3D HDM parameters. Each data set included gravimetric data from two samples of the same ply-count (six, twelve, or forty-ply) but different planar dimensions, which were simultaneously fit to the 3D HDM using least-squares regression.  The diffusion

behavior was assumed to be orthotropic, based on the orthotropic nature of the fiber reinforcement. Therefore, five parameters were recovered using the least-squares method: through-thickness diffusivity ($D_z$), edge diffusivity ($D_e = D_x = D_y$), probability of a mobile molecule becoming bound ($\gamma$), probability of a bound molecule becoming mobile ($\beta$), and equilibrium moisture content ($M_\infty$). The quality of the fit was measured by calculating the root-mean squared (RMS) error of the predicted moisture content relative to the experimental gravimetric data. In order to eliminate any dependence of the recovered parameters on initial estimates, multiple initial guesses are used for each parameter. For our purposes, accuracy is assumed when the recovered value of a parameter does not vary more than one percent regardless of the initial estimate.

The six-ply data set included gravimetric data from the 40 x10 mm and 40 x 20 mm samples. The least-squares curve fit to the 3D HDM yielded the parameters shown in Table 16. The RMS error between the prediction and the experimental data is 2.5 x $10^{-3}$ and 3 x $10^{-3}$ for the 40 x 10 mm and 40 x 20 mm samples, respectively. The experimental data and the corresponding 3D HDM predictions are shown in Figure 36. The quality of the prediction is excellent for both sample dimensions.

The recovered hindered diffusion parameters from the twelve-ply data set are shown in Table 16. A slightly higher equilibrium moisture content and edge

diffusivity are recovered relative to the six-ply samples. The twelve-ply data set

again included gravimetric data from the 40 x10 mm and 40 x 20 mm samples,

and yielded RMS errors of 2.4 x $10^{-3}$ and 3.2 x $10^{-3}$, respectively. The

experimental data and the corresponding 3D HDM predictions are shown in

Figure 37.  Again, the quality of the prediction is excellent for both sample sizes.

**Table 16 - 3D HDM parameters recovered from each of three experimental**

**data sets.**

|  | Six-ply | Twelve-ply | Forty-ply |
|---|---|---|---|
| $D_e$ (mm$^2$/hour) | 1.98 x $10^{-3}$ | 2.89 x $10^{-3}$ | 4.07 x $10^{-3}$ |
| $D_z$ (mm$^2$/hour) | 1.73 x $10^{-4}$ | 1.47 x $10^{-4}$ | 3.12 x $10^{-4}$ |
| $\gamma$ | 2.98 x $10^{-6}$ | 1.22 x $10^{-6}$ | 2.3 x $10^{-5}$ |
| $\beta$ | 1.25 x $10^{-5}$ | 6.64 x $10^{-6}$ | 4.7 x $10^{-5}$ |
| $\mu$ | 0.807 | 0.844 | 0.671 |
| $M_\infty$ (%) | 1.72 | 1.69 | 1.84 |

**Figure 36 - Experimental gravimetric data and corresponding 3D HDM predictions for six-ply laminate samples of 40 x 10 mm and 40 x 20 mm planar dimensions.**

**Figure 37 - Experimental gravimetric data and corresponding 3D HDM predictions for twelve-ply laminate samples of 40 x 10 mm and 40 x 20 mm planar dimensions.**

The longer times required to reach equilibrium moisture content for very thick samples, such as the forty-ply samples used in this study, resulted in experimental data that is further from reaching equilibrium. Therefore, the least-squares curve fit to the third data set, the experimental data from the two forty-ply sample sizes, exhibits a slight dependence on the initial estimates. Therefore, initial estimates were set according to the parameters recovered from the twelve-ply experimental data. The best fit was obtained for equilibrium moisture content of 1.84 %, which

is considerably higher than the values obtained for the six and twelve-ply samples. The recovered parameters (See Table 16) yield an excellent fit to the data, as evidenced by RMS error of 2.4 x $10^{-3}$ and 2 x $10^{-3}$ for planar dimensions of 40 x 10 mm and 30 x 30 mm, respectively. The quality of the prediction as applied to the experimental data is shown in Figure 38.
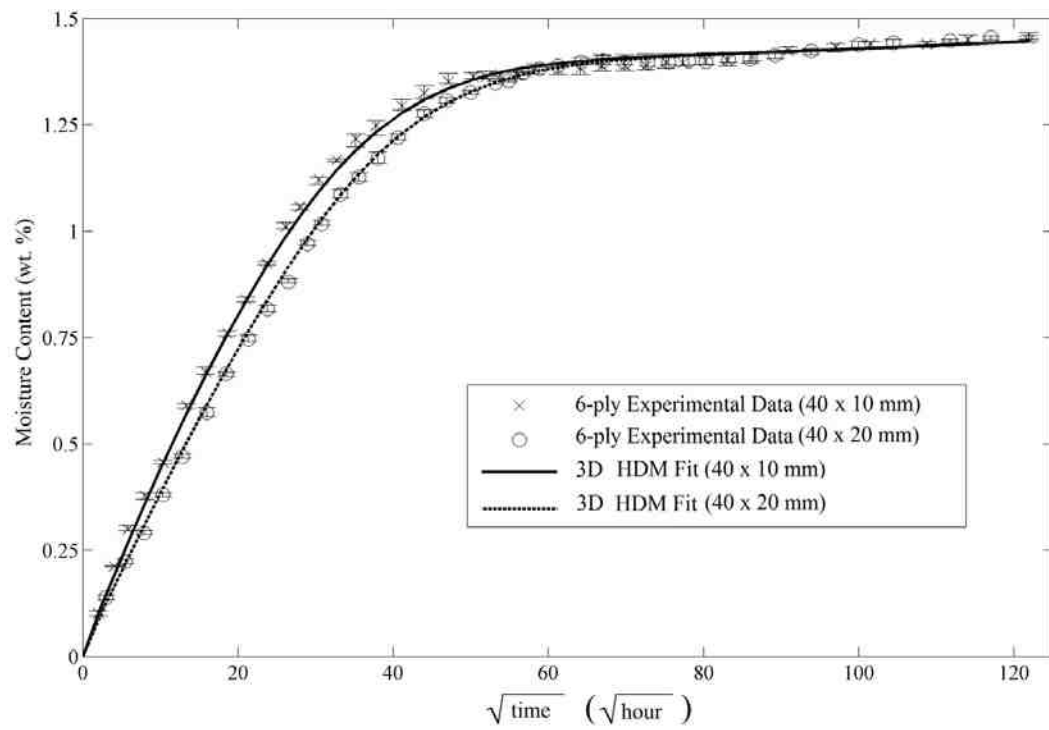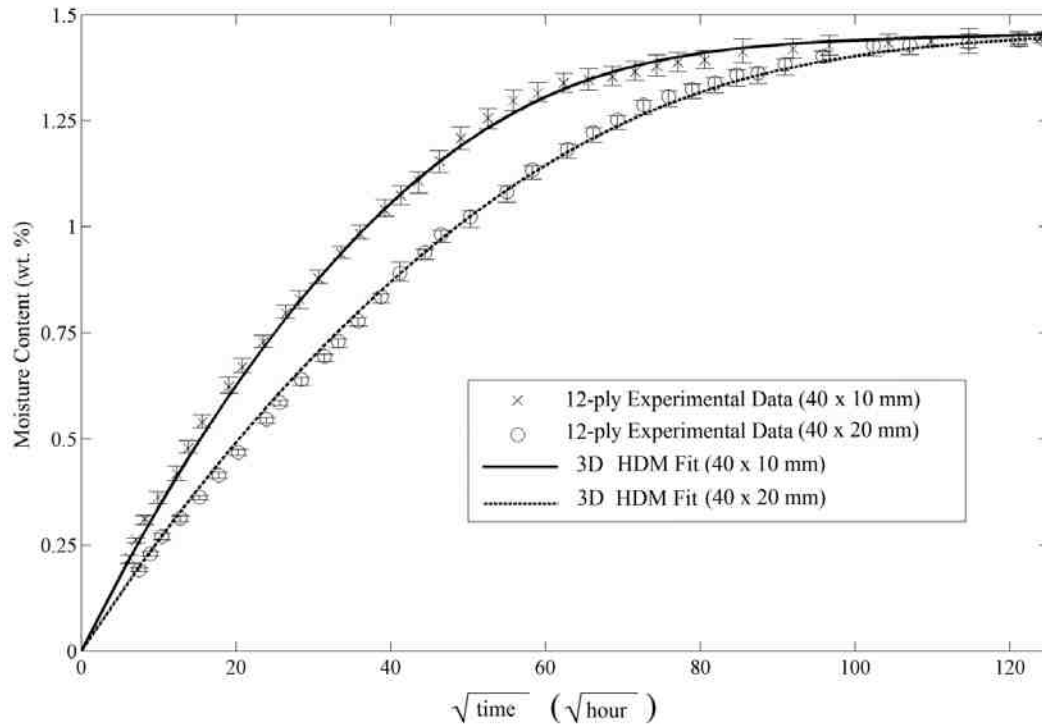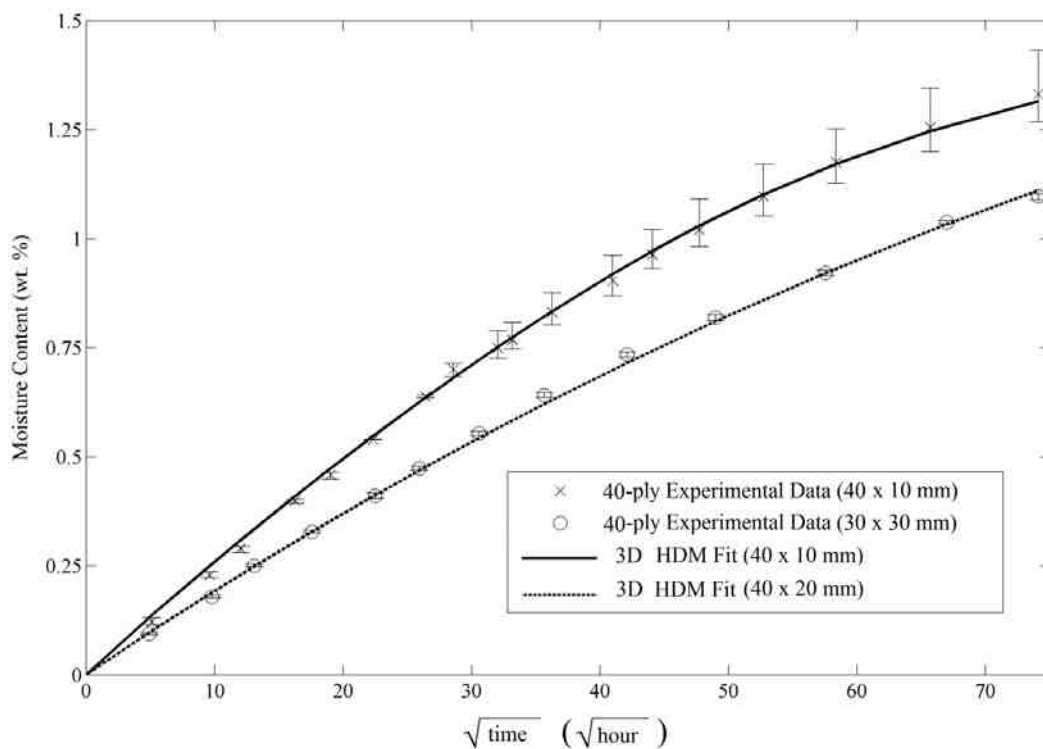


**Figure 38 – Experimental gravimetric data and corresponding 3D HDM predictions for forty-ply laminate samples of 40 x 10 mm and 30 x 30 mm planar dimensions.**

The relationship between the recovered edge and through-thickness diffusivity further highlights the importance of including three-dimensional anisotropic diffusion effects in any comprehensive model of moisture absorption in polymeric composites. Diffusion through the edges of the laminate (along the fiber) proceeds at 11.4, 19.7, and 13 times faster than through the thickness (transverse to the fiber) for the six, twelve, and forty-ply samples, respectively. These values are basically consistent with those reported for other materials in the literature. Blikstad [60], for example, observed a ten-fold increase in diffusion through the edges of a graphite/epoxy laminate relative to through-thickness diffusion. In addition, Aronhime et al. studied the anisotropic moisture absorption behavior of unidirectional Kevlar/epoxy and found that the ratio of diffusion along the fiber to diffusion transverse to the fiber varied from 3 to over 100, depending on the fiber volume fraction [61]. The contribution of moisture absorption into the Kevlar fiber itself was assumed to play a role. In addition, Arao et al. report edge diffusivities between 2 and 4 times greater than through-thickness diffusivity for a woven carbon-fiber reinforced epoxy laminate [62].

The separate recovery of 3D HDM parameters for each laminate thickness highlights the effect of laminate construction on diffusion properties. Despite simultaneous layup, cure, and post-cure under identical conditions, variations exist depending on the ply-count which are apparent in the recovered diffusion parameters. Variations in the recovered diffusion properties may be the result of

different fiber volume fractions and void content, or the existence of degree of cure gradients within thick laminates.

One of the most likely contributors to the variation in diffusion properties according to laminate thickness is the fiber volume fraction as measured by the average ply thickness for each sample. The six, twelve, and forty-ply samples have an average thickness of 1.34, 2.63, and 10.55 mm, respectively. Therefore, the average per-ply thickness for the six, twelve, and forty-ply laminates is 0.223, 0.219, and 0.264 mm, respectively (see Table 15). This higher resin content in the forty-ply samples is consistent with what was observed in the SEM image in Figure 28. These variations in per-ply thickness exist despite the simultaneous cure of all three laminates under the same conditions. The specific gravity reported by the manufacturer of 1.78 is consistent with the six and twelve-ply samples, which have an average specific gravity of 1.75 and 1.77, respectively. The forty-ply samples, however, have an average specific gravity of 1.69, which is indicative of higher resin content. The higher predicted equilibrium moisture content of the forty-ply laminate, therefore, is to be expected. The quartz fibers are assumed to be impermeable, and all absorbed moisture is contained within voids, the fiber/matrix interface, or the resin itself. Not surprisingly, the predicted equilibrium moisture content for the six, twelve, and forty-ply laminates correlates well to the per-ply thickness, which is related to the resin content. The highest per-ply thickness and highest equilibrium moisture content is observed in

the forty-ply laminate. The lowest per-ply thickness and lowest equilibrium moisture content is seen in the twelve-ply laminate. The six-ply laminate has a slightly higher per-ply thickness relative to the twelve-ply laminate, in addition to slightly higher equilibrium moisture content.

In addition to different fiber volume fractions, temperature gradients that develop during the cure process of thick composites may lead to variations in the degree of cure throughout the thickness of the laminate [84]. A number of studies have been performed on the variation in the degree of cure of thick polymer composites due to the existence of temperature gradients [84-89]. Additionally, thick laminates may experience internal temperatures exceeding the cure temperature due to the exothermic cross-linking reactions of the polymer. In some cases, this internal temperature may reach levels that are likely to induce degradation of the polymer matrix [89]. These variations in the structure of the polymer through the thickness of the laminate may contribute to changes in diffusivity as thickness increases. Specific studies on this phenomenon are very limited. However, the degree of cure and crosslink density was found to influence the moisture absorption properties of an epoxy in a study performed by Perrin [90]. Specifically, a fully cross-linked epoxy network was found to absorb more water and at a faster rate than a less cross-linked network.

Variation in the recovered probabilities of molecular binding and unbinding based on the laminate thickness is also observed. However, the diffusion hindrance coefficient is relatively consistent, ranging from 0.67 to 0.84 with an average value of 0.79. A hindrance coefficient of unity indicates Fickian diffusion, in which mobile molecules are free to diffuse by random molecular motion. A lower hindrance coefficient indicates a greater degree of disruption of the diffusion of mobile molecules. In this case, the recovered hindrance coefficient of 0.67 indicates that moisture absorption in the forty-ply laminates is more hindered than in the other laminate sizes. However, the recovered values are consistent with hindered diffusion reported in BMI resins. Li et al., for example, report $\gamma$ and $\beta$ values corresponding to hindrance coefficients of 0.78, 0.80, 0.83, and 0.88 depending on post-cure temperature and exposure temperature [44]. The hindrance coefficient may also be influenced by any changes in the structure of the polymer as a result of a temperature gradient during the cure cycle. Kumosa et al. [26] suggest a correlation between sample thickness and the values of $\gamma$ and $\beta$ for moisture absorption of a unidirectional glass-reinforced polymer composite exposed to 80% relative humidity at 50°C. The extent of laminate compaction during the cure process that led to different per-ply thickness likely contributes to the change in hindrance coefficient. The lower resin flow and higher resin content observed in the forty-ply laminate may lead to changes in the structure of the polymer, such as increased microvoids. This non-homogenous structure may contribute to the increased diffusion hindrance in the forty-ply laminate. In

145

addition, changes in the polymer structure due to degree of cure gradient may contribute to increased diffusion hindrance.

## (5.6) Application of Recovered Diffusion Parameters to Samples of Different Planar Dimensions

The ability of the three-dimensional hindered diffusion model to capture the moisture absorption behavior of two samples of the same ply-count and different planar aspect ratio was demonstrated in the previous section. In order to further validate the recovered diffusion parameters and the applicability of the 3D HDM to the moisture absorption behavior of the laminates, the parameters were applied to gravimetric data to samples not included in the least-squares curve fit. In this way, we can establish the ability to apply parameters recovered from two laminate sizes to other laminates of the same thickness but different planar dimensions.

Additional gravimetric data from six-ply samples of 45 x 15 mm and 30 x 30 mm planar dimensions and twelve-ply samples of 30 x 30 mm planar dimensions were not used in the curve-fit process for either ply-count. The recovered six-ply parameters were applied to the two other six-ply sample sizes, 45 x 15 mm and 30 x 30 mm, with only slightly higher RMS error of $3.9 \times 10^{-3}$ and $3.5 \times 10^{-3}$, respectively, when compared to the gravimetric data from the 40 x 10 mm and 40 x 20 mm sample sizes. In addition, the twelve-ply parameters were applied to the

gravimetric data from the twelve-ply 30 x 30 mm sample with excellent

agreement. The RMS error in this case was 3.7 x $10^{-3}$, again only slightly higher

than the error associated with the gravimetric data used in the curve-fit process.

The gravimetric data from the two six-ply samples and one twelve-ply sample are

shown in Figure 39, along with the corresponding 3D HDM predictions.

The applicability of the recovered parameters from samples of one thickness to

samples of a different thickness was also investigated. Based on the differences in

the laminate physical properties, it is assumed that the recovered model

parameters will only be applicable to laminates of the same ply-count. The 3D

HDM parameters recovered using data from six-ply samples were used in an

attempt to predict moisture absorption behavior in the twelve and forty-ply

samples. The average RMS error of the six-ply 3D HDM prediction relative to the

six-ply experimental data is 3.2 x $10^{-3}$. Applying those parameters to the twelve-

ply experimental data yields an average RMS error of 8.1 x $10^{-3}$, over 250%

higher. Further, applying those parameters to the forty-ply experimental data

yields an average RMS error of 34.6 x $10^{-3}$, over 10 times higher than the error

associated with the fit to the six-ply data.
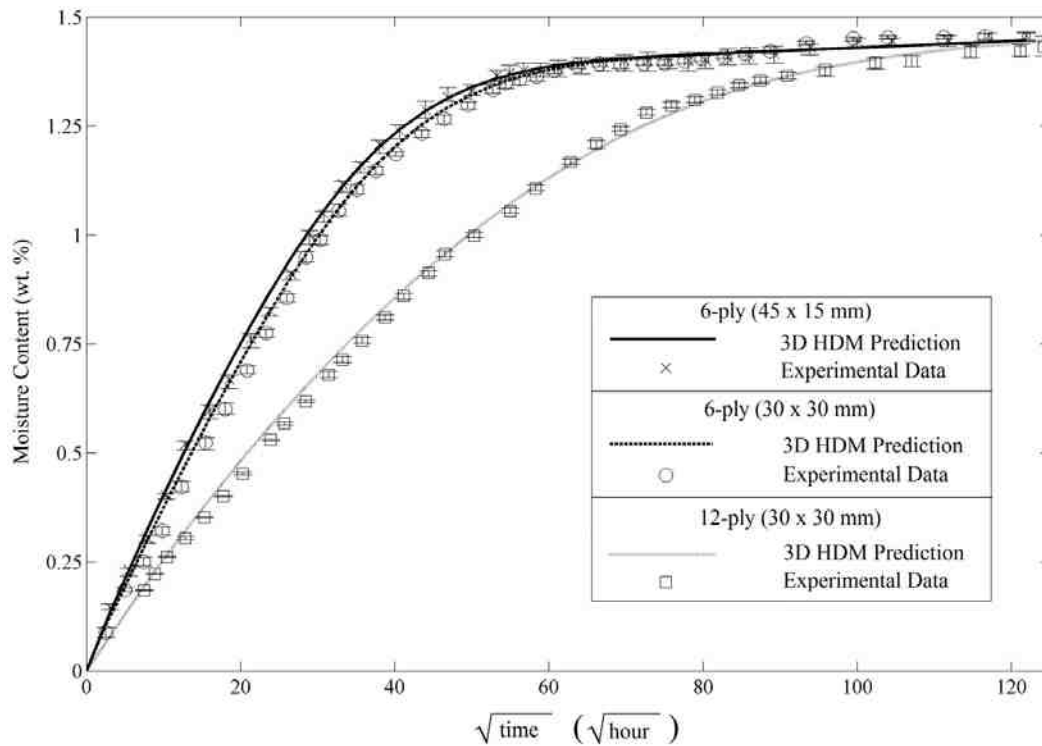
**Figure 39 – Application of recovered 3D HDM parameters to gravimetric data from samples not used in the least-squares regression process.**

The 3D HDM parameters recovered using only experimental data from the six-ply samples are applied to twelve-ply experimental data from 40 x 10 mm samples in Figure 40. The error between the prediction and the experimental data demonstrates the failure of this set of parameters to predict moisture absorption behavior of the thicker samples.

**Figure 40 - 3D HDM parameters recovered using only experimental data from the six-ply samples applied to six, twelve, and forty-ply experimental data from 40 x 10 mm samples.**

The 3D HDM parameters recovered using data from only twelve-ply samples were then used in an attempt to predict moisture absorption behavior in the six and forty-ply samples. The average RMS error of the twelve-ply curve fit applied to the twelve-ply experimental data is 3.1 x 10$^{-3}$. Applying those parameters to the six-ply experimental data yields an average RMS error of 4.1 x 10$^{-3}$, an increase of 32%. When applied to the forty-ply experimental data, the average RMS error is 14.1 x 10$^{-3}$, approximately 4.5 times higher than the error associated with the fit

to the twelve-ply data.  The 3D HDM parameters recovered using only

experimental data from the twelve-ply samples are applied to six, twelve, and

forty-ply experimental data from 40 x 10 mm samples in Figure 41.  Again, the

error between the prediction and the experimental data demonstrates the failure of

this set of parameters to predict moisture absorption behavior of all but the

twelve-ply samples.


Lastly, the 3D HDM parameters recovered using data from only forty-ply samples

were used in an attempt to predict moisture absorption behavior in the six and

twelve-ply samples. The average RMS error of the forty-ply curve fit applied to

the forty-ply experimental data is 2.8 x $10^{-3}$. Applying those parameters to the

twelve-ply experimental data yields an average RMS error of 11.4 x $10^{-3}$, an

increase of over 350%. In addition, applying those parameters to the six-ply

experimental data yields an RMS error of 12.9 x $10^{-3}$, approximately 4.6 times

higher than the error associated with the fit to the forty-ply data.  The 3D HDM

parameters recovered using only experimental data from the forty-ply samples are

applied to six, twelve, and forty-ply experimental data from 40 x 10 mm samples

in Figure 42.
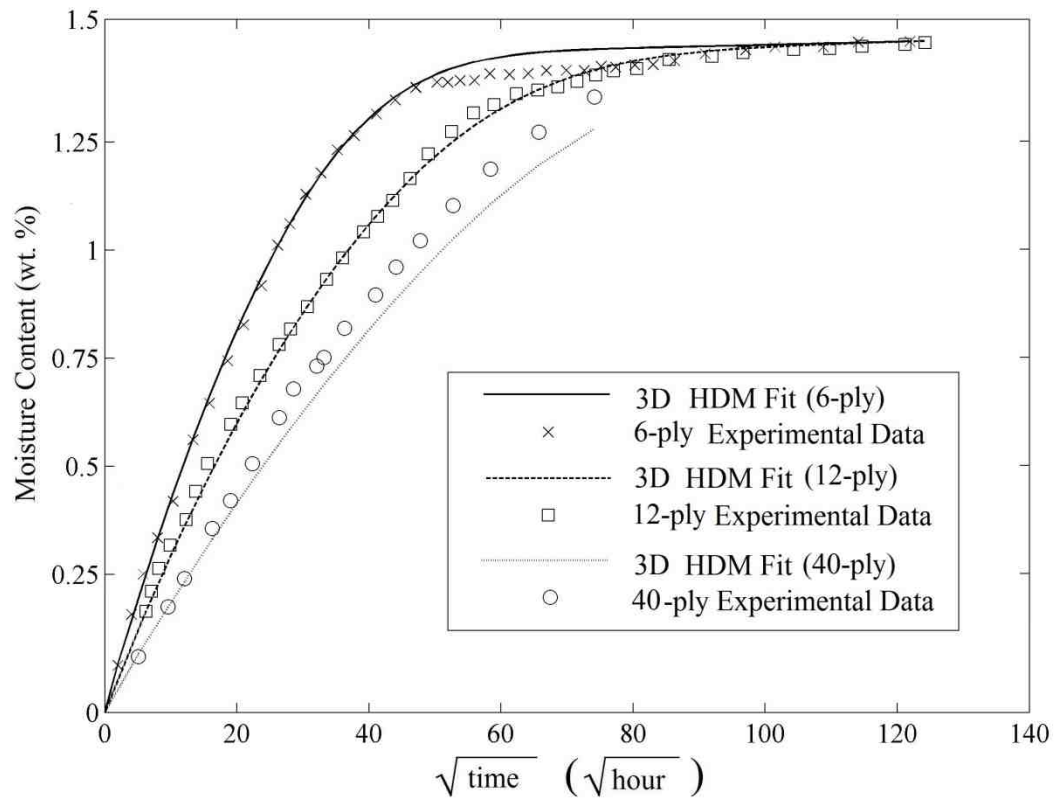
**Figure 41 – 3D HDM parameters recovered using experimental data from the 40 x 10 mm, twelve-ply samples applied to six, twelve, and forty-ply data.**

Again, the error between the prediction and the experimental data demonstrates the failure of this set of parameters to predict moisture absorption behavior of all but the twelve-ply samples.
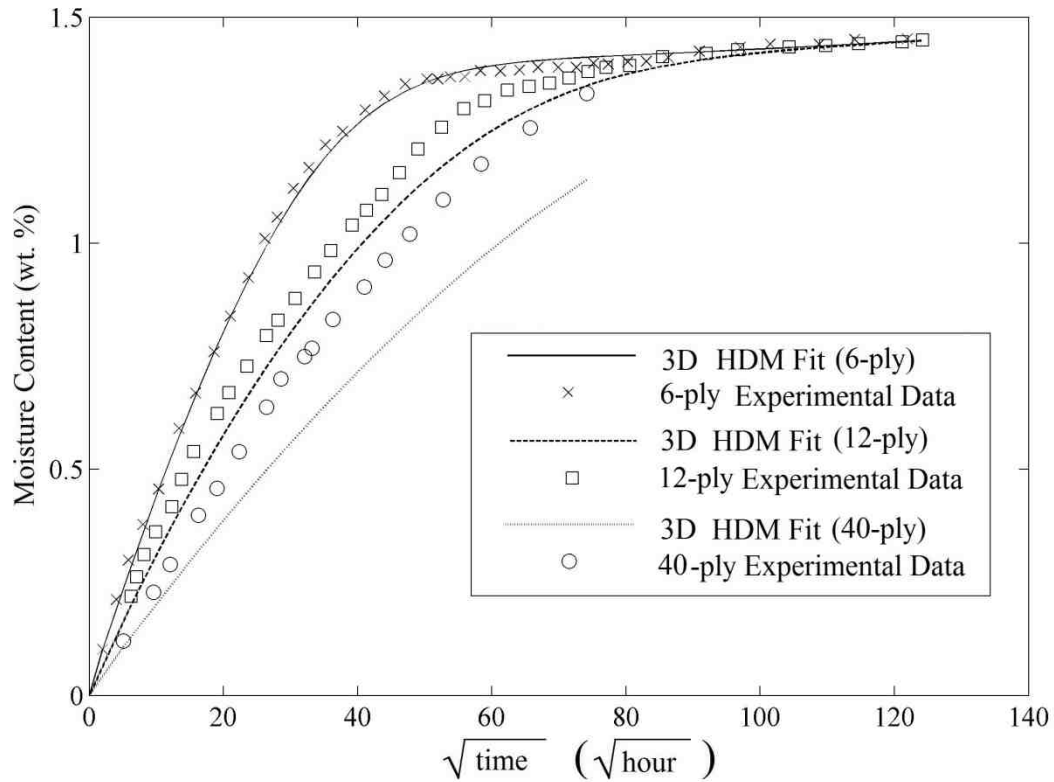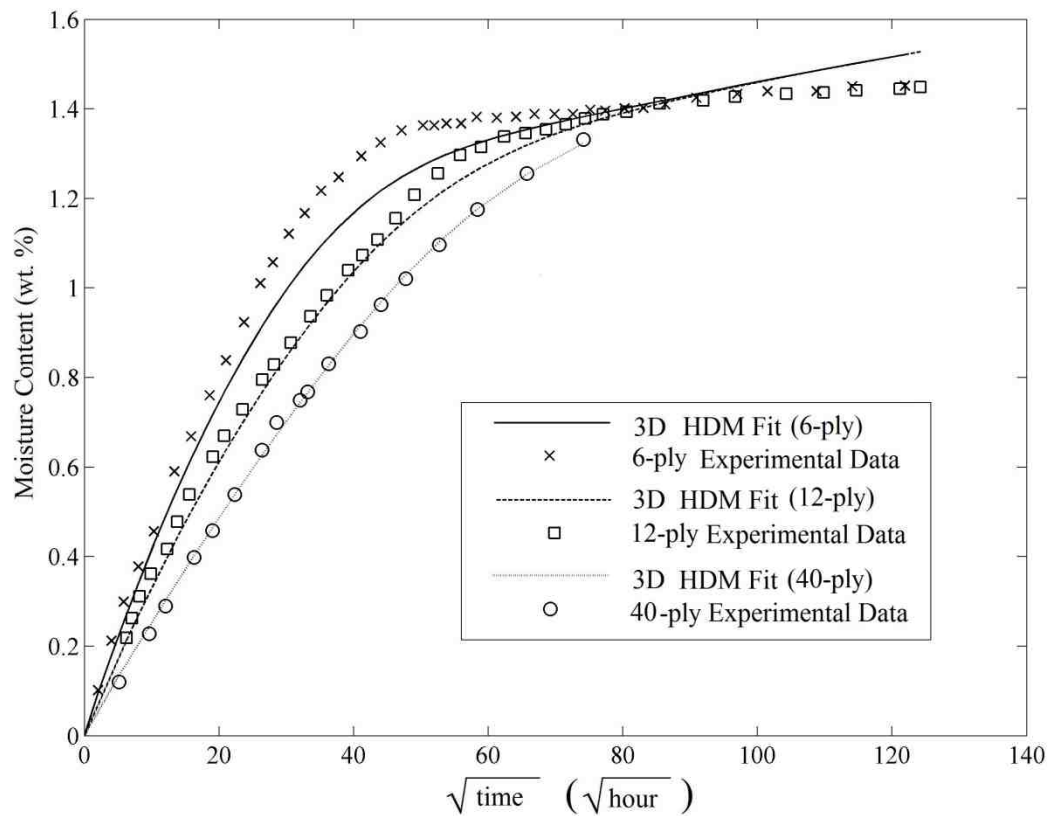
**Figure 42 - 3D HDM parameters recovered using only experimental data from the six-ply samples applied to six, twelve, and forty-ply experimental data from 40 x 10 mm samples.**

### (5.7)   3D HDM Parameter Recovery Prior to Experimental Equilibrium

The maximum moisture content of a composite in a specific environment plays a critical role in engineering design decisions due to the relationship between moisture and material property degradation. The pseudo-equilibrium moisture

content of 1.38% illustrated in Figure 35 corresponds with the equilibrium moisture content reported by the manufacturer for this material when fabricated according to the manufacturer's recommendations. However, experimental gravimetric data indicates that moisture absorption continues at a slower rate after this point and clearly deviates from the Fickian equilibrium plateau. The moisture content reached experimentally after 21 months of exposure is 1.46%, which is higher than the value reported by the manufacturer, but lower than what is predicted by the 3D HDM. The ability to accurately predict equilibrium moisture content prior to experimentally reaching a saturation point was demonstrated in Chapter 4.

As suggested in Chapter 4, the 3D HDM was applied to experimental data at exposure times throughout the moisture absorption study. The accuracy with which the model parameters may be recovered is affected by the length of the experimental time frame and the proximity of the experimental moisture content to the actual moisture equilibrium. The initial, relatively fast moisture uptake is largely controlled by diffusion of mobile molecules by random molecular motion. As a result, the three-dimensional diffusivities are relatively immune to changes in the initial estimates when experimental data is used that reaches or exceeds Fickian "pseudo-equilibrium". The recovered diffusion hindrance coefficient and equilibrium moisture content, however, may vary widely based on initial estimates if sufficient experimental data is not used.

In this case, the model parameters are consistently recovered within 1% after

approximately 16.5 months of exposure, regardless of initial estimates.

Subsequent measurements up to 21 months confirm the validity of the predictions.

Prior to 16.5 months, however, a range of model parameters may be recovered

which exhibit equivalent RMS error. An attempt to recover the model parameters

based on 4.5 months of experimental data, just after Fickian "pseudo-equilibrium"

exhibited significant dependence on the initial parameter estimates. A range of

hindrance coefficients from unity to 0.56 and moisture equilibrium from 1.4% to

2.3% were recovered, depending on the initial guess. Within these upper and

lower bounds, an infinite set of model parameters exist which yield RMS error of

less than 3 x $10^{-3}$ relative to experimental data. The recovered hindrance

coefficient of unity indicates unimpeded Fickian diffusion of mobile molecules,

while 0.56 indicates a highly hindered diffusion process. The range of recovered

model parameters narrows as the experimental data increases. At 6 months, the

window for hindrance coefficient and equilibrium moisture content narrows to

0.89 – 0.61 and 1.57% - 2.14%, respectively. The window narrows further at 11.5

months, where the hindrance coefficient may fall between 0.82 and 0.77 and

equilibrium moisture content may fall between 1.69% and 1.74%. After 16.5

months of exposure time, the parameters vary little with changes in initial

estimates. The parameters determined from 21 months of experimental data are

tightly bounded by the parameters recovered at 16.5 months. The hindrance

coefficient of 0.807, for example, is between the range of hindrance coefficient

values recovered at 16.5 months, which are 0.804 and 0.808. Similarly, the equilibrium moisture content of 1.723% falls between the 16.5 month range of 1.716% to 1.725%. The results of the parameter recovery based on experimental data from 4.5, 6, 11.5, and 16.5 months are presented in Figure 43 along with the gravimetric data from the six-ply, 40 x 10 mm samples.
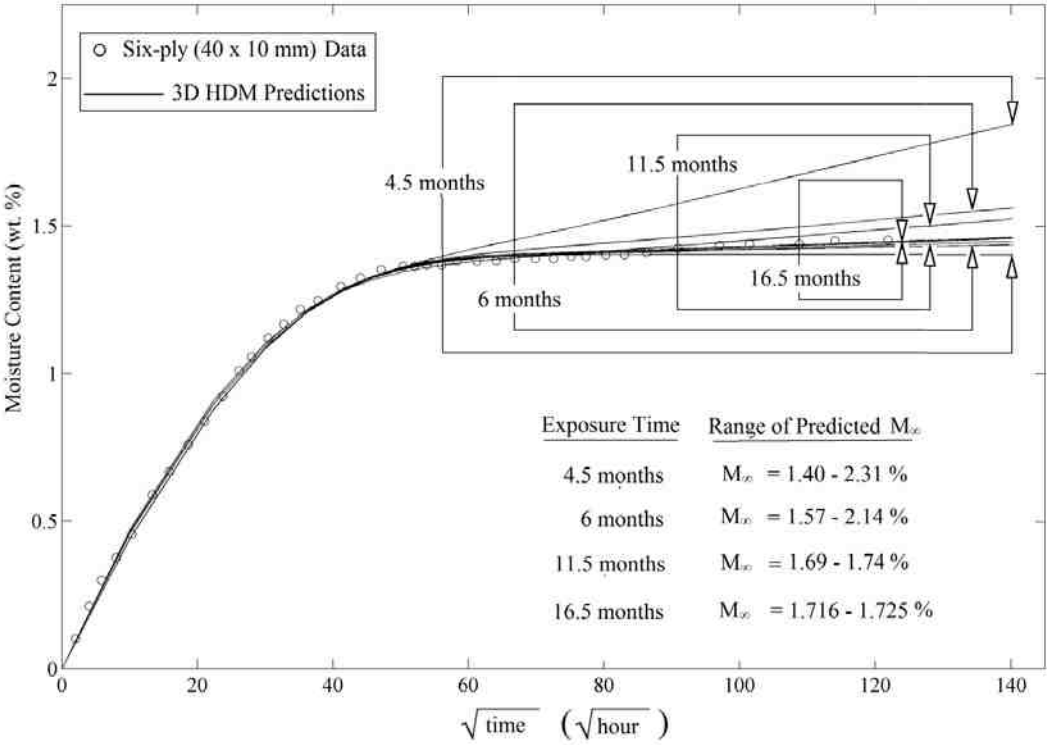


**Figure 43 – Effect of experimental time frame on recovery of three-dimensional hindered diffusion model parameters, with emphasis on equilibrium moisture content recovery.**

## (5.8)   Conclusions

Gravimetric moisture absorption data from six, twelve, and forty-ply BMI/quartz laminate specimens immersed in water at 25°C was collected over 21 months. The moisture absorption behavior was shown to deviate from the widely-used Fickian diffusion model.  The three-dimensional hindered diffusion model was successfully implemented in the recovery of orthotropic diffusion parameters. Excellent agreement is achieved between experimental gravimetric data and the 3D HDM for each laminate thickness.  Recovered model parameters show considerable differences in diffusion properties between six, twelve, and forty-ply laminates. However, diffusion parameters are consistent for all laminates of different planar dimensions and the same ply-count, regardless of inclusion in the least-square curve-fit. Equilibrium moisture content of 1.72, 1.69, and 1.84% and corresponding diffusion hindrance coefficients of  0.807, 0.844, and 0.671 are recovered for six, twelve, and forty-ply laminates, respectively.  Edge diffusivity of 1.98 x $10^{-3}$, 2.89 x $10^{-3}$, and 4.07 x $10^{-3}$ mm$^2$/hour was recovered for six, twelve, and forty-ply laminates, respectively. Diffusion through the laminate edges (in the fiber direction) occurs 11.4, 19.7, and 13 times faster than diffusion through the thickness (transverse to the fibers) for six, twelve, and forty-ply laminates, respectively. Moisture absorption parameters were shown to be successfully recovered after 16.5 months of exposure, prior to experimentally

reaching equilibrium moisture content. Subsequent gravimetric data up to 21

months were consistent with the predicted behavior.

# Chapter 6: Concluding Remarks and Recommendations for Future Work

## (6.1) Concluding Remarks

As composite usage increases, accurate characterization of environmental degradation of polymeric composites is critical. Moisture ingress is particularly important, due to the extent of the potential damage and the ubiquitous nature of moisture in nearly all operational environments. Further, accurate prediction of the reduction in mechanical and electrical properties due to moisture ingress is crucial to engineering design decisions. The incorporation of expected material property degradation into design decision is necessary to prevent in-service failure of composite structures. In addition to the increasing usage of composite materials, the longevity expected of composite structures is also increasing. The widely-used Fickian diffusion model, while applicable in many cases, fails to capture the slow increase in moisture content often seen in polymer composites exposed to moisture for long times. As a result, moisture content and resultant material property degradation may be underestimated at long times.

The simplicity of the Fickian diffusion model, and in particular the one-dimensional version, is one of the model's most important advantages. Additionally, the model is capable of predicting the basic shape of the moisture uptake curve in polymeric composites with significant success in many cases. The mechanics of simple diffusion by random molecular motion are incorporated in the Fickian diffusion model, and moisture absorption driven wholly by this phenomenon show excellent agreement with the model. The inhomogeneous nature of fiber-reinforced polymer composites, both physically and chemically, complicates the moisture diffusion process. The extent of this complication dictates the applicability of the Fickian diffusion model.

As a result, researchers are left with a decision to use the Fickian diffusion model or any of a number of models that predict anomalous diffusion behavior. The aforementioned "complication" that is a result of inhomogeneous polymeric composites was assumed in this work to be quantifiable as diffusion *hindrance*. The existing body of work on moisture diffusion in polymer reinforced composites does not include a sufficiently sophisticated model capable of capturing varying degree of this non-Fickian phenomenon. This disruption of normal diffusion due to random molecular motion can be represented by associating a probability of becoming bound and unbound with the diffusing molecules. These probabilities can be further simplified by combining them into the dimensionless hindrance coefficient proposed in this work.

The three-dimensional hindered diffusion model developed herein, therefore, is capable of predicting a wide range of moisture absorption behavior and is a novel and important improvement on predictive models of diffusion in polymer composites. The model's ability to predict *both* Fickian and non-Fickian moisture absorption with equal ease by moderating the hindrance coefficient, while incorporating material anisotropy and three-dimensional effects, make it truly comprehensive. The numerical solution method required for exact predictions is a drawback. However, the analytical approximation developed in Chapter 4 is valid for most cases, and is computationally feasible for use in an iterative curve-fitting process for recovery of diffusion parameters from experimental data.

An analytical solution to the three-dimensional anisotropic hindered diffusion model was developed in order to increase the utility of the model in recovering these diffusion properties based on experimental data. A parameter recovery method employing the analytical solution of the 3D HDM and least-squares regression was presented. The recovery method was applied successfully to synthetic moisture absorption data generated using both the 3D Fickian mass gain function and the numerical solution to the 3D HDM. Anisotropic diffusivities and equilibrium moisture content, $M_\infty$ were recovered with less than 1% error for both cases. The hindrance coefficient, $\mu$, which is dependent on the values of $\gamma$ and $\beta$, was consistently recovered with less than 1% error for both Fickian and non-Fickian synthetic data regardless of initial estimates. The ability to accurately

recover $M_\infty$ using experimental data prior to reaching equilibrium moisture

saturation was investigated with varying amounts of artificially induced

measurement error.  Accurate recovery of $M_\infty$ is possible long before it is reached

experimentally, though the time required is dependent on measurement error and

frequency. The results indicated that increased measurement error lengthens the

experimental time required to accurately predict equilibrium moisture content. A

typical measurement error of 2 % was shown to increase the required

experimental time frame by nearly 150% compared to data collected with no

error.  In addition, collecting experimental gravimetric measurements twice as

often may decrease the time required to recover $M_\infty$ by as much as 40%.

The applicability and superiority of the 3D HDM over the 3D Fickian model was

further demonstrated by application of the model to experimental gravimetric data

from a BMI/Quartz laminate immersed in water at 25°C for 21 months. The

moisture absorption behavior was shown to deviate from the widely-used Fickian

diffusion model, but conform well to the Hindered Diffusion model for all sample

sizes. Recovery of the 3D HDM parameters revealed slight differences in

diffusion behavior based on sample thickness, highlighting the potential for error

if using experimental data from one sample thickness to predict another. Potential

causes of the variations in the recovered diffusion properties may be the result of

the different contributions of diffusion through the edges relative to the face of a

sample, different fiber volume fractions according to laminate thickness, or the

existence of degree of cure gradients within thick laminates. Equilibrium moisture content of 1.72, 1.69, and 1.84% and corresponding diffusion hindrance coefficients of 0.807, 0.844, and 0.671 are recovered for six, twelve, and forty-ply laminates, respectively. Edge diffusivity of $1.98 \times 10^{-3}$, $2.89 \times 10^{-3}$, and $4.07 \times 10^{-3}$ $mm^2$/hour was recovered for six, twelve, and forty-ply laminates, respectively. Diffusion through the laminate edges (in the fiber direction) occurs 11.4, 19.7, and 13 times faster than diffusion through the thickness (transverse to the fibers) for six, twelve, and forty-ply laminates, respectively. Moisture absorption parameters were shown to be successfully recovered after 16.5 months of exposure, prior to experimentally reaching equilibrium moisture content. Subsequent gravimetric data up to 21 months were consistent with the predicted behavior.

## (6.2)    Recommendations for Future Work

### (6.2.1) The Physical Cause of Hindered Diffusion

The ability of the three-dimensional hindered diffusion model to capture Fickian and non-Fickian moisture absorption behavior has been demonstrated. However, the physical nature of the disruption in molecular diffusion remains unknown. The most likely causes are molecular binding of the water to polar sites on the polymer chain, capture of the diffusing molecules in microvoids, or long-term

relaxation of the polymer due to the introduction of a penetrant.  The ability to relate the chemical composition of the polymer or the size and distribution of microvoids may allow prediction of the hindrance coefficient based on these factors, without time-consuming gravimetric experiments. For example, a baseline hindrance coefficient may be expected for BMI which may be adjusted up or down based on the size and distribution of microvoids. Alternatively, a specific chemical structure may be expected in bismaleimide resins cured under known conditions for which molecular binding and unbinding probabilities may be predicted with accuracy.

*(6.2.2) The Relationship between Laminate Thickness, Resin Content, Void Content, and Moisture Absorption Properties*

The use of thin composite samples in gravimetric moisture absorption studies is the most efficient method for diffusion property recovery in terms of both experimental time required and material costs. However, variations in the recovered diffusion parameters depending on the material thickness found in this study of BMI/Quartz moisture absorption behavior suggest that the use of thin samples is inadequate. The obvious differences in laminate physical properties (i.e., fiber volume fraction, per-ply thickness, etc.) are undoubtedly largely to blame for the variance in recovered diffusion parameters. However, such cure-process induced differences are inevitable and not easily controlled among

laminates of different thickness. Therefore, from a practical standpoint, relating moisture absorption properties of thin composite samples to the behavior of thicker samples is difficult at best and impossible at worst. Establishing a correlation between the physical characteristics of the laminate and the change in the moisture absorption properties that would allow the use of thin samples for experiments would be extremely beneficial.  A known relationship between void content or fiber volume fraction and equilibrium moisture content, for example, would allow adjustment of diffusion properties based on these laminate physical characteristics.

*(6.2.3) The Effect of Exposure Temperature and Humidity Level on*

*Diffusion Hindrance Coefficient*

A known relationship exists between exposure temperature and diffusion coefficients in polymeric composites.  As expected and as reported throughout the literature, increased temperature increases the rate of diffusion. The primary contribution to moisture gain in polymeric composites is traditional diffusion according to Fick's law, which is gradient driven and due to random molecular motion. Increases in temperature and the subsequent increase in molecular motion lead to increased diffusion at higher temperatures. Similarly, higher humidity levels increases the rate of diffusion in polymeric composites. However, the effect of temperature and humidity on the hindrance coefficient has not yet been

established. Developing a relationship between exposure temperature, humidity, and hindrance coefficient would increase the applicability of the model to a wider range of environmental conditions. Experimental determination of diffusion hindrance at multiple temperatures and humidity levels may lead to a basic understanding of the change in diffusion hindrance that can be associated with temperature and humidity change. Such knowledge would allow diffusion parameters recovered from experimental gravimetric data at one temperature and humidity level to be used to predict the hindered moisture absorption behavior at other environmental conditions.

### (6.2.4) Degree-of-Cure Gradients and Diffusion Hindrance Coefficient

The effect of the degree of cure through the thickness of a laminate on the moisture absorption properties is an important consideration, especially in the case of very thick laminates. In thick laminates, the exothermic reactions during the cure process are very likely to cause a temperature overshoot in the center of the laminate. Hence, a variation in the degree of cure through the thickness may exist. Such a variation may cause a gradient in the diffusion hindrance through the thickness, due to the different physical and chemical structure that would result from the temperature gradient. If this were the case, diffusion properties would not be geometrically scalable between samples of different thickness, even with identical fiber volume fractions and void content.

# References

[1]     Kumar, B.G., Singh, R.P., Nakamura, T. (2002). Degradation of Carbon Fiber-reinforced Epoxy Composites by Ultraviolet Radiation and Condensation, *Journal of Composite Materials*, 36(24): 2713-2733.

[2]     Kutz, Myer. Handbook of Environmental Degradation of Materials. Norwich, NY: William Andrew Pub., 2005.

[3]     Cochran, R.C., Donnellan, T.M., Trabocco, R.E. (1992). Environmental Degradation of High Temperature Composites. Naval Air Development Center (1992). DTIC. Apr. 1992. Web. Mar. 2011. <http://handle.dtic.mil/100.2/ADP006820>.

[4]     Fischer, P., DeLuccia, J.J. (1976). Effects of Graphite/Epoxy Composite Materials on the Corrosion Behavior of Aircraft Alloys, *American Society for Testing and Materials* ASTM STP 602 (1976): 50-66.

[5]     Tucker, W.C., Brown, R. (1989). Blister Formation on Graphite/Polymer Composites Galvanically Coupled with Steel in Seawater, *Journal of Composite Materials,* 23: 389-395.

[6]     Ozcelik, O., Aktas, L., Altan, M.C. (2009). Thermo-oxidative Degradation of Graphite/Epoxy Composite Laminates: Modeling and Long-term Predictions, *Express Polymer Letters*, 3(12), 797-803.

[7]     Rauwendaal, C. (2001). *Polymer Extrusion*. Cincinnati, OH: Hanser Gardner Publications.

[8]     Roy, S., Singh, S., Schoeppner, G.A. (2008). Modeling of Evolving High-Temperature Polymer Matrix Composites Subjected to Thermal Oxidation, *Journal of Material Science*. 43: 6651-6660.

[9]     Carroll, J.R., Hammond, C.L. (1978). Environmental Effects on Composites*,  AIAA*  Paper 78-498, American Institute of Aeronautics and Astronautics / American Society of Mechanical Engineers / American Society of Civil Engineers / American Helicopter Society 19th Structures, Structural Dynamics, and Materials Conference, Bethesda, MD, April 1978.

[10]     Abdelmagid, B., Ziaee, S., Gass, K. and Schneider, M. (2005). The Combined Effects of Load, Moisture and Temperature on the Properties of E-glass/epoxy Composites, *Composite Structures*, 71(3-4): 320-26.

[11]     Akay, M. (1997). Influence of Moisture on the Thermal and Mechanical Properties of Autoclaved and Oven-cured Kevlar-49/epoxy Laminates, *Composites Science and Technology*, 57(5): 565-571.

[12]     Jankowsky, J.L., Wong, D.G., DiBerardino, M.F., Cochran, R.C. (1993). Evaluation of upper use temperature of toughened epoxy composites, *Proceedings of the Symposium on Assignment of the Glass Transition*, March 4, 1993 – March 5, 1993; Atlanta, GA: 277–92.

[13]     Viña, J., Garcia, E. A., Argüelles, A., and Viña, I. (2000). The Effect of Moisture on the Tensile and Interlaminar Shear Strengths of Glass or Carbon Fiber Reinforced PEI, *J. Mater. Sci. Lett.*, 19(7): 579–581.

[14]     Cerny, I. and Mayer, R.M. (2010). Evaluation of Static and Fatigue Strength of Long Fiber GRP Composite Material Considering Moisture Effects, *Composite Structures*, 92(9): 2035-038.

[15]     Naceri, A. (2009). Modeling of the Mechanical Behavior of Composite at Different Relative Humidities, *Strength of Materials*, 41(4): 444-448.

[16]     Chu, W., and Karbhari, V. M. (2005). Effect of Water Sorption on Performance of Pultruded E-Glass/Vinylester Composites, *Journal of Materials in Civil Engineering*, 17(1): 63.

[17]     Kalfon, E., Harel, H., Marom, G., Drukker, E., Green, A. K., and Kressel, I. (2005). Delamination of Laminated Composites Under the Combined Effect of Nonuniform Heating and Absorbed Moisture, *Polymer Composites*, 26(6): 770-777.

[18]     Papanicolaou, G.C., Kosmidou, T.V., Vatalis, A.S. and Delides, C.G. (2006). Water Absorption Mechanism and Some Anomalous Effects on the Mechanical and Viscoelastic Behavior of an Epoxy System, *Journal of Applied Polymer Science*, 99(4): 1328-339.

[19]    Lin, Y., and Chen, X. (2005). Moisture Sorption–Desorption–Resorption Characteristics and its Effect on the Mechanical Behavior of the Epoxy System, *Polymer*, 46(25): 11994-12003.

[20]    Aktas, L., Hamidi, Y., and Altan, M. C. (2002). Effect of Moisture Absorption on Mechanical Properties of Resin Transfer Molded Composites - Part I: Absorption, *Journal of Materials Processing and Manufacturing Science,* 10: 239-254.

[21]    Aktas, L., Hamidi, Y., and Altan, M. C. (2002). Effect of Moisture Absorption on Mechanical Properties of Resin Transfer Molded Composites - Part II: Desorption, *Journal of Materials Processing and Manufacturing Science,* 10: 255-267.

[22]    Barraza, H.J., Aktas, L., Hamidi, Y., Long, J., O'Rear, E.A., and Altan, M.C. (2003). Moisture Absorption and Wet-adhesion Properties of Resin Transfer Molded (RTM) Composites Containing Elastomer-coated Glass Fiber, *Journal of Adhesion Science and Technology,* 17(2): 217-242.

[23]    Pillay, S., Vaidya, U.K., Janowski, G.M. (2009). Effects of Moisture and UV Exposure on Liquid-Molded Carbon Fabric Reinforced Nylon 6 Composite Laminates, *Composites Science and Technology*, 69: 839-846.

[24]    Wan, Y., Wang, Y., Huang, Y., Zhou, F., He, B., Chen, G., and Han, K. (2005). Moisture Sorption and Mechanical Degradation of VARTMed Three-dimensional Braided Carbon-epoxy Composites, *Composites Science and Technology*, 65(7-8): 1237-243.

[25]    Cotinaud, M., Bonniau, P. and Bunsell, A.R. (1982). The Effect of Water Absorption on the Electrical Properties of Glass-fibre Reinforced Epoxy Composites, *Journal of Materials Science*, 17(3): 867-77.

[26]    Kumosa, L. (2004). Moisture Absorption Properties of Unidirectional Glass/polymer Composites Used in Composite (non-ceramic) Insulators, *Composites Part A: Applied Science and Manufacturing*, 35(9): 1049-063.

[27]    Fick, A. (1855). Ueber Diffusion. *Annalen Der Physik Und Chemie*, 170(1): 59-86.

[28] Rao, R.M.V.G.K., H.V.S Kumari and K.S. Raju. (1995). Moisture Diffusion Behaviour of T300-914C Laminates, *Journal of Reinforced Plastics and Composites*, 14(5): 513-22.

[29] Hayward, D., Hollins, E., Johncock, P., McEwan, I., Pethrick, R. and Pollock, E. (1997). The Cure and Diffusion of Water in Halogen Containing Epoxy/amine Thermosets, *Polymer* 38(5): 1151-168.

[30] Rao, R.M.V.G.K., Chanda, M. and Balasubramanian, N. (1983). A Fickian Diffusion Model for Permeable Fibre Polymer Composites, *Journal of Reinforced Plastics and Composites*, 2(4): 289-99.

[31] Al-Harthi, M., Loughlin, K., and Kahraman, R. (2007). Moisture Diffusion into Epoxy Adhesive: Testing and Modeling, *Adsorption,* 13(2): 115-20.

[32] Mensitieri, G., Lavorgna, M., Musto, P., and Ragosta, G. (2006). Water Transport in Densely Crosslinked Networks: A Comparison between Epoxy Systems Having Different Interactive Characters, *Polymer*, 47(25): 8326-336.

[33] Glaskova, T., and Aniskevich, A. (2009). Moisture Absorption by Epoxy/montmorillonite Nanocomposite, *Composites Science and Technology*, 69(15-16): 2711-2715.

[34] Liu, W., Hoa, S., and Pugh, M. (2008). Water Uptake of Epoxy-clay Nanocomposites: Experiments and Model Validation, *Composites Science and Technology* 68(9): 2066-072.

[35] Liu, W., Hoa, S., and Pugh, M. (2007). Water Uptake of Epoxy-clay Nanocomposites: Model Development, *Composites Science and Technology,* 67(15-16): 3308-315.

[36] Abacha, N., Kubouchi, M., Sakai, T. and Tsuda, K. (2009). Diffusion Behavior of Water and Sulfuric Acid in Epoxy/Organoclay Nanocomposites, *Journal of Applied Polymer Science*, 112(2): 1021-029.

[37]     Bao, L., and Yee, A. (2002). Moisture Diffusion and Hygrothermal Aging in Bismaleimide Matrix Carbon Fiber Composites - Part I: Uni-weave Composites, *Composites Science and Technology*, 62(16): 2099-110.

[38]     Bao, L., and Yee, A. (2002). Moisture Diffusion and Hygrothermal Aging in Bismaleimide Matrix Carbon Fiber Composites: Part II - Woven and Hybrid Composites, *Composites Science and Technology*, 62(16): 2111-119.

[39]     Bao, L. and Yee, A. (2002). Effect of Temperature on Moisture Absorption in a Bismaleimide Resin and Its Carbon Fiber Composites, *Polymer*, 43(14): 3987-997.

[40]     Glaskova, T.I., Guedes, R.M., Morais, J.J., and Aniskevich, A. N. (2007). A Comparative Analysis of Moisture Transport Models as Applied to an Epoxy Binder, *Mechanics of Composite Materials*, 43(4): 377-88.

[41]     Jacobs, P. M., and Jones, F.R. (1989). Diffusion of Moisture into Two-Phase Polymers, *Journal of Materials Science*, 24(7): 2331-336.

[42]     Hamerton, I., Herman, H., Rees, K., Chaplin, A. and Shaw, S. (2001). Water Uptake Effects in Resins Based on Alkenyl-modified Cyanate Ester-bismaleimide Blends, *Polymer International*, 50(4): 475-83.

[43]     LaPlante, G., Ouriadov, A.V., Lee-Sullivan, P., and Balcom, B.J. (2008). Anomalous Moisture Diffusion in an Epoxy Adhesive Detected by Magnetic Resonance Imaging, *Journal of Applied Polymer Science,* 109(2): 1350-359.

[44]     Li, Y., Miranda, J., and Sue, H. (2002).  Moisture Diffusion Behavior in Bismaleimide Resin Subjected to Hygrothermal Cycling, *Polymer Engineering & Science,* 42(2): 375-81.

[45]     Musto, P., Ragosta, G., Scarinzi, G. and Mascia, L. (2002). Probing the Molecular Interactions in the Diffusion of Water through Epoxy and Epoxy–Bismaleimide Networks, *Journal of Polymer Science Part B: Polymer Physics*, 40(10): 922-38.

[46]     Popineau, S., Rondeaumouro, C., Sulpice-Gaillet, C. and Shanahan, M. (2005). Free/bound Water Absorption in an Epoxy Adhesive, *Polymer*, 46(24): 10733-0740.

[47]     Cotugno, S., Mensitieri, G., Musto, P., and Sanguigno, L. (2005). Molecular Interactions in and Transport Properties of Densely Cross-Linked Networks:  A Time-Resolved FT-IR Spectroscopy Investigation of the Epoxy/HO System, *Macromolecules*, 38(3): 801-811.

[48]     Wong, T. C., and Broutman, L.J. (1985). Moisture Diffusion in Epoxy Resins. Part I. Non-Fickian Sorption Processes, *Polymer Engineering and Science*, 25(9): 521-28.

[49]     Yeh, R., Lin, P. and Lin, K. (2002). Two-Stage Moisture Absorption Behavior and Hydrolysis of Cured Dicyanate Ester Resins, *Journal of Polymer Research*, 9(1): 31-36.

[50]     Mubashar, A., Ashcroft, I. A., Critchlow, G. W., and Crocombe, A. D. (2009). Modeling Cyclic Moisture Uptake in an Epoxy Adhesive, *The Journal of Adhesion*, 85(10): 711-35.

[51]     Kotsikos, G., Gibson, A.G. and Mawella, J. (2007). Assessment of Moisture Absorption in Marine GRP Laminates with Aid of Nuclear Magnetic Resonance Imaging, *Plastics, Rubber and Composites* 36(9): 413-18.

[52]     Carter, H. G., and Kibler, K.G. (1978). Langmuir-Type Model for Anomalous Moisture Diffusion in Composite Resins, *Journal of Composite Materials* 12(2): 118-31.

[53]     Roy, S., Xu, W. X., Park, S. J., and Liechti, K. M. (2000). Anomalous Moisture Diffusion in Viscoelastic Polymers: Modeling and Testing, *Journal of Applied Mechanics*, 67(2): 391.

[54]     Maggana, C., and Pissis, P. (1999). Water Sorption and Diffusion Studies in an Epoxy Resin System, *Journal of Polymer Science Part B: Polymer Physics,* 37(11): 1165-182.

[55]    Berens, A.R. and Hopfenberg, H.B. (1978). Diffusion and Relaxation in Glassy Polymer Powders: 2. Separation of Diffusion and Relaxation Parameters, *Polymer*, 19: 489-496.

[56]    Berens, A.R. and Hopfenberg, H.B. (1979). Induction and Measurement of Glassy-state Relaxations by Vapour Sorption Techniques, *Journal of Polymer Science: Polymer Physics*, 17: 1757-1770.

[57]    Shen, C.H., and Springer, G.S. (1976). Moisture Absorption and Desorption of Composite Materials, *Journal of Composite Materials,* 10(1): 2-20.

[58]    Cai, L.W., and Weitsman, Y., (1994). Non-Fickian Moisture Diffusion in Polymeric Composites, *Journal of Composite Materials,* 28(2): 130-154.

[59]    Bond, D.A., (2005). Moisture Diffusion in a Fiber-reinforced Composite: Part I – Non-Fickian Transport and the Effect of Fiber Spatial Distribution, *Journal of Composite Materials,* 39(23): 2113-2141.

[60]    Blikstad, M. (1986). Three-Dimensional Moisture Diffusion in Graphite/Epoxy Laminates, *Journal of Reinforced Plastics and Composites*, 5(1): 9-18.

[61]    Aronhime, M. T., Neumann, S., and Marom, G. (1987). The Anisotropic Diffusion of Water in Kevlar-epoxy Composites, *Journal of Materials Science*, 22(7): 2435-446.

[62]    Arao, Y., Koyanagi, J., Hatta, H., and Kawada, H. (2008). Analysis of Time-Dependent Deformation of CFRP Considering the Anisotropy of Moisture Diffusion, *Advanced Composite Materials*, 17(4): 359-72.

[63]    Pierron, F., Poirette, Y. and Vautrin, A. (2002). A Novel Procedure for Identification of 3D Moisture Diffusion Parameters in Thick Composites: Theory, Validation and Experimental Results, *Journal of Composite Materials*, 36(19): 2219-243.

[64]    Aktas, L., Hamidi, Y.K. and Altan, M.C. (2004). Combined Edge and Anisotropy Effects on Fickian Mass Diffusion in Polymer Composites, *Journal of Engineering Materials and Technology*, 126(4): 427-434.

[65] Waters, D.J. and Frank, C.W. (2009). Hindered Diffusion of Oligosaccharides in High Strength Poly(ethylene Glycol)/Poly(acrylic Acid) Interpenetrating Network Hydrogels: Hydrodynamic Versus Obstruction Models, *Polymer,* 50(26): 6331-339.

[66] Li, J. and Cantwell, F. (1996). Intra-particle Sorption Rate and Liquid Chromatographic Bandbroadening in Porous Polymer Packings III. Diffusion in the Polymer Matrix as the Cause of Slow Sorption, *Journal of Chromatography A*, 726(1-2): 37-44.

[67] Masoud, H. and Alexeev, A. (2010). Permeability and Diffusion through Mechanically Deformed Random Polymer Networks, *Macromolecules*, 43(23): 10117-0122.

[68] Shao, J. and Baltus, R.E. (2000). Hindered Diffusion of Dextran and Polyethylene Glycol in Porous Membranes, *AIChE Journal,* 46(6): 1149-1156.

[69] Hassanzadeh, H., Pooladi-Darvish, M. (2007). Comparison of Different Numerical Laplace Inversion Methods for Engineering Applications, *Applied Mathematics and Computation*, 189: 1966-1981.

[70] Youssef, G., Freour, S. and Jacquemin, F. (2009). Stress-dependent Moisture Diffusion in Composite Materials, *Journal of Composite Materials*, 43(15): 1621-637.

[71] Dehgan, M. (2004). Numerical Solution of the Three-Dimensional Advection-Diffusion Equation, *Applied Mathematics and Computation,* 150(1): 5-19.

[72] Yu, Y. and Pochiraju, K. (2003). Three-Dimensional Simulation of Moisture Diffusion in Polymer Composite Materials, *Polymer-Plastics Technology and Engineering*, 42(5): 737-56.

[73] Ouyang, Z. and Wan, B. (2008). Modeling of Moisture Diffusion in FRP Strengthened Concrete Specimens, *Journal of Composites for Construction*, 12(4): 425-34.

[74] Yang, J., Yang, Q., Ma, L. and Liu, W. (2010). Moisture Diffusion Behavior of Permeable Fiber-reinforced Polymer Composite, *Frontiers of Mechanical Engineering in China*, 5(3): 347-52.

[75] Li, Y., Miranda, J., and Sue, H. (2001). Hygrothermal Diffusion Behavior in Bismaleimide Resin, *Polymer*, 42(18): 7791-7799.

[76] ASTM D5229 / D5229M. (2010). Standard Test Method for Moisture Absorption Properties and Equilibrium Conditioning of Polymer Matrix Composite Materials, *ASTM International - Standards Worldwide*.

[77] Tang, X., Whitcomb, J.D., Li, Y., and Sue, H. (2005). Micromechanics Modeling of Moisture Diffusion in Woven Composites, *Composites Science and Technology*, 65(2005): 817-826.

[78] Sava, M., Sava, I., Cozan, V., Tanasa, F. (2007). Preparation and Polymerization of Bismaleimide Compounds, *Journal of Applied Polymer Science*, 106: 2185-2191.

[79] Ju, J., Morgan, R.J. (2004). Characterization of Microcrack Development in BMI-Carbon Fiber Composite under Stress and Thermal Cycling. *Journal of Composite Materials*, 38(22): 2007-2024.

[80] Liang, G., Zhang, Z., Yang, J., Wang, X. (2007). BMI Based Composites with Low Dielectric Loss, *Polymer Bulletin,* 59: 269-278.

[81] Garnich, M.R., Dalgarno, R.W., Kenik, D.J. (2011). Effects of Moisture on Matrix Cracking in a Cryo-cycled Cross-ply Laminate, *Journal of Composite Materials*, 45(26): 2783-2795.

[82] Seo, J., Jang, W., Han, H. (2007). Thermal Properties and Water Sorption Behaviors of Epoxy and Bismaleimide Composites, *Macromolecular Research,* 15(1): 10-16.

[83] HexPly® F650 Product Data Sheet, Hexcel Corporation, Stamford, Connecticut. www.hexcel.com/Resources/DataSheets/Prepreg-Data.../F650_us.pdf. (accessed December 2011).

[84]    R.A. Chaudhuri, R.A., Kabir, H.R.H. (1992). Influence of Lamination and Boundary Constraint on the Deformation of Moderately Thick Cross-ply Rectangular Plates, *Journal of Composite Materials,* 26(1): 51–77.

[85]    Hojjati M., and Hoa S.V. (1994). Curing Simulation of Thick Thermosetting Composites, *Composites Manufacturing,* 5(3): 159–169.

[86]    Bogetti, T.A., and Gillespie, J.W. (1991). Two-dimensional Cure Simulation of Thick Thermosetting Composite, *Journal of Composite Materials,* 25: 239-273.

[87]    Yi S., Hilton H.H., and Ahmad M.F. (1997).  A Finite Element Approach for Cure Simulation of Thermosetting Matrix Composite, *Computers & Structures,* 64(1–4): 383–388.

[88]    Kim J.S., and Lee D.G. (1997). Development of an Autoclave Cure Cycle with Cooling and Reheating Steps for Thick Thermoset Composite Laminates, *Journal of Composite Materials,* 31(22): 2264–2282.

[89]    Guo, Z., Du, S., and Zhang, B. (2004). Temperature Field of Thick Thermoset Composite Laminates During Cure Process, *Composites Science and Technology,* 65(2005): 517-523.

[90]    Perrin, F.X., Nguyen, M.H., and Vernet, J.L. (2009). Water Transport in Epoxy-aliphatic Networks: Influence of Curing Cycles, *European Polymer Journal*, 45(2009): 1524-1534.

# Appendix A:   Raw Experimental Gravimetric Data for
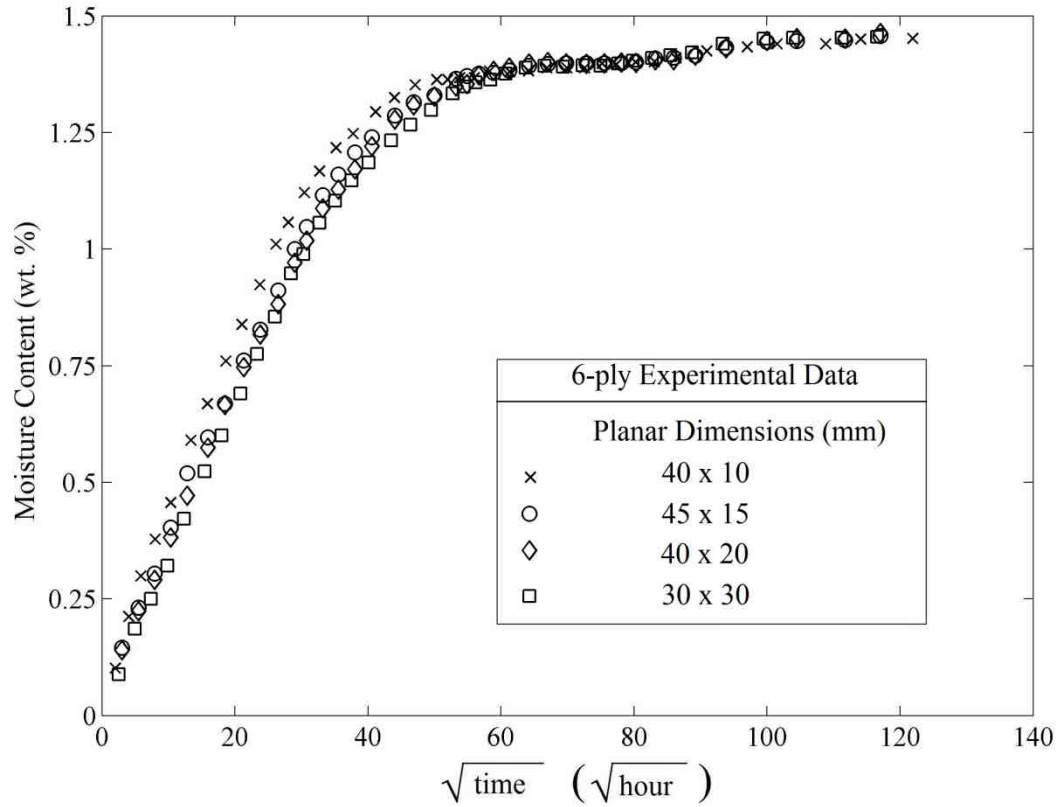
# BMI/Quartz Laminates



**Fig. A1 -  Graphical representation of average six-ply experimental data**
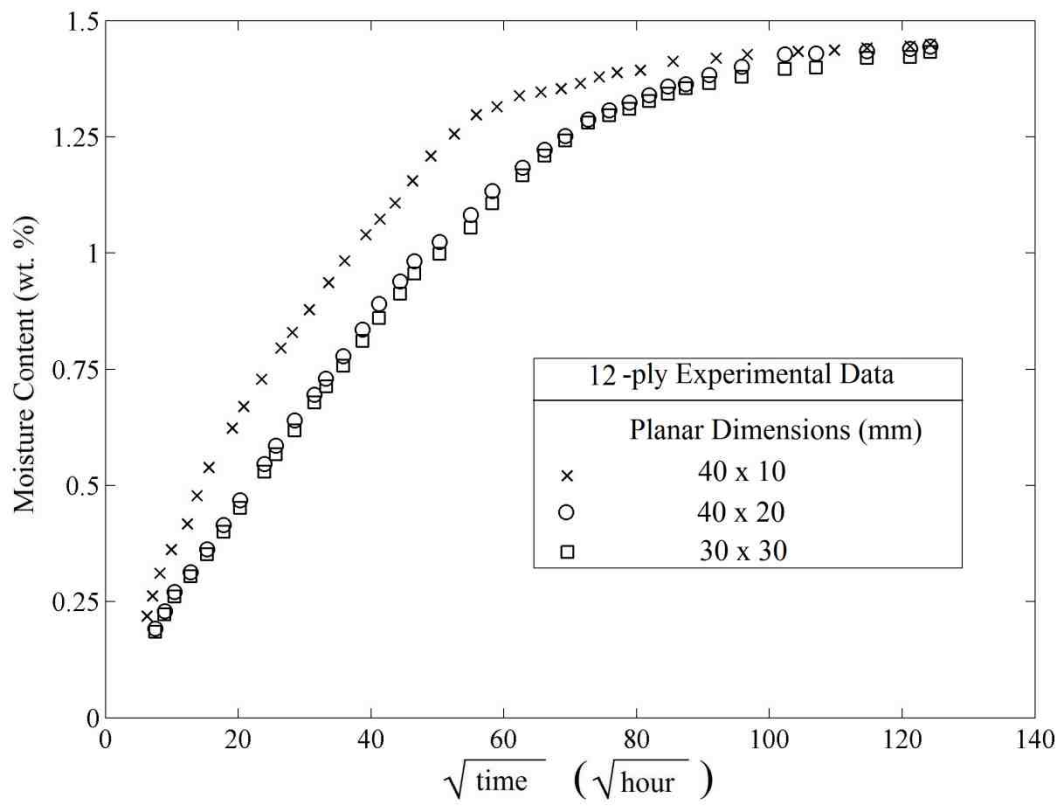
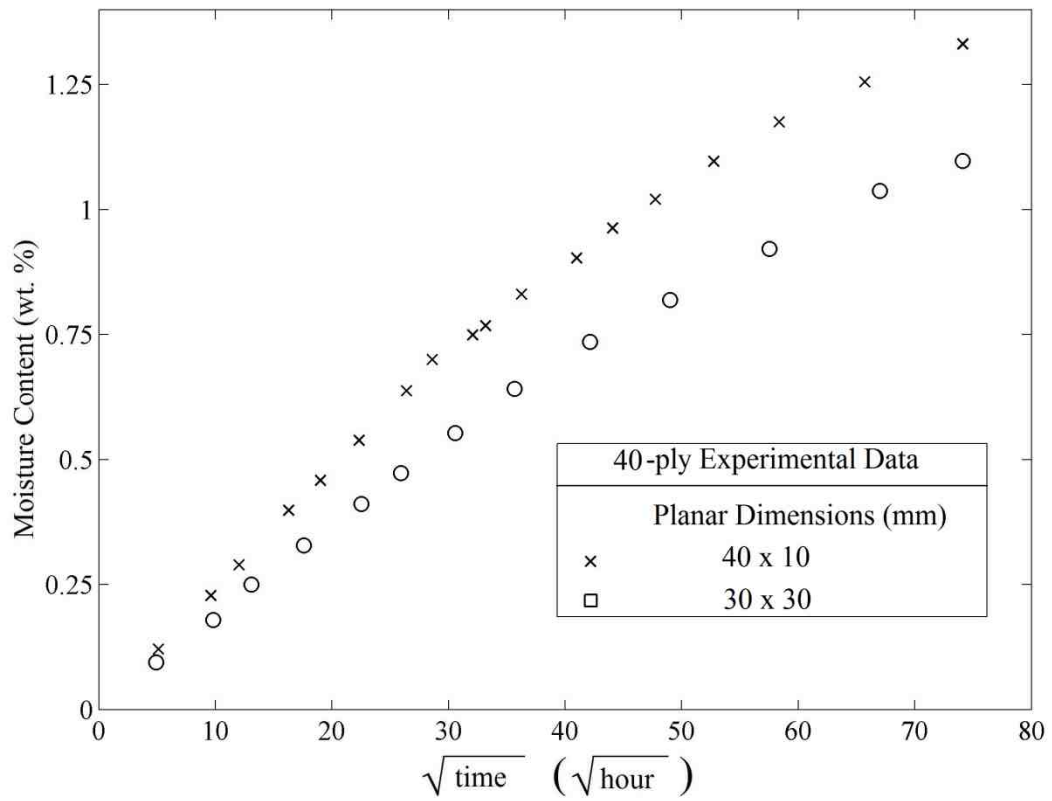**Fig. A2 - Graphical representation of average twelve-ply experimental data**

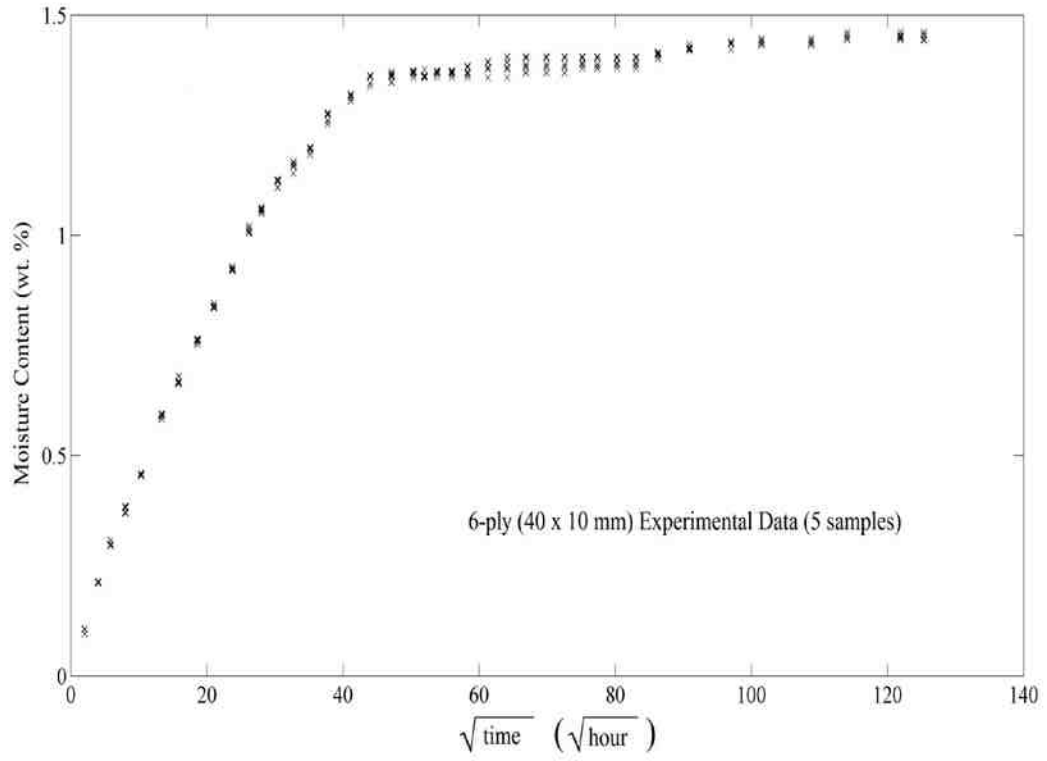**Fig. A3 - Graphical representation of average forty-ply experimental data**

**Fig. A4 - Raw experimental data for six-ply, 40 x 10 mm BMI/Quartz composite specimens**
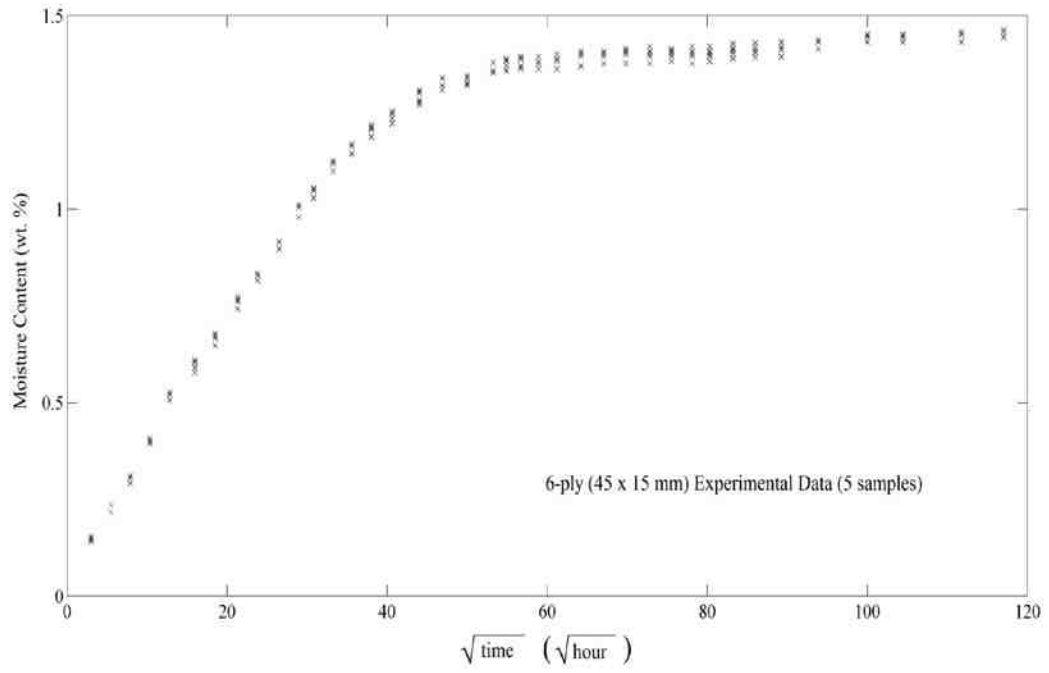
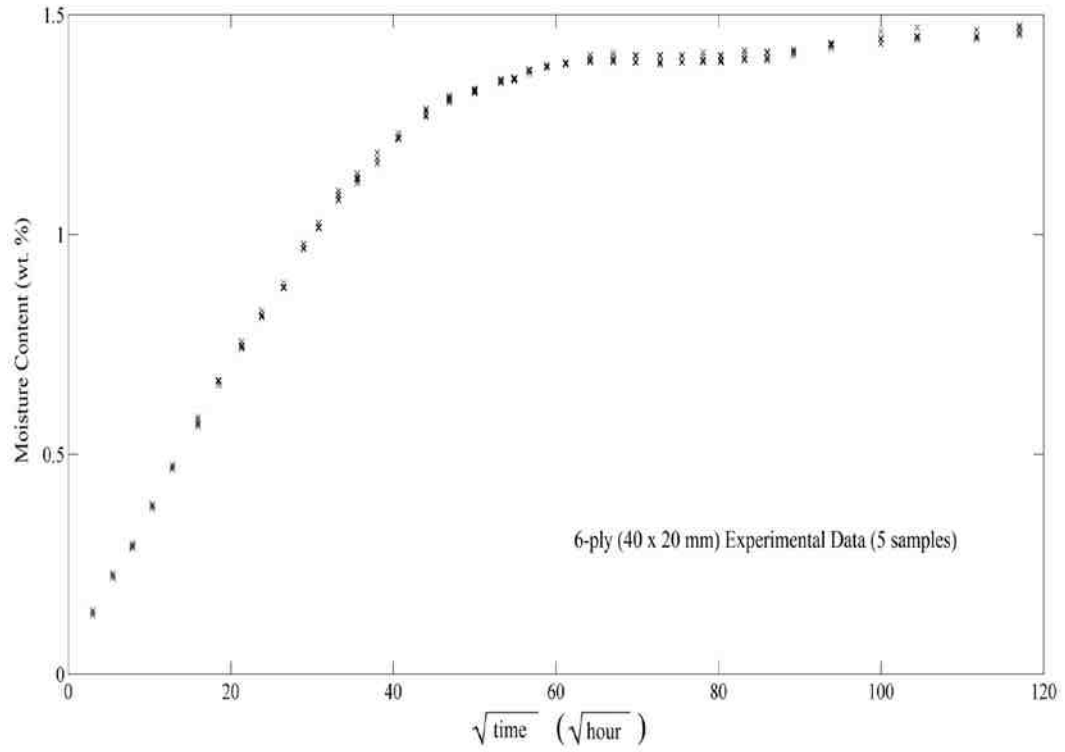**Fig. A5 - Raw experimental data for six-ply, 45x 15 mm BMI/Quartz composite specimens**

**Fig. A6 - Raw experimental data for six-ply, 40 x 20 mm  BMI/Quartz composite specimens**
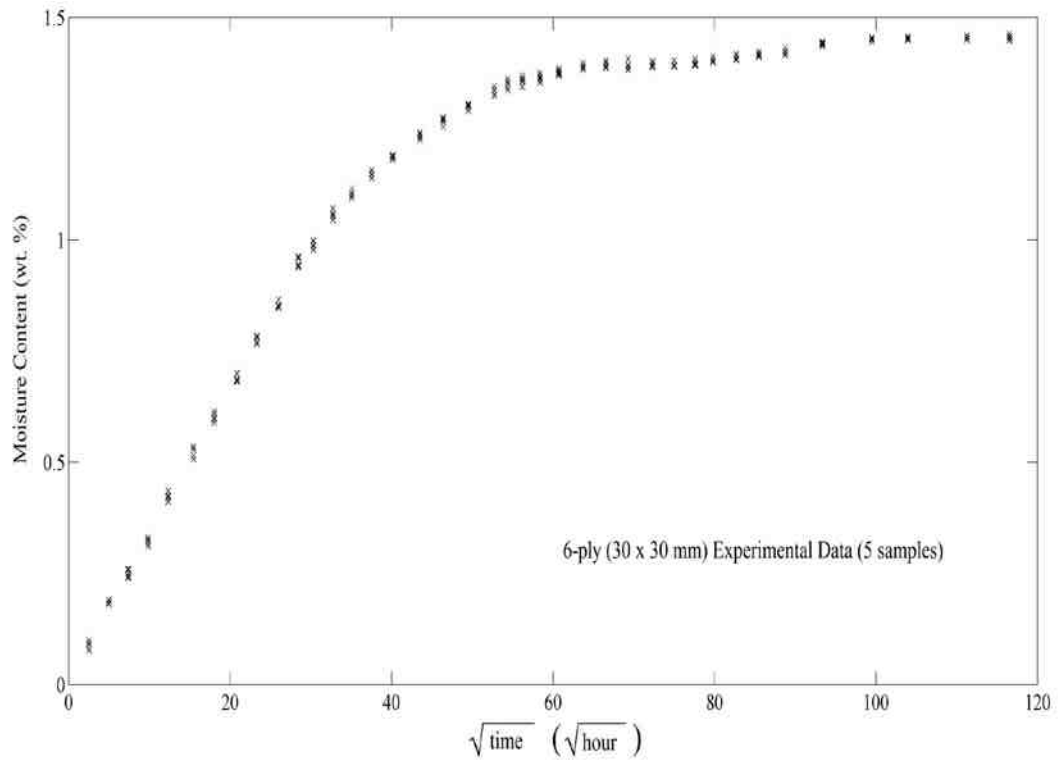
**Fig. A7 - Raw experimental data for six-ply, 30 x 30 mm  BMI/Quartz composite specimens**
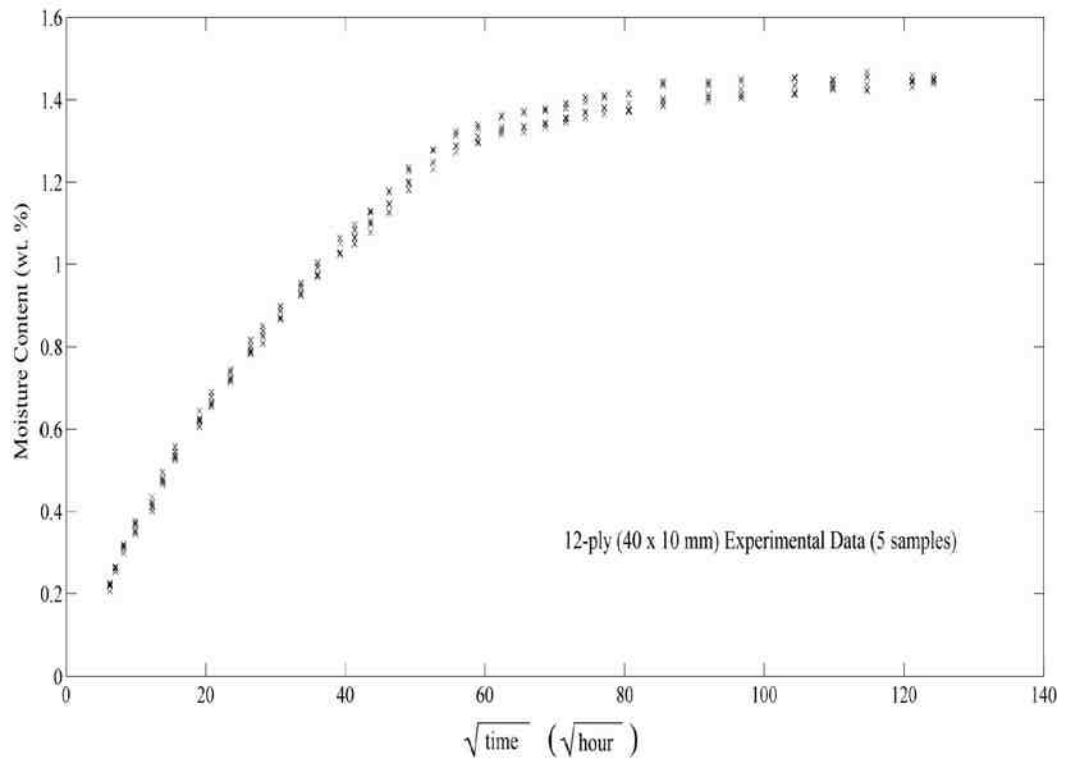
**Fig. A8 - Raw experimental data for twelve-ply, 40 x 10 mm  BMI/Quartz specimens**
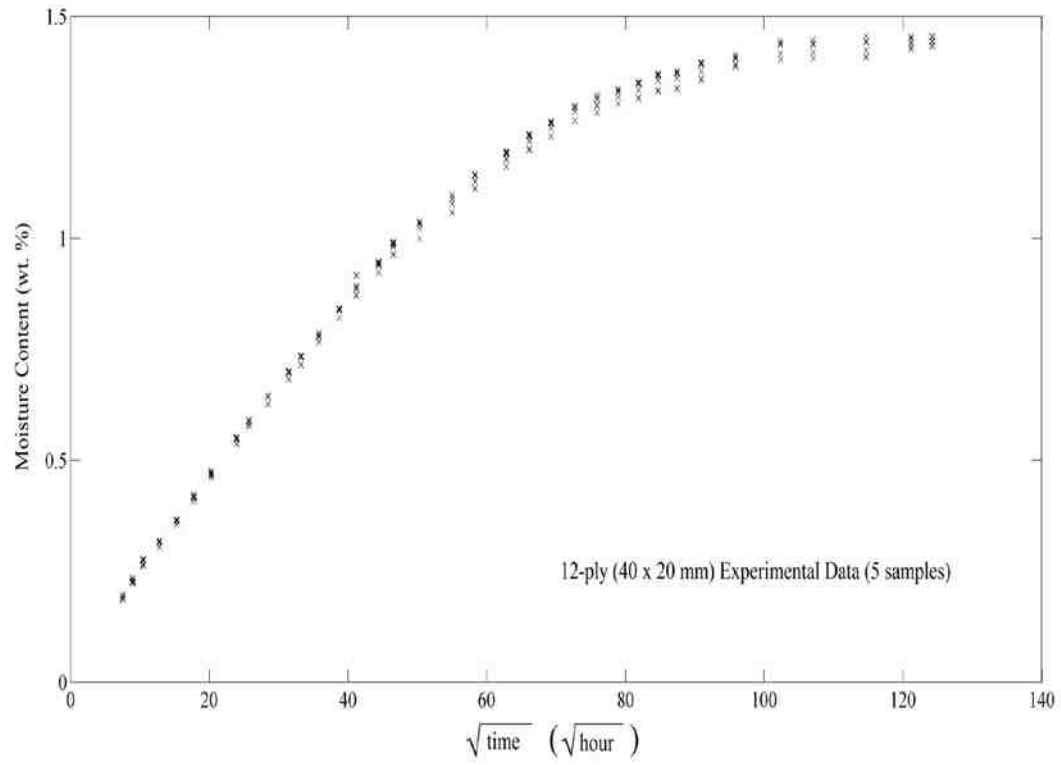
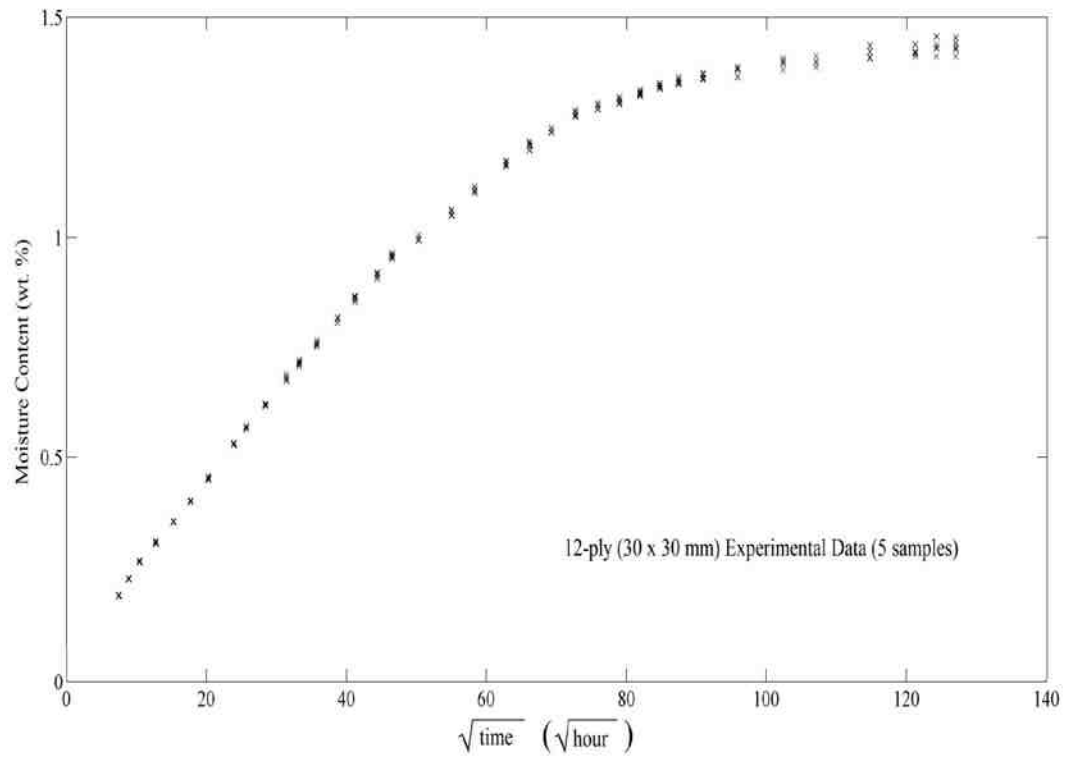**Fig. A9 - Raw experimental data for twelve-ply, 40 x 20 mm  BMI/Quartz specimens**

**Fig. A10 - Raw experimental data for twelve-ply, 30 x 30 mm  BMI/Quartz specimens**
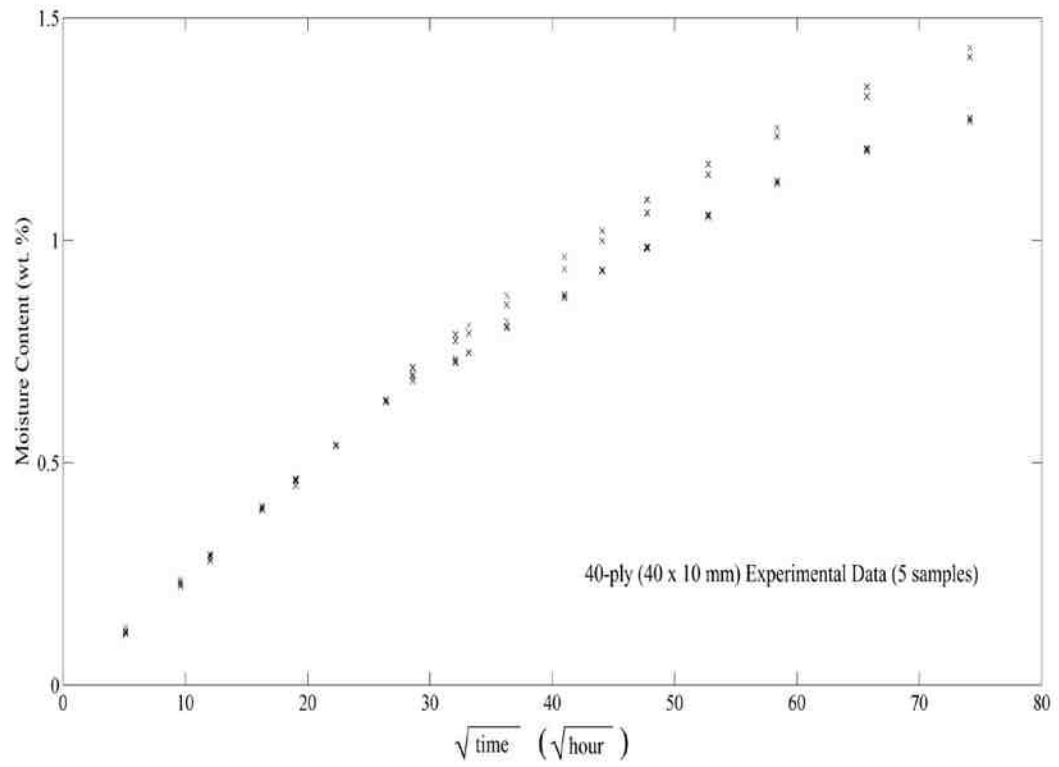
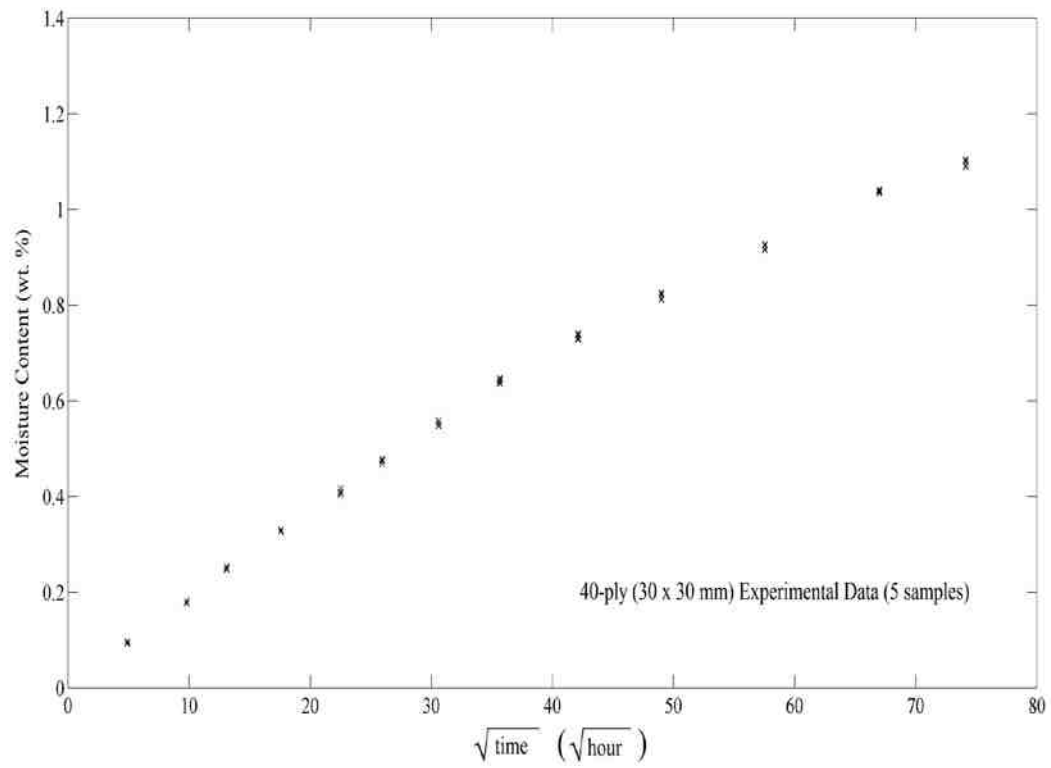**Fig. A11 - Raw experimental data for forty-ply, 40 x 10 mm  BMI/Quartz specimens**

**Fig. A12 - Raw experimental data for twelve-ply, 30 x 30  mm  BMI/Quartz**
**specimens**

# Appendix B:  Nomenclature

| Symbol | Meaning | Typical Unit |
|---|---|---|
| $M$ | Moisture content | $mg/mm^3$ |
| $M_\infty$ | Equilibrium moisture content | % |
| $\gamma$ | Probability of mobile molecule becoming bound | $hour^{-1}$ |
| $\beta$ | Probability of bound molecule becoming mobile | $hour^{-1}$ |
| $n$ | Concentration of mobile molecules | $mg/mm^3$ |
| $n_\infty$ | Equilibrium concentration of mobile molecules | $mg/mm^3$ |
| $N$ | Concentration of bound molecules | $mg/mm^3$ |
| $N_\infty$ | Equilibrium concentration of bound molecules | $mg/mm^3$ |
| $D_x$ | Diffusivity in $x$ direction | $mm^2/hour$ |
| $D_y$ | Diffusivity in $y$ direction | $mm^2/hour$ |
| $D_z$ | Diffusivity in $z$ direction | $mm^2/hour$ |
| $D_e$ | Diffusivity through the edges of an orthotropic laminate | $mm^2/hour$ |
| $h$ | Laminate thickness, $z$ direction | mm |
| $w$ | Laminate width, $x$ direction | mm |
| $l$ | Laminate length,  $y$ direction | mm |
| $s$ | Slope of initial section of Fickian moisture absorption curve | - |
| $D_c$ | Corrected diffusivity to account for edge effects | $mm^2/hour$ |
| $k$ | Parameter that determines overall rate of saturation | $hour^{-1}$ |

| | | |
|---|---|---|
| $k_x$ | Parameter that determines rate of saturation in $x$ direction | hour$^{-1}$ |
| $k_y$ | Parameter that determines rate of saturation in $y$ direction | hour$^{-1}$ |
| $k_z$ | Parameter that determines rate of saturation in $z$ direction | hour$^{-1}$ |
| $M_d$ | Equilibrium moisture content of dense phase in dual-diffusivity model | % |
| $M_l$ | Equilibrium moisture content of less dense phase in dual-diffusivity model | % |
| $D_d$ | Diffusivity of dense phase in dual-diffusivity model | mm$^2$/hour |
| $D_l$ | Diffusivity of dense phase in dual-diffusivity model | mm$^2$/hour |
| $m_d$ | Diffusivity of dense phase in dual-diffusivity model | mm$^2$/hour |
| $m_l$ | Slope of moisture uptake curve of dense phase in dual-diffusivity model | - |
| $V_d$ | Slope of moisture uptake curve of less dense phase in dual-diffusivity model | - |
| $\Phi$ | Diffusive absorption fraction in Diffusion-Relaxation Model | - |
| $\Omega$ | Relaxation rate constant in Diffusion-Relaxation Model | - |
| $M_F$ | Fickian mass gain | % |
| $M^*$ | Dimensionless moisture content, values between 0 – 1 | - |
| $A1$ | Dimensionless diffusivity in $x$ direction | - |

| | | |
|---|---|---|
| *A2* | Dimensionless diffusivity in *y* direction | - |
| *A3* | Dimensionless diffusivity in *z* direction | - |
| *µ* | Diffusion Hindrance Coefficient | - |
| *E* | Error between prediction and experimental data | % |
| $M_{exp}$ | Experimentally determined moisture content | % |
| *W* | Experimentally determined sample weight | mg |
| $W_i$ | Initial sample weight | mg |
| $T_g$ | Glass transition temperature | °C |